

Electronic and Magnetic Properties of Manganese Doped Quantum Dots

D i s s e r t a t i o n

zur Erlangung des Doktorgrades
des Department Physik
der Universität Hamburg

vorgelegt von

Peter Moraczewski

aus Löwenberg

Hamburg

2009

Gutachterin / Gutachter der Dissertation: Prof. Dr. Daniela Pfannkuche
Prof. Dr. Detlef Heitmann

Gutachterin / Gutachter der Disputation: Prof. Dr. Daniela Pfannkuche
Prof. Dr. Ulrich Merkt

Datum der Disputation: 21.12.2009

Vorsitzender des Prüfungsausschusses: PD Dr. Alexander L. Chudnovskiy

Vorsitzender des Promotionsausschusses: Prof. Dr. Robert Klanner

Dekan der Fakultät für Mathematik,
Informatik und Naturwissenschaften: Prof. Dr. Heinrich Graener

Abstract

In semiconductor quantum dots electrons and holes are confined in all three spatial directions. Their eigenstates can be tailored by the use of appropriate materials, the size and the shape of the dot and also by applied electric and magnetic fields. When we dope the quantum dot with atoms possessing a large magnetic moment, like manganese, they interact with the electrons or holes via pd exchange interaction. In III-V semiconductors such as $GaAs$ or $InAs$ the Mn atom is an acceptor. So, holes will be the main charge carriers. The interaction of holes with the magnetic manganese impurities is stronger than the interaction of electrons from the conduction band. We calculate numerically the eigenstates of several holes in a quantum dot using $\mathbf{k} \cdot \mathbf{p}$ theory, under the influence of a magnetic field fully taking into account their Coulomb interaction. The direct interaction between several manganese atoms is very short ranged and, therefore, can be neglected for sufficiently separated magnetic impurities. An interaction, however, is mediated by the holes confined in the quantum dot. We examine the possibility to control the alignment of several manganese atoms in $GaAs$ and $InAs$ quantum dots by changing the hole eigenstates via a manipulation of the confining potentials and the magnetic field.

We show the high importance of the hole-band mixing to the Coulomb energy of up to three holes. It also significantly influences the dispersion of the hole in the magnetic field and the coupling between the spins of the hole and the manganese impurity. We show the influence of the acceptor potential in dependence of the strength of the different dot-potential configurations. In magnetic fields the properties of the hole- and manganese-spin compound coupled by the pd -interaction are dominated in $GaAs$ dots by the manganese spin whereas in $InAs$ the spin of the hole is dominant. Finally we demonstrate the control of the ferromagnetic Mn - Mn coupling by the number of the confined holes.

Inhaltsangabe

Quantenpunkte aus Halbleitern können Elektronen und Löcher in drei Dimensionen einschließen. Die von den Teilchen ausgebildeten Quantenzustände können durch die Wahl der Halbleiter, durch die Größe und die Form der Punkte sowie von äußeren elektromagnetischen Feldern beeinflusst werden. In die Quantenpunkte eingebrachte Fremdatome wie Mangan beeinflussen die gefangenen Elektronen und Löcher über die pd -Wechselwirkung. Mangan eingebracht in III-V Halbleiter wie $GaAs$ oder $InAs$ wird zu einem Akzeptor und bringt deshalb hauptsächlich Löcher in den Halbleiterkristall ein. Auch ist die Spin-Wechselwirkung der Löcher mit dem Mangan stärker als die der Leitungsband-Elektronen. Wir berechnen numerisch die Eigenzustände einiger Löcher in einem Quantenpunkt mit Hilfe der $\mathbf{k} \cdot \mathbf{p}$ -Theorie. Dabei betrachten wir den Einfluss des magnetischen Feldes sowie der Coulomb-Abstoßung zwischen den Löchern. Die direkte Wechselwirkung zwischen mehreren Mangan-Atomen hat eine kurze Reichweite und kann deshalb für genügend von einander getrennte Atomen vernachlässigt werden. Eine gegenseitige Beeinflussung kann dennoch mittels der im Quantenpunkt eingeschlossenen Löcher induziert werden. Wir untersuchen die Möglichkeit diese wechselseitige Beeinflussung durch Veränderung der Eigenzustände der Löcher zu kontrollieren. Dies wird wiederum durch Variation der Quantenpunkt-Potentiale und des magnetischen Feldes erreicht.

Wir zeigen die besondere Bedeutung auf, die dem Mischen der Bloch-Bänder des Loches für die Coulomb-Energie von bis zu drei Löchern zukommt. Dieses Mischen beeinflusst sowohl die Dispersion der Löcher im Magnetfeld als auch die Wechselwirkung mit den Spins der Mangan Atome. Wir zeigen den Einfluss des Akzeptor-Potentials in Abhängigkeit von verschiedenen Konfigurationen des Quantenpunktpotentials. Unter der Wirkung des Magnetfeldes wird der Spin-Verbund des Lochs und des Mangan in $GaAs$ -Quantenpunkten dominiert von der Zeeman-Energie des Mangan. In Quantenpunkten aus $InAs$ dominiert die Zeeman Energie des Lochs. Schließlich zeigen wir die Kontrolle der ferromagnetischen Kopplung zwischen den Mangan-Atomen durch die Anzahl der eingefangenen Löcher.

Contents

1	Introduction	7
2	Theoretical Basis	10
2.1	$\mathbf{k} \cdot \mathbf{p}$ -theory	10
2.1.1	Effective Mass	10
2.2	Envelope Function Approximation	14
2.2.1	Hole Density in the Quantum Dots	15
2.3	Exact Diagonalisation	16
2.4	Numerical Routines	17
2.5	Quantum Dot Model	17
2.6	Basis Functions	19
2.6.1	Motion in xy plane	20
2.6.2	Algebra for the Fock-Darwin States	21
2.6.3	Elliptic Quantum Dots	24
2.6.4	Motion in z direction	25
2.6.5	Basis States for One Hole	26
2.7	Energy dependence on the magnetic field	27
2.8	Many-Body Interaction	27
2.9	Manganese Impurity	29
2.10	Time Inversion Symmetry	31
3	Quantum Dot With Holes	33
3.1	Single-Particle States	33
3.1.1	GaAs Quantum Dots	34
3.1.2	Band Coupling Effects	37
3.1.3	InAs Quantum Dots	40
3.1.4	Elliptical Quantum Dots	41
3.2	Many-Particle States	42
3.2.1	Two Holes	43
3.2.2	Three Holes	46

3.2.3	Variation of Confining Potentials	48
3.3	Quantum Dot with One Mn Impurity	49
3.3.1	Strength of the Used Potentials	51
3.3.2	<i>GaAs</i> Quantum Dots	52
3.3.3	Influence of the Lateral Confinement	58
3.3.4	<i>InAs</i> Quantum Dots	60
3.3.5	Off-Axis Mn Atoms	62
3.3.6	<i>GaAs</i> Dots, Mn Off-Axis	64
3.3.7	<i>InAs</i> Dots, Mn Off-Axis	71
3.3.8	Elliptic Dots with Mn	72
3.4	2 Mn 1 Hole	73
3.4.1	<i>GaAs</i> Dots	73
3.4.2	<i>InAs</i> Dots	80
3.5	2 Holes with Manganese	81
3.5.1	2 Holes, 1 Manganese	82
3.5.2	2 Holes, 2 Manganese	86
3.6	Precision of the calculations	87
4	Conclusions and Outlook	90
5	Appendix	92
5.1	Polarisation	92
5.2	Coefficients for relative coordinates	93
6	Bibliography	94
7	Publications	100

Chapter 1

Introduction

Semiconductor quantum dots are regions in a semiconductor crystal, where charge carriers are confined in all three spatial directions. Confined in a small volume the charge carriers show quantum mechanical behavior. The development in the fabrication techniques of semiconductor structures by “molecular beam epitaxy” (MBE) and “metal-organic chemical vapor deposition” (MOCVD) allows a high degree of control over the confinement. This makes it possible to engineer the form of the wave function of the confined carriers. This possibility has triggered a large interest in the research field of quasi zero-dimensional semiconductor nanostructures. Manifold experimental techniques were developed to map the electronic states in the quantum dots. In “cyclotron resonance” (CR) experiments confined particles are excited directly between the dot states [1], [2]. Optically created electron-hole pairs (excitons) are attracted by the dot potentials and recombine inside the dot enlightening its inner structure [3]. Also the charging [4] and electron transport through the dot [5], [6] reveals its characteristics.

Another fascinating development in the field of semiconductors was the occurrence of “diluted magnetic semiconductors” (DMS). After mastering the electrical properties of these materials the question arose if such a high degree of control is also possible on their magnetic behavior. In DMS magnetic impurities are coupled to a ferromagnetic regime by itinerant charge carriers of the semiconductor crystal [7], [8]. Obviously, control on the magnetic impurities can be gained by engineering the hole wave function in the quantum dot. This technique lets us influence the magnetic properties as well as the quantum mechanical states of single spins [9].

Beside the scientific interest many applications are envisaged. Maybe the most exciting one is “spintronic”, the aim to use the spin degree of freedom of the charge carrier and the impurity in computation and data storage. There are proposals for quantum-bit gates made from quantum dots [10], [11]. They are promising systems for the realization of a solid state quantum computer [12] because of the high degree of control on the spin states already possible in these systems [13], [14], [15]. To realize such devices still more knowledge is necessary about the behavior of the confined charge carriers and their interaction with impurities. Especially the characteristics of charge carriers from the valence band of the used semiconductors is complicated and often

broadly approximated. The aim of this work is to provide more insight into the eigenstates of such confined holes in large quantum dots. Their mutual Coulomb interaction as well as the interaction with magnetic impurities will be covered. We use numerical calculations to investigate the influence of dot-potential symmetry and strength, band-coupling effects, acceptor-potential position and spin interactions on the quantum mechanical eigenstates of the hole-impurity system. The eigenstates of the holes are calculated by means of a 4-band $\mathbf{k} \cdot \mathbf{p}$ theory and the envelope function approximation. The pd exchange interaction of the hole spin with the spin of the magnetic impurity is modeled by an effective Heisenberg Hamiltonian.

The need for a good insight in the eigenstates of holes in quantum dots can be motivated in many ways: Manganese has a large magnetic moment of $S = 5/2$ and is commonly used in diluted magnetic semiconductors. On the other hand *GaAs* and *InAs* belong to the best understood and technologically best controlled quantum dot materials. Now, manganese acts mostly as an acceptor in these III-V semiconductors and holes will be the main charge carriers. Secondly, the now most widely used investigation method on quantum dots is the photoluminescence spectroscopy of excitons confined in the dots. To interpret the measured spectra a good knowledge of the hole part of the total wave function is necessary. In the past the hole wave function was considered only in a very simplified form. The effects of band coupling and dot anisotropy are commonly neglected. Thirdly, the hole-spin degree of freedom is coupled to the orbital movement of the holes. It then becomes possible to modify the hole-spin/manganese-spin interaction by changing the dot confinement and thus the orbital movement of the holes. Another characteristic of confined holes is the possibility to access the effects of mutual many-particle interaction with cyclotron resonance investigations. Due to the band coupling in the Kohn-Luttinger Hamiltonian the theorem of Kohn [16] is validated. Thus, the center of mass movement does not decouple from the relative movement of the holes. Only the former is affected by the long-wave electromagnetic field in this setup [17].

During the investigation for a suitable system to realize a quantum bit [18] the question on the spin coherence time of particles confined in quantum dots arose. It turns out that the main mechanism for the loss of the coherence is the interaction with the spin of the nuclei of the host crystal [19], [20]. For holes this interaction is much smaller since the valence bands develop from atomic p orbitals with vanishing density at the position of the lattice atoms [21]. Additionally a large degree of control over the hole spin was shown [22].

Confinement of charge carriers can be achieved by different means. The now most widely used quantum dot fabrication technique is the Stranski-Krastanow growth [23], [24]. The obtained quantum dots have a rather strong confinement with dot-level separations from several tens to hundreds of meV [3]. Here, the inner electronic structure of the dots is rather simple and due to the strong confinement in the growth direction the band-coupling effects are small. We will therefore concentrate on larger dots which can be fabricated with lithographic and etching techniques [25]. Dots fabricated in this way are often etched from two dimensional electron- or hole-gas samples. They also can be defined by top metal gates. We will concentrate on dots

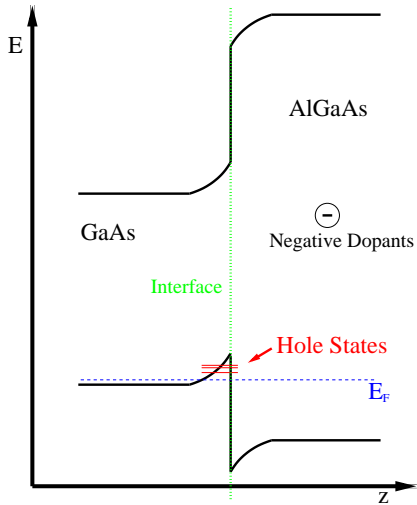


Figure 1.1: Schematic band regime at the interface of *GaAs/GaAlAs* under the influence of negative dopants in *GaAlAs*.

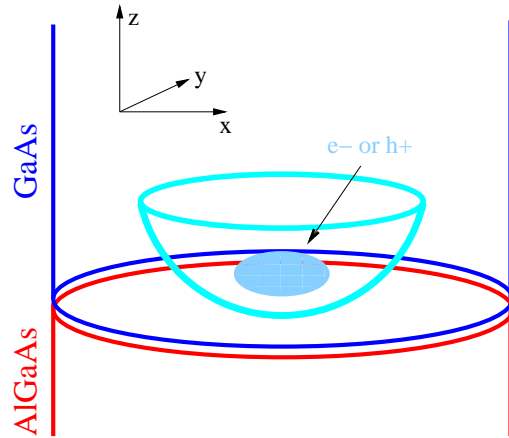


Figure 1.2: Schematic diagram of an etched pillar of *GaAs/GaAlAs* with a quantum dot formed at the interface.

formed at a single hetero-interface by modulation doping. Figure 1.1 shows the band regime in the vicinity of the interface. In this configuration due to the triangular potential the overlap of light- and heavy-hole wave functions in z direction is larger than in quantum well structures. This enhances the band-coupling effects. The confinement in the interaction plane occurs through charges on the outside of an etched pillar. It is modeled by an effective harmonic potential. Figure 1.2 shows an schematic example.

Finally we will show how the interaction between two magnetic impurities in a quantum dot arises due to the mediation of confined holes. We will stress the changes to this interaction due to the change of the dot potentials and number of confined charge carriers (holes).

To our knowledge there have been no experiments on the hole levels in the quantum dots we want to deal with until now (November 2009). The experiments investigating excitons are carried out in self-assembled quantum dots and deal mostly only with the ground state of the system. Due to this lack of experimental data we will not give any spectra of light absorption or photoluminescence which could be directly compared to the experiments. They can, nevertheless, be readily calculated from the obtained eigenstates. We will concentrate on the description of the eigenstates' character and the transitions triggered by the change of our free parameters. We hope, this will enable the reader to gain a better understanding in the processes going on in the system.

Chapter 2

Theoretical Basis

2.1 $\mathbf{k} \cdot \mathbf{p}$ -theory

The effects caused by electrons in semiconductor crystals originate often only from several electrons occupying the conduction band. Also the absence of several electrons forming holes in the valence band can fully determinate the electrical behaviour of such crystals. In equilibrium the electrons stay at the minimum of the conduction band and the holes at the maximum of the valence band. The strength of most of the electric and magnetic fields we apply to the specimen of such crystals do not move the crystal momentum \mathbf{k} of these particles far away from the extrema of the bands. This gives us the possibility to approximate the dispersion relation $E(\mathbf{k})$ of such particles by expanding it around the extreme points. The $\mathbf{k} \cdot \mathbf{p}$ -theory, I want to use to describe the hole states inside a quantum dot, is such a approximative scheme. It treats the influence of the crystal lattice on an electron or hole as a perturbation. In this description the influence of the crystal potential is transferred to an effective mass of the particle. This mass is different from the vacuum mass. It can also become anisotropic due to an anisotropic crystal symmetry. I will give only fundamental equations from which the Hamiltonian of my system follows. Derivation of this theory can be found e.g. in [26], [27], [28].

2.1.1 Effective Mass

Let us assume that the extreme point of a band under consideration lies at $\mathbf{k} = 0$, the Γ point of the crystal. This is often the case as for the interesting crystals of *GaAs* and *InAs*. For a perfect, bulk crystal the Hamiltonian and its eigenstates will be

$$H\Psi_{\mathbf{k}n} = E_n(\mathbf{k})\Psi_{\mathbf{k}n} \quad (2.1)$$

$$H = \frac{\mathbf{p}^2}{2m_e} + V(\mathbf{r}) \quad \Psi_{\mathbf{k}n}(\mathbf{r}) = e^{i\mathbf{k}\mathbf{r}}u_{\mathbf{k}n}(\mathbf{r}). \quad (2.2)$$

Here, m_e is the free electron mass, $V(\mathbf{r})$ the potential of the lattice atoms and $u_{\mathbf{k}n}(\mathbf{r})$ is the Bloch function for the n th band at \mathbf{k} . In order to take advantage of the known symmetry of the crystal, it is convenient to describe all the eigenstates $\Psi_{\mathbf{k}n}(\mathbf{r})$ in terms of a special set of functions

$$\chi_{\mathbf{k}n} = e^{i\mathbf{k}\mathbf{r}} u_{0n}(\mathbf{r}) \quad \Psi_{\mathbf{k}n}(\mathbf{r}) = \sum_n \int d\mathbf{k} a_n(\mathbf{k}) e^{i\mathbf{k}\mathbf{r}} u_{0n}(\mathbf{r}). \quad (2.3)$$

The functions $u_{0n}(\mathbf{r})$ are the Bloch functions for band n and $\mathbf{k} = 0$. Taking all n bands into account, we get a complete and orthogonal set of functions. Their advantage lies in their symmetry, which follows the symmetry of the crystal lattice. Thus their matrix elements with some basic operators can be determined just by symmetry considerations. By inserting (2.3) in (2.1), multiplying from left with $\exp(-i\mathbf{k}\mathbf{r})u_{0n}$ and integrating over the whole crystal we get

$$\sum_{n'} \int d\mathbf{k}' \langle \mathbf{k}n | H | \mathbf{k}'n' \rangle a_{n'}(\mathbf{k}') = E_n(\mathbf{k}) a_n(\mathbf{k}) \quad (2.4)$$

where the matrix elements $\langle \mathbf{k}n | H | \mathbf{k}'n' \rangle$ are

$$\begin{aligned} \langle \mathbf{k}n | H | \mathbf{k}'n' \rangle &= \int d\mathbf{r} e^{-i\mathbf{k}\mathbf{r}} u_{0n}^* \left(\frac{\mathbf{p}^2}{2m_e} + V(\mathbf{r}) \right) e^{i\mathbf{k}'\mathbf{r}} u_{0n'} \\ &= \int d\mathbf{r} e^{i(\mathbf{k}'-\mathbf{k})\mathbf{r}} u_{0n}^* \left(E_n(0) + \frac{\mathbf{k}' \cdot \mathbf{p}}{m} + \frac{k'^2}{2m_e} \right) u_{0n'} \\ &= \delta(\mathbf{k} - \mathbf{k}') \left[\left(E_n(0) + \frac{k^2}{2m_e} \right) \delta_{nn'} + \frac{1}{m_e} \sum_{\alpha} k_{\alpha} P_{nn'}^{\alpha} \right] \end{aligned} \quad (2.5)$$

The Bloch functions u_{0n} are eigenfunctions to the periodic crystal potential $V(\mathbf{r})$ and fulfil $(\mathbf{p}^2/2m_e + V(\mathbf{r}))u_{0n} = E_n(0)u_{0n}$.

$$P_{nn'}^{\alpha} = \frac{(2\pi)^3}{V_{u.c.}} \int_{u.c.} d\mathbf{r} u_{0n}^* (-i\partial_{\alpha}) u_{0n'} \quad (2.6)$$

is a momentum matrix element. The integration goes over one unit cell of the crystal. The term $\mathbf{k} \cdot \mathbf{p}$ in (2.5) gives the name to this theory. The electrons in the valence band, which we are interested in, experience a strong spin orbit coupling¹. This is because the valence bands develop from p like atomic orbitals with angular momentum $l = 1$. Conduction bands, however, are formed from s like orbitals without orbital angular momentum. We can incorporate the effect of spin-orbit coupling into our description without changing it much. We change the basis Bloch functions u_{0n} to some linear combinations of them belonging to the same band \tilde{u}_{0n} , which are also eigenstates to the spin-orbit coupling operator [26]

$$\left(\frac{\mathbf{p}^2}{2m_e} + V(\mathbf{r}) + \frac{\hbar}{4m_e^2 c^2} \sigma [\nabla V(\mathbf{r}) \times \mathbf{p}] \right) \tilde{u}_{0n} = \tilde{E}_n(0) \tilde{u}_{0n}. \quad (2.7)$$

¹Note that the only kind of spin-orbit coupling we are dealing with here, is the one caused by the strong Coulomb potential of the lattice atoms. Spin-orbit coupling effects caused by additional potentials, e.g. dot or acceptor potentials, are neglected. Their influence is very small [29].

Notice, that in the last line of (2.5) the Bloch function enter only via the momentum matrix-elements $P_{nn'}^\alpha$. We just have to change this matrix elements to

$$\tilde{P}_{nn'}^\alpha = \frac{(2\pi)^3}{V_{u.c.}} \int_{u.c.} d\mathbf{r} \tilde{u}_{0n}^* (-i\partial_\alpha + \frac{\hbar}{4m_e^2 c^2} [\boldsymbol{\sigma} \times \nabla V]_\alpha) \tilde{u}_{0n'}. \quad (2.8)$$

In the following, I will drop the tilde sign but we have to remember, that we are now dealing with the basis \tilde{u}_{0n} .

Now, to proceed further, we have to make some approximations. Since, as described above, the crystal momenta \mathbf{k} , we will usually encounter, are small, we can get rid of the $\mathbf{k}' \cdot \mathbf{p}$ term in (2.5) by treating it as a perturbation. In the valence band the three p states with orbital angular momentum $l = 1$ are coupled to the two hole spin states $s = 1/2$. From the six resulting states two blocks are created, one with total angular momentum $\mathbf{J} = \mathbf{L} + \mathbf{s}$ of $|\mathbf{J}| = 3/2$ and one of $|\mathbf{J}| = 1/2$. The four topmost valence bands in *GaAs* and *InAs* consist of the $|\mathbf{J}| = 3/2$ sates according to the four possible z components of $|\mathbf{J}| = 3/2$. In the bulk crystal at $\mathbf{k} = 0$ the band is fourfold degenerate. The split-off band with $|\mathbf{J}| = 1/2$ lies about 340 meV lower in *GaAs* and 380 meV in *InAs* [30]. The large energetic distance of this split-off band as well as the large distance to the conduction band makes it possible to treat the coupling to these bands via the $\mathbf{k}' \cdot \mathbf{p}$ term as a perturbation. The coupling between the topmost degenerate bands, however, we have to treat explicitly. We can only expect, that the influence of bands separated by some energy ΔE from our degenerate set can be treated in a perturbative manor. The separation ΔE has to be much larger than a typical kinetic energy of an electron $E(0) - E(\mathbf{k})$. We expand the term in \mathbf{k} . The terms of the perturbative expansion linear in \mathbf{k} are very small [26] so we can drop them. Then, up to second order in \mathbf{k} the coefficients in the expansion 2.3 fulfil

$$\left(E_n(0) + \frac{k^2}{2m_e} + \frac{k_\alpha k_\beta}{m_e^2} \sum_{n' \neq n} \frac{P_{nn'}^\alpha P_{n'n}^\beta}{E_n - E_{n'}} \right) b_n(\mathbf{k}) = E_n(\mathbf{k}) b_n(\mathbf{k}). \quad (2.9)$$

The index n counts the four top valence bands, $j = 3/2, j_z = \pm 3/2, \pm 1/2$. The index n' counts all the remote bands, whose influence is taken into account only through the momentum matrix-elements $P_{nn'}^\alpha$. In the formula above α runs through x, y, z and we use Einstein's summation convention. The coefficients $b_n(\mathbf{k})$ represent our approximative solution to (2.1) with spin orbit coupling. When we set the zero energy at $E_n(0) = 0$, we can define

$$\frac{1}{\mu_n^{\alpha\beta}} = \frac{1}{m_e} \delta_{\alpha\beta} + \frac{2}{m_e^2} \sum_{n' \neq n} \frac{P_{nn'}^\alpha P_{n'n}^\beta}{E_n - E_{n'}} \quad (2.10)$$

as the inverse effective mass tensor.

If we look at a single energetically isolated and isotropic (no dependence on α, β) band, e.g. the

conduction band of III-V semiconductors, the tensor becomes a scalar $\mu_n^{\alpha\beta} = m^*$. The dispersion relation for an electron in such a band then reads

$$E_c(\mathbf{k}) = \frac{\hbar^2 k^2}{2m^*} \quad (2.11)$$

i.e. it is the one of a free particle with some effective mass m^* .

For the topmost four valence bands the kinetic energy takes the form of a four by four matrix. It is called the Kohn-Luttinger Hamiltonian [26],[31]

$$H_{KL} = \begin{pmatrix} P + Q & S & R & 0 \\ S^\dagger & P - Q & 0 & R \\ R^\dagger & 0 & P - Q & -S \\ 0 & R^\dagger & -S^\dagger & P + Q \end{pmatrix} \quad (2.12)$$

with

$$P = \frac{\gamma_1}{2m_e} (k_x^2 + k_y^2 + k_z^2) \quad (2.13)$$

$$Q = \frac{\gamma_2}{2m_e} (k_x^2 + k_y^2) - \frac{2\gamma_2}{2m_e} k_z^2 \quad (2.14)$$

$$R = -\frac{\sqrt{3}}{2} \left(\frac{\gamma_2 + \gamma_3}{2m_e} (k_x - ik_y)^2 - \frac{\gamma_2 - \gamma_3}{2m_e} (k_x + ik_y)^2 \right) \quad (2.15)$$

$$S = -\frac{\gamma_3}{2m_e} \left(-2\sqrt{3} \right) (k_x - ik_y) k_z. \quad (2.16)$$

The order of the basis functions is $j_z = (3/2, 1/2, -1/2, -3/2)$. The γ 's are called the Kohn-Luttinger parameters. They correspond to the summations in (2.10) but are usually determined experimentally [32]. The experimental results correspond, of course, to the spin-orbit coupled momentum matrix elements $\tilde{P}_{nn'}^\alpha$. The presence of the term $(k_x + ik_y)^2$ in the operator R of (2.12) reduces the symmetry of the whole Kohn-Luttinger matrix from spherical to cubic. In order to simplify the calculations and not have to choose a specific direction inside the crystal we want to drop it. The pre-factor of this term has a value proportional to $\gamma_2 - \gamma_3$. For *GaAs* these parameters are $\gamma_2 = 2.1$ and $\gamma_3 = 2.9$. So their difference is small against e.g. their sum and the other Luttinger parameter. In comparison to the other terms in (2.12) this term will be small. Neglecting the cubic part of the Kohn-Luttinger matrix is called the spherical approximation. With this assumption we do not take account of the band warping, i.e. the anisotropy of the holes dispersion. This effect becomes significant only at higher values of \mathbf{k} where the $\mathbf{k} \cdot \mathbf{p}$ theory becomes less reliable anyway. Calculations on the reliability of the spherical approximation can be found e.g. in [33].

There is some ambiguity concerning the representation of this matrix. Luttinger uses the four

dimensional representation of the angular momentum operator to set up this matrix. The matrix here is the one following from the representation for the angular momentum operator from [34],p.144. With this representation all the matrix elements become real valued. This is favourable for numerical calculations. This representations differs slightly from the one used by [31].

2.2 Envelope Function Approximation

In the previous section we found a description for the dispersion relation of a hole in the valence band of a bulk III-V semiconductor crystal. When additional potentials, i.e. electric and magnetic fields, are present inside such a crystal the periodicity of the crystal is destroyed and we can no longer use this description. However, we want to restrict the magnitude of such disturbances to be small in comparison with potentials exerted by the atoms of the crystal on the electrons in the bands. We can then expect that over some unit cells of the crystal such an additional potential will not change significantly and the periodicity will be preserved at this length scale. The eigenstate of an electron in such a crystal will therefore vary only over long distances compared to e.g. the lattice constant. One can expect that over long distances we can find the electron more often at positions with low potential and rarer where the potential is high. We assume that for the partially conserved periodicity the eigenstate of the electron will resemble some combination of Bloch states. Now due to the additional potentials the Bloch state will gain a slowly varying space dependant modulation in amplitude [35]. This can be written as

$$\psi(\mathbf{r}) = \sum_n F_n(\mathbf{r})u_{n0}. \quad (2.17)$$

The modulating function $F_n(\mathbf{r})$ is called the envelope function. Since the Bloch functions u_{n0} at the Γ point are known, we just have to find the right envelope functions. The form of F_n will depend on the symmetry of the additional potential.

The electron in the bulk crystal could be described by a free particle with some effective mass. Now we have to solve a problem of a particle with an effective mass and subjected to an additional potential $U(\mathbf{r})$. For a free particle the solutions to the Schrödinger equation are plane waves. They are eigenfunctions to the translation operator. In a bulk crystal all the possible translations yield all the possible eigenstates of the electron [36], [37].

$$e^{i\mathbf{k}\mathbf{r}}u_{n\mathbf{k}}(\mathbf{r}) \quad (2.18)$$

where the values of \mathbf{k} are restricted by boundary conditions. Now, one can envision the plane waves also as envelope functions for the case of translational symmetry, the symmetry of the underlying crystal lattice. In this picture the crystal momentum \mathbf{k} is just some quantum number counting the eigenfunctions. For an additional potential the envelope function will in general not be a plane wave. We expand it in some set of functions F_n^i , where n counts the expansion in the

Bloch states while the multi-index i stands for the expansion of the envelope function. Eq. (2.3) then becomes

$$\Psi(\mathbf{r}) = \sum_n \sum_i c_n^i F_n^i(\mathbf{r}) u_{n0}(\mathbf{r}). \quad (2.19)$$

The summation over i replaces the integration over \mathbf{k} . In the calculation of the matrix elements (2.5) all the k 's result from derivation of the envelope function $\exp(-i\mathbf{k}\mathbf{r})$. Since now we do not know the explicit form of the envelope function $F_n^i(\mathbf{r})$ we can not perform this operation yet. We can pursue our investigation as in the bulk case. We have only to replace all the \mathbf{k} 's by the momentum operator \mathbf{p} which acts only on the envelope function. By choosing a complete and orthogonal set of functions for the F_n^i and calculating the matrix elements $\langle n'i' | \mathcal{O}(\mathbf{p}) | ni \rangle$ we come to a representation for H_{KL} and to a matrix equation for the coefficient vector $\mathbf{c} = (\dots c_n^i \dots)^T$. We assume, that the additional potential $U(\mathbf{r})$ varies so slowly that it can be taken as constant over one unit cell. Then it will be diagonal in the band index n : $\langle n'i' | U(\mathbf{r}) | ni \rangle = \delta_{n'n} I(i'i)$. We then have to solve

$$(H_{KL} + \mathbb{1}U(\mathbf{r}))\psi(\mathbf{r}) = E\psi(\mathbf{r}) \quad (2.20)$$

where $\mathbb{1}$ is the unit matrix.

2.2.1 Hole Density in the Quantum Dots

It is instructive to look at the probability density of the holes inside the dot. But it is necessary to discuss the meaning of this term. The probability to find a hole at \vec{r} can be obtained by calculating the expectation value of a delta function $\langle \Psi | \delta(\vec{r}) | \Psi \rangle$. Using 2.17 we obtain

$$\langle \delta(\vec{r}) \rangle = \sum_{nm} \sum_{ij} c_n^{i*} c_m^j \int_{crystal} d\mathbf{r} F_n^{i*} u_n^* \delta(\vec{r}) F_m^j u_m. \quad (2.21)$$

Now, in the envelope function approximation, we can not account for structures of the dimension of one lattice cell. Since we have assumed that the envelope function is almost constant on the length scale of one lattice cell we can tread such a cell just as one point. We take the density of the hole as constant in one cell. We can express this by changing the δ function in 2.21 in a function $\tilde{\delta}(\vec{r})$ which is constant and equal 1 inside the cell under consideration and zero outside.

We get

$$\begin{aligned}
 \langle \Psi | \delta(\vec{r}) | \Psi \rangle &= \sum_{nm} \sum_{ij} c_n^{i*} c_m^j \int_{cr} d\mathbf{r} F_n^{i*} \tilde{\delta}(\vec{r}) F_m^j \int_{UC} d\mathbf{r} u_n^* u_m \\
 &= \sum_n \sum_{ij} c_n^{i*} c_n^j \int_{cr} d\mathbf{r} F_n^{i*} \tilde{\delta}(\vec{r}) F_n^j \\
 &\approx \sum_n \sum_{ij} c_n^{i*} c_n^j \int_{cr} d\mathbf{r} F_n^{i*} \delta(\vec{r}) F_n^j \\
 &= \sum_n \sum_{ij} c_n^{i*} c_n^j F_n^{i*}(\vec{r}) F_n^j(\vec{r}).
 \end{aligned} \tag{2.22}$$

In this picture the density of the hole is just the sum of the envelope function densities for each of the four bands.

2.3 Exact Diagonalisation

To find the eigenvalues and eigenstates of my system I used the Exact Diagonalisation calculation scheme. All the equations we want to solve are too difficult to be analytically treated in this form. When we represent our Hamiltonian in a complete set of orthogonal basis functions, it becomes a matrix of numbers. We can treat this matrix using a computer. If we are interested in finding the eigenvalues and eigenvectors of a system we have to diagonalise the matrix representing our Hamiltonian. Let this matrix be \mathbf{M} . Then an eigenvalue equation will be

$$\mathbf{M}\mathbf{v} = \lambda\mathbf{v} \tag{2.23}$$

with some eigenvalue λ and corresponding eigenvector \mathbf{v} . We can now transform this equation to an other equation, which yields the same eigenvalues. We do so by using an unitary matrix \mathbf{S} with $\mathbf{S}\mathbf{S}^+ = \mathbf{1}$. We get

$$\mathbf{S}\mathbf{M}\mathbf{S}^+\mathbf{S}\mathbf{v} = \lambda\mathbf{S}\mathbf{v} \quad \rightarrow \quad \mathbf{D}\mathbf{v}' = \lambda\mathbf{v}' \tag{2.24}$$

$$\mathbf{D} = \mathbf{S}\mathbf{M}\mathbf{S}^+, \quad \mathbf{v}' = \mathbf{S}\mathbf{v}. \tag{2.25}$$

We can find \mathbf{S} such, that \mathbf{D} is diagonal and contains all possible λ 's. The \mathbf{v}' are then Cartesian vectors. It follows, that the rows of the transformation matrix \mathbf{S}^+ contain the eigenvectors \mathbf{v}_i of the original problem to the eigenvalue λ_i .

$$\mathbf{S}^+\mathbf{v}'_i = \mathbf{S}^+\mathbf{S}\mathbf{v}_i = \mathbf{v}_i = \mathbf{S}^+(\dots 1_i \dots)^T. \tag{2.26}$$

In this manner it is possible, to solve every problem exactly. Therefore the name of this procedure: Exact Diagonalisation. In practice the applicability of this strategy is often limited. The

sets of functions in which we expand the Hamiltonian are always of infinite dimension yielding matrices of infinite size, which in the most cases can not be solved whether analytically nor numerically. The approximation we have to apply to our calculations is to cap the size of the basis. When we choose a set of basis functions for our expansion with a similar symmetry as our problem, we can expect that already a small number of basis functions will describe our eigenstates very exactly. The missing of higher functions of our complete set will not alter the resulting eigenstate very much. Since we are mostly interested in the eigenvalues and eigenstates with the lowest energy, we just take those basis functions in our expansion, which are expected to give a good approximation to the energetically lowest eigenvectors. There is no rigorous method to choose. One has to use some intuition and maybe vary the basis to be sure not to miss an important basis function. Our strategy is to find a basis, which resembles the symmetry of our system as good as possible. Then we have to calculate the matrix representation of the Hamilton operator describing our problem and diagonalise this matrix using numerical routines on a computer.

2.4 Numerical Routines

Many different problems can be formulated in such a way, that the solution involves the diagonalisation of a matrix. So there are already a lot of numerical routines available, which perform this aim. One has only to deliver to this procedure the correct matrix describing the problem. The routines themselves are taken from numerical algebra packages like LAPACK and ARPACK. These routines are proven for reliability and optimised to deliver the best performance. LAPACK, the Linear Algebra PACKage, offers routines to manipulate matrices and to calculate normal and generalised eigenvalue problems. The performance of the routine strongly declines, when the matrices become larger. For problems containing several electrons or holes the matrices can become so large, that an other routine has to be used. Matrices describing many-body problems are large but often only very sparse. In this case the ARnoldi PACKage offers to us very well performing routines.

2.5 Quantum Dot Model

The quantum dots in my calculations are represented by potentials, which restrict the movement of holes inside a semiconductor crystal. In my work I want to simulate the behaviour of up to three holes inside a quantum dot while regarding the mutual Coulomb repulsion of the holes, the influence of an acceptor potential of an impurity and a spin-spin interaction between the impurity and the holes. The influence of the mutual hole Coulomb interaction in relation to their orbital energies rises with the size of the dot. So we have to deal with dots with a diameter of at least several tens of nanometres. Such dots can be fabricated e.g. by lithographic methods from two

dimensional hole gas (2DHG) structures.

The kind of description I will use here is particularly useful for larger quantum dots. In small quantum dots the confinement of charge carriers is so strong, that a hole can be confined only in one or two orbital states. Therefore effects regarding the orbital movement of the holes inside the dot are blurred due to a lack of different eigenstates the hole can occupy. Such systems are typically described by much simpler Hamiltonians containing only the spin degree of freedom of the concerned particles.

I simulate a quantum dot formed at the interface of two semiconducting materials with different band gaps such as $Al_xGa_{1-x}As$ and $GaAs$. The band gap in pure $GaAs$ is much smaller than in $AlGaAs$. Holes at the top of the valence band in $GaAs$ cannot enter into the $Al_xGa_{1-x}As$ crystal due to this band offset. Between the valence bands in these two materials the offset depends on the fraction x of Al in the $GaAs$ host crystal and can vary between 100 meV and 400 meV [38]. Such 2D structures are typically fabricated by molecular beam epitaxy. In this process the semiconductor crystal is grown layer by layer of atoms. Let us call the direction of the growth the z direction. Then the band offset constrains the motion of the holes to the $GaAs$ part of the crystal. By a technique called modulation doping it is possible to introduce charged impurities into the $Al_xGa_{1-x}As$ at a precisely chosen point in the vicinity of the interface. To confine holes one has to choose an attractive, i.e. negative, Coulomb potential. It then lowers the energy of the holes near the interface and attracts them towards it. This potential and the band offset form two potential barriers perpendicular to the z direction and thus confine the holes to the interface. For calculational simplicity I assume the band offset in my calculations as infinite. This approximation is valid because we deal with much smaller typical confinement energies than the energetical band offset. In the quantum dot the confinement energy amounts to several tens of meV. Also taking a finite size of the interface potential into account leads only to a stronger mixing between the light and heavy hole bands. In our system this mixing will be large anyway. No additional features will occur or become blurred. In the $GaAs$ part of the crystal the potential of this additional ions is approximated by a linearly rising potential. This results in a triangular shape for the confining potential in z direction.

The assumption of infinite potential barriers at interfaces of different semiconductors has a larger impact in quantum well structures. This is because here this strong restriction is applied on both sides of the quantum well. The energies and band mixing in such structures depends very strongly on the penetration depth of the hole wave function into the barrier. This is especially true for small dots. In this potential configurations good approximations have to be found to obtain the correct eigenenergies. Due to a change of the effective mass of the hole behind the barrier in $AlGaAs$ and the unknown composition of the crystal at the interface this task can become difficult. For heterojunctions this problem is much less prominent due to an infinite potential on just one side of the structure. Also the assumption of a linearly rising potential on the other side is only valid in the vicinity of the interface. States with higher energy and thus larger extend in z direction will experience a much weaker potential. Both approximations will become worse

when the total energy of the hole system approaches 300 – 400 meV. In dots considered here this can happen especially for systems with more than three holes. In calculations on 2-dimensional electron and hole systems one has typically to deal with many charge carriers. They can screen the potential imposed by the ions behind the barrier. Therefore, the slope of the linear potential in such systems has to be calculated self-consistently. In my system, I will deal only with up to three holes. Their charge will not alter the dot potentials.

To get a 0 dimensional structure we still have to restrict the movement of the holes in the plane of the interface, the xy plane. This can be done by some electrodes on top of the crystal or by etching pillars out of the grown crystal perpendicular to the interface. In both cases the holes are confined in the xy plane due to a potential of charge carriers surrounding the confined holes. The additional charge is located inside the electrodes or at the surface of the pillars in dependence on the realisation of the quantum dots. In both cases this xy potential can be approximated to a very good degree by a 2-dimensional harmonic potential [39].

2.6 Basis Functions

To minimise the error by capping the size of our basis we have to find basis functions, which resemble the symmetry of the system under consideration as good as possible. Its symmetry is mainly determined by the potentials forming the dot, a harmonic potential in the xy plane and a triangular potential in z direction. We also want to apply a magnetic field along the z direction of our system (Faraday configuration). Such a field is represented by an additional vector potential. A good ansatz is the choice of eigenfunctions for the one-band problem with the considered potentials. In our case such a problem can be solved analytically. The basis functions we have to use are Airy functions for the z direction and Fock-Darwin states for the xy motion[40]. Unlike for electrons, this functions are not the eigenfunctions of the system. This is because we take now into account the four different valence bands simultaneously. The mixture of these bands and thus the effective masses of the holes depend on their momentum. For numerical calculations we have to choose a basis with a particular effective mass. This basis functions can not be eigenfunction to all states. To ease the implementation of the matrix in the program we choose basis functions that will be eigenfunctions to some of the operators in the diagonal of the Hamiltonian matrix. This diagonal operators have a large weight on the eigenstates so we can expect our truncated basis to give better results for the low-energy sector of the spectrum.

2.6.1 Motion in xy plane

Let us first start with the xy motion. The xy part of the diagonal element for the $j_z = 3/2$ band of the Kohn-Luttinger Hamiltonian together with the potential in xy plane reads

$$H_{xy}^{\frac{3}{2}} = \frac{\gamma_1 + \gamma_2}{2m_e} (\mathbf{p} - e\mathbf{A})^2 + \frac{K_0}{2} (x^2 + y^2). \quad (2.27)$$

$\mathbf{A} = B/2(-y, x, 0)$ is the vector potential in symmetric gauge, K_0 describes the strength of the harmonic potential, m_e is the mass of a free electron and γ_1, γ_2 are Luttinger parameters. It turns out to be more convenient not to choose eigenfunctions of the operator above as basis functions but functions, where the effective mass of the particle is just $\gamma_1/2m$. In this basis, all matrix elements concerning the xy motion can be calculated analytically. It is also convenient to describe the harmonic and vector potential in terms of frequencies. With our choice of the mass we get

$$\omega_0 = \sqrt{\frac{K_0\gamma_1}{m_e}} \quad \omega_c = \frac{eB\gamma_1}{m_e} \quad \omega_h = \sqrt{\omega_0^2 + \left(\frac{\omega_c}{2}\right)^2}. \quad (2.28)$$

Here, ω_0 describes the strength of the confining potential. ω_c is the cyclotron frequency and describes the confinement due to the magnetic field. ω_h is the hybrid frequency, which finally determines the energy and the spatial extent of the system. Eq. (2.27) becomes

$$H = \frac{\gamma_1}{2m_e} (p_x^2 + p_y^2) + \frac{m_e}{2\gamma_1} \omega_h^2 (x^2 + y^2) - \frac{\omega_c}{2} (xp_y - yp_x). \quad (2.29)$$

There are two convenient methods to find the eigenvalues and eigenvectors to this Hamiltonian. One can straight solve the differential equation or translate the problem into an algebraic one. The last method is most convenient, when we want to solve the problem of just one hole in a quantum dot. Now, the Coulomb repulsion between two holes or the acceptor potential of an impurity can not be solved with this algebraic method. We then have to resort to numerical calculations and are forced to know the spatial representation of the eigenvectors. In the following I will therefore give a short insight into both ways to solve (2.29).

The confining potential has rotational symmetry around the z axis so the eigenfunctions of H should also be eigenfunctions to the z component of the angular momentum $xp_y - yp_x = L_z$. It is therefore convenient to describe the operator in cylindric coordinates. Now (2.27) becomes

$$H = -\frac{\hbar\gamma_1}{2m_e} \left[\frac{1}{r} \frac{\partial}{\partial r} + \frac{\partial^2}{\partial r^2} - \frac{1}{r^2} \frac{\partial}{\partial \varphi^2} \right] + \frac{1}{2} \frac{\gamma_1}{m_e} \omega_h^2 r^2 + \frac{i\hbar\omega_c}{2} \frac{\partial}{\partial \varphi}. \quad (2.30)$$

When we introduce the characteristic length of the system l , we can come to a differential operator for a dimensionless quantity ξ

$$l = \sqrt{\frac{\hbar\gamma_1}{m_e\omega_h}} \quad \xi = \frac{r}{l}. \quad (2.31)$$

Then, (2.30) reads

$$H = -\frac{\hbar\omega_h}{2} \left[\frac{1}{\xi} \frac{\partial}{\partial \xi^2} + \frac{\partial^2}{\partial \xi^2} - \frac{1}{\xi^2} \frac{\partial^2}{\partial \varphi^2} - \xi^2 \right] + \frac{i\hbar\omega_c}{2} \frac{\partial}{\partial \varphi}. \quad (2.32)$$

Eigenfunctions of this operator have the form

$$\langle \mathbf{r} | nm \rangle = \frac{1}{l} \phi_m(\varphi) \rho_{nm}(r/l) \quad (2.33)$$

$$\phi_m(\varphi) = \frac{1}{\sqrt{2\pi}} e^{im\varphi} \quad \rho_{nm}(\xi) = \sqrt{\frac{2n!}{(n+|m|)!}} \xi^{|m|} e^{-\xi^2/2} L_n^{|m|}(\xi^2). \quad (2.34)$$

Here L_n^m are Laguerre polynomials[41]. $\langle \mathbf{r} | nm \rangle$ are the Fock-Darwin states [40],[42]. Finally the energy eigenvalues of such an operator with the eigenfunctions above are

$$E_{nm} = \hbar\omega_h(2n + |m| + 1) + \frac{\hbar\omega_c}{2}m. \quad (2.35)$$

Since (2.34) are not quite the eigenstates of our problem, (2.35) is not quite the energy eigenvalue. For the algebraic calculation of matrix elements it is instructive, however, to take a closer look at these functions.

2.6.2 Algebra for the Fock-Darwin States

Similar to the case of a 1-dimensional harmonic oscillator we can solve the problem of the two-dimensional harmonic oscillator in a magnetic field using an algebraic method. Let us therefore define the following operators [42], [43]:

$$\hat{a}_x^+ = \frac{1}{\sqrt{2}} \left(\frac{1}{l}x - \frac{il}{\hbar}p_x \right) \quad \hat{a}_x = \frac{1}{\sqrt{2}} \left(\frac{1}{l}x + \frac{il}{\hbar}p_x \right) \quad (2.36)$$

$$\hat{a}_y^+ = \frac{1}{\sqrt{2}} \left(\frac{1}{l}y - \frac{il}{\hbar}p_y \right) \quad \hat{a}_y = \frac{1}{\sqrt{2}} \left(\frac{1}{l}y + \frac{il}{\hbar}p_y \right) \quad (2.37)$$

and

$$\hat{a}_+^+ = \frac{1}{\sqrt{2}}(\hat{a}_x^+ + i\hat{a}_y^+) \quad \hat{a}_+ = \frac{1}{\sqrt{2}}(\hat{a}_x - i\hat{a}_y) \quad (2.38)$$

$$\hat{a}_-^+ = \frac{1}{\sqrt{2}}(\hat{a}_x^+ - i\hat{a}_y^+) \quad \hat{a}_- = \frac{1}{\sqrt{2}}(\hat{a}_x + i\hat{a}_y). \quad (2.39)$$

Because of the commutator $[x_i, p_i] = i\hbar$ one can show

$$[\hat{a}_+, \hat{a}_+^+] = [\hat{a}_-, \hat{a}_-^+] = \mathbf{1} \quad (2.40)$$

while all other commutators vanish. We can further define the operators

$$\hat{n}_+ = \hat{a}_+^\dagger \hat{a}_+ \quad \hat{n}_- = \hat{a}_-^\dagger \hat{a}_-. \quad (2.41)$$

They commute, so there is a set of states, which are eigenstates to both of them.

$$\hat{n}_+ |n_+, n_- \rangle = n_+ |n_+, n_- \rangle \quad \hat{n}_- |n_+, n_- \rangle = n_- |n_+, n_- \rangle \quad (2.42)$$

Similar to the rising and lowering operators for e.g. the angular momentum [42] one can show the following relations:

$$\hat{a}_+^\dagger |n_+, n_- \rangle = \sqrt{n_+ + 1} |n_+ + 1, n_- \rangle \quad \hat{a}_+ |n_+, n_- \rangle = \sqrt{n_+} |n_+ - 1, n_- \rangle \quad (2.43)$$

$$\hat{a}_-^\dagger |n_+, n_- \rangle = \sqrt{n_- + 1} |n_+, n_- + 1 \rangle \quad \hat{a}_- |n_+, n_- \rangle = \sqrt{n_-} |n_+, n_- - 1 \rangle. \quad (2.44)$$

Then, an arbitrary state $|n_+, n_- \rangle$ can be written as

$$|n_+, n_- \rangle = \frac{(\hat{a}_+^\dagger)^{n_+} (\hat{a}_-^\dagger)^{n_-}}{\sqrt{n_+!} \sqrt{n_-!}} |0, 0 \rangle. \quad (2.45)$$

We can also describe the common space and momentum operators in terms of the new ones:

$$x = \frac{l}{2} (\hat{a}_+ + \hat{a}_+^\dagger + \hat{a}_- + \hat{a}_-^\dagger) \quad p_x = \frac{\hbar}{2il} (\hat{a}_+ - \hat{a}_+^\dagger + \hat{a}_- - \hat{a}_-^\dagger) \quad (2.46)$$

$$y = \frac{il}{2} (\hat{a}_+ - \hat{a}_+^\dagger - \hat{a}_- + \hat{a}_-^\dagger) \quad p_y = \frac{\hbar}{2l} (\hat{a}_+ + \hat{a}_+^\dagger - \hat{a}_- - \hat{a}_-^\dagger) \quad (2.47)$$

$$x^2 + y^2 = l^2 (\mathbf{1} + \hat{n}_+ + \hat{n}_- + \hat{a}_+ \hat{a}_- + \hat{a}_+^\dagger \hat{a}_-^\dagger) \quad (2.48)$$

$$p_x^2 + p_y^2 = \frac{\hbar^2}{l^2} (\mathbf{1} + \hat{n}_+ + \hat{n}_- - \hat{a}_+ \hat{a}_- - \hat{a}_+^\dagger \hat{a}_-^\dagger) \quad (2.49)$$

$$xp_y - yp_x = \hbar (\hat{n}_+ - \hat{n}_-). \quad (2.50)$$

Our Hamiltonian (2.29) can be written in terms of the new operators as

$$H = \hbar\omega_h (\mathbf{1} + \hat{n}_+ + \hat{n}_-) - \frac{\hbar\omega_c}{2} (\hat{n}_+ - \hat{n}_-). \quad (2.51)$$

The states $|n_+, n_- \rangle$, which are eigenstates to \hat{n}_+, \hat{n}_- , can differ from the Fock-Darwin states we already found only by a phase factor. The old quantum numbers n, m are related to the new ones n_+, n_- by

$$n = \min(n_+, n_-) = \frac{n_+ + n_- - |n_+ - n_-|}{2} \quad m = n_+ - n_-. \quad (2.52)$$

To calculate the phase factor we can determine the spatial probability amplitude $\langle (r, \varphi) | n_+ n_- \rangle$. The rising operators a_+^\dagger, a_-^\dagger can be described in terms of the position and momentum operators \mathbf{x}, \mathbf{p} as

$$\hat{a}_+^\dagger = \frac{e^{i\varphi}}{2} \left(\frac{r}{l} - l \frac{\partial}{\partial r} - \frac{il}{r} \frac{\partial}{\partial \varphi} \right) \quad \hat{a}_-^\dagger = \frac{e^{-i\varphi}}{2} \left(\frac{r}{l} - l \frac{\partial}{\partial r} + \frac{il}{r} \frac{\partial}{\partial \varphi} \right). \quad (2.53)$$

We get $\langle (r, \varphi) | n_+ n_- \rangle$ by applying (2.53) to the ground state function

$$\langle (r, \varphi) | 00 \rangle = \frac{1}{l\sqrt{\pi}} e^{-r^2/(2l^2)}. \quad (2.54)$$

By comparison we obtain

$$\langle (r, \varphi) | n_+ n_- \rangle = \frac{1}{\sqrt{2\pi}} e^{im\varphi} \frac{(-1)^n}{l} \sqrt{\frac{2n!}{(n+|m|)!}} \left(\frac{r}{l} \right)^{|m|} e^{-r^2/(2l^2)} L_n^{|m|} \left(\left(\frac{r}{l} \right)^2 \right). \quad (2.55)$$

The usefulness of the n_+, n_- basis is revealed, when we try to calculate the matrix elements describing the motion of the hole in the xy plane. The operators of the Kohn-Luttinger matrix read in this basis

$$(P_{xy} + V_{xy}) \frac{1}{\hbar\omega_h} = (1 + n_+ + n_-) - \frac{\omega_c}{2\omega_h} (n_+ - n_-). \quad (2.56)$$

With the effective mass $m^* = m_e/\gamma_1$ the operator P_{xy} is diagonal. This is no longer true for Q_{xy} because of its different effective mass. Q_{xy} couples states with the same angular momentum of the envelope function and different n .

$$\begin{aligned} (Q_{xy} + V_{xy}) \frac{1}{\hbar\omega_h} &= \frac{1}{2} \left(1 + \frac{\gamma_2}{\gamma_1} + \left(\frac{\gamma_2}{\gamma_1} - 1 \right) \left(\frac{\omega_c}{2\omega_h} \right)^2 \right) (1 + n_+ + n_-) \\ &+ \frac{\gamma_2}{\gamma_1} \frac{\omega_c}{2\omega_h} (n_+ - n_-) \\ &+ \frac{1}{2} \left(1 - \frac{\gamma_2}{\gamma_1} + \left(\frac{\gamma_2}{\gamma_1} - 1 \right) \left(\frac{\omega_c}{2\omega_h} \right)^2 \right) (a_+ a_- + a_+^\dagger a_-^\dagger) \end{aligned} \quad (2.57)$$

In the axial approximation the operator R reads

$$R \frac{1}{\hbar\omega_h} = \frac{\sqrt{3}}{2} \frac{\gamma_2 + \gamma_3}{2} \frac{1}{\gamma_1} \left[\left(\frac{\omega_c}{2\omega_h} + 1 \right)^2 (a_+)^2 + \left(\left(\frac{\omega_c}{2\omega_h} \right)^2 - 1 \right) a_+ a_-^\dagger + \left(\frac{\omega_c}{2\omega_h} - 1 \right)^2 (a_-^\dagger)^2 \right]. \quad (2.58)$$

Analogously the S operator is

$$S \frac{1}{\hbar\omega_h} = \sqrt{3} \frac{\gamma_3}{\gamma_1} \frac{l_{HO}}{l_z} \left[\left(\frac{\omega_c}{2\omega_h} - 1 \right) a_+ + \left(\frac{\omega_c}{2\omega_h} + 1 \right) a_-^\dagger \right] \frac{\partial}{\partial z}.$$

$$\frac{1}{l_z} = \begin{cases} \left(\frac{2m_e e F}{\hbar^2 (\gamma_1 - 2\gamma_2)} \right)^{\frac{1}{3}} & HH \\ \left(\frac{2m_e e F}{\hbar^2 (\gamma_1 + 2\gamma_2)} \right)^{\frac{1}{3}} & LH \end{cases} \quad (2.59)$$

Here l_z is what we could call the characterising length of the system in z direction. By dividing

the operators by ω_h we immediately can see the behaviour of the system with rising magnetic field. From (2.28) follows $\omega_c/2\omega_h \rightarrow 1$ as the magnetic field strength increases. Therefore, all parts of the operators above with pre factors like $(\omega_c/2\omega_h - 1)$ become small. Then, all basis states which appeared in the expansion of the eigenstates of the system due to the coupling through the operators with these pre factors, will loose weight in the expansion of the eigenstates for higher magnetic field. This is a manifestation of the symmetry breaking between the states with the same absolute value but different sign of the total angular momentum by the magnetic field.

Using (2.38) and (2.39) we can now easily calculate all matrix elements for the xy motion.

2.6.3 Elliptic Quantum Dots

Quantum dots fabricated by any process often do not possess rotational symmetry in the xy plane. This can have significant influence on the eigenstates of these dots. Elliptic quantum dots, i.e. dots with an elliptic contour of constant potential in the xy plane, are an approximation to these non-circular dots. For single-band quantum dot models, as in case of electrons in the conduction band, one can show that the elliptical potential lifts the degeneracy of the excited states in the Fock-Darwin spectrum [44], [45],[46]. In the case of holes the dependence on the anisotropy of the potential is more complicated. The elliptic potential acts on the orbital movement of the holes, the Fock-Darwin states. We will see that hole eigenstates consist of different Fock-Darwin

states and the spin is coupled to the orbital movement. Thus the influence of the elliptic potential is different. The elliptic shape is created by changing the xy potential in (2.27) to

$$V_{xy} = \frac{K_0}{2}(x^2 + y^2) + K_e y^2. \quad (2.60)$$

The constant K_e describes the strength of the additional harmonic potential. In the basis for the xy plane y^2 can be described as follows in terms of the creation and annihilation operators

$$y^2 = l^2 \left[\hat{a}_+ \hat{a}_- - \hat{a}_+ \hat{a}_-^+ - \hat{a}_+^+ \hat{a}_- + \hat{a}_+^+ \hat{a}_-^+ + \hat{a}_+ \hat{a}_+^+ + \hat{a}_- \hat{a}_-^+ - 1 \right. \\ \left. - \frac{1}{2} (\hat{a}_+^2 + \hat{a}_+^{+2} + \hat{a}_-^2 + \hat{a}_-^{+2}) \right]. \quad (2.61)$$

Since this additional operator breaks the circular symmetry of the dot, the Hamiltonian of the system no longer resolves into blocks belonging only to a single value of the z component of the total angular momentum $M = m_{FD} + j_z$. So, we have to include all possible values of the angular momentum in our calculations. Here and in all cases where the circular symmetry of the problem is broken, to maintain a computable matrix I consider only values of M belonging to the energetically lowest states. They go from $M = -7/2$ to $M = +7/2$. This assures, that all states with a strong coupling to the ground states $M = \pm 3/2$ are considered.

2.6.4 Motion in z direction

For the triangular potential in z direction one cannot calculate the required matrix elements analytically. This is due to the cumbersome functions and the different masses for the light and heavy holes. The used Airy-Functions [47] are solutions to the differential equation

$$\left(\frac{1}{2m^*} p_z^2 + eFz \right) \zeta(z) = E\zeta(z) \quad \zeta(z=0) = \zeta(z=\infty) = 0 \quad (2.62)$$

$$\zeta_p(z) = Ai \left[\left(\frac{2m^* eF}{\hbar^2} \right)^{\frac{1}{3}} \left(z - \frac{E_p}{eF} \right) \right]. \quad (2.63)$$

F describes the strength of the linear potential in z direction. E_p is the p th eigenvalue of the differential equation (2.62). E_p/eF are the roots of the Airy function. For the Bloch bands with $j_z = \pm 3/2$, we insert the effective mass $m^* = m_e/(\gamma_1 - 2\gamma_2)$, where m_e is the mass of a free electron. For the Bloch bands with $j_z = \pm 1/2$, we use Airy functions with the effective mass $m^* = m_e/(\gamma_1 + 2\gamma_2)$. We expand the z component of the eigenstate envelope-function not in one but in two orthogonal sets of functions. They are not orthogonal with respect to each other, because of the different masses used to define them. This procedure assures a good description of the hole wave function with a minimal set of basis functions.

The mass in the z direction for the $j_z = \pm 3/2$ bands $m_{3/2}^z = m_e/(\gamma_1 - 2\gamma_2)$ is bigger then the

one for $j_z = \pm 1/2$ bands $m_{1/2}^z = m_e/(\gamma_1 + 2\gamma_2)^2$. Therefore, the $j_z = \pm 3/2$ bands are called the Heavy-Hole bands whereas the $j_z = \pm 1/2$ ones are called Light-Hole bands. Notice (see Eq. 2.12) that for the xy direction the situation is reversed. The $j_z = \pm 3/2$ mass $m_{3/2}^{xy} = m_e/(\gamma_1 + \gamma_2)$ is light and the $j_z = \pm 1/2$ mass $m_{1/2}^{xy} = m_e/(\gamma_1 - \gamma_2)$ is heavy. The names originate from the description of 2D hole systems, where the holes are only confined in the z direction. The energy of the different states was then determined by the $m_{3/2}^z$ and $m_{1/2}^z$ terms.

While expanding the z states in two non-orthogonal sets of functions, we have to calculate some matrix elements, which appear due to the non-orthogonality. In the \mathbf{R} operator of the Kohn-Luttinger Hamiltonian we have to calculate $\langle \zeta_i^{HH} | \zeta_j^{LH} \rangle$ and for the \mathbf{S} operator $\langle \zeta_i^{HH} | p_z | \zeta_j^{LH} \rangle$. Here $HH(LH)$ denotes the functions with heavy(light) mass in z direction. These calculations have to be performed numerically, which can be readily accomplished using Mathematica. Then the results of the integration are saved in a file and read out to set up the matrix.

2.6.5 Basis States for One Hole

The wave function of a hole from the topmost valence band of GaAs inside a quantum dot is described by the sum over all four top valence bands, where the summands are products of Bloch states $u_{j_z}(\mathbf{r})$ times some envelope functions $F_m(\mathbf{r})$

$$\Psi_M(\mathbf{r}) = \sum_{j_z} c_{M-j_z}^{j_z} F_{M-j_z}^{j_z}(\mathbf{r}) u_{j_z}(\mathbf{r}). \quad (2.64)$$

Here $M = m + j_z$ is the sum of two z components of different angular momenta of the hole. The angular momentum \mathbf{j} , with z component j_z , appears due to the spin-orbit coupled movement of an electron around the atoms constituting the crystal lattice. In the Tight-Binding model for the formation of bands in the crystal, they develop from orbitals of the atoms forming the lattice. In this process the particles retain their angular momentum. The topmost valence bands in *GaAs* develop from p orbitals. With spin-orbit coupling this gives a total angular momentum of $|\mathbf{j}| = 3/2$. The movement of the hole inside the circularly symmetric quantum dot gives rise to the conservation of a component of the angular momentum. With our choice of the coordinate axes it is L_z . The Fock-Darwin states are eigenstates to this operator and m is the conserved quantum number. The sum $M = m + j_z$ is a good quantum number, i.e. the matrix representing the system becomes block-diagonal with respect to M . There is no interaction between states from different blocks and we can diagonalise each block at a time. Since the j_z value changes for every band, the envelope function for every band must have a different m .

As mentioned above, we expand the envelope functions F in a complete and orthogonal set of

² Without any confinement the masses are isotropic according to the spherical approximation. The particular form of the confining potentials defines the mass of the holes in confined states.

functions, namely the Fock-Darwin states. With our choice form above we get

$$F_{M-j_z}^{j_z}(\mathbf{r}) = \sum_p \sum_n C_{n,|M-j_z|}^{j_z} \zeta_p^{HH(LH)}(\mathbf{z}) \phi_{|M-j_z|}(\varphi) \frac{1}{l} \rho_{n,|M-j_z|}(r/l). \quad (2.65)$$

We have to choose the heavy-hole masses (HH) for $j_z = \pm 3/2$ and light-hole masses (LH) for $j_z = \pm 1/2$. From the exact diagonalisation we get the eigenvalues of the system and the expansion coefficients $C_{n,|M-j_z|}^{j_z}$. They represent the eigenstates in the chosen single-particle basis.

2.7 Energy dependence on the magnetic field

The magnetic field appears in two points in the description of a hole confined in a quantum dot. Following the theory of Luttinger [31] the interaction of the z component of the total angular momentum \mathbf{J} of the hole has the form $E_z = 2\mu_B \kappa j_z \mathbf{B}$. μ_B is the Bohr magneton, j_z the z component of \mathbf{J} and the Luttinger constant κ is a material dependant parameter. It describes the effect of the remote bands on the alignment of j_z in the magnetic field. This whole description is valid in the basis of the four topmost valence bands with $|\mathbf{J}| = 3/2$. The influence on the movement in the dot orbitals is described by changing the momentum operator $\tilde{p}_\alpha \rightarrow p_\alpha - qA_\alpha$. \mathbf{A} is the vector potential and q the charge of the particle. In quantum dots the field is often applied perpendicular to the xy plane, where the electrons are confined by a harmonic potential. Then the influence of the field on the energy due to the orbital movement described by the envelope functions is $m\omega_c/2B$. Here, m is the z component of the orbital angular momentum and ω_c the cyclotron frequency. Quantum numbers m and j_z with the same sign must both increase or lower the energy in their respective terms. To describe the movement of electrons in the valence band one can stay in the familiar picture and has to deal with negative electron masses. Alternatively one can switch to the hole picture, where the holes retain positive masses. Luttinger worked in the electron picture and chose $-e$ for the charge of the moving particles. Then negative j_z lower the energy. In my calculation I use the hole picture i.e. I assume $q = +e$. But I dropped accidentally the also necessary transformation of the particle momenta $\mathbf{p}_e = -\mathbf{p}_h$. The momentum of the hole must have the opposite direction of the electron momentum in the band. This inconsistency can be levelled by assuming the magnetic field to point in the $-z$ direction. This is equivalent to changing the charge q back to be $-e$. Due to this feature in my calculations Zeeman-like terms with positive quantum numbers lower the energy of the state.

2.8 Many-Body Interaction

We want to treat a quantum dot with several holes and their mutual repulsion. Since we use the full quantum mechanical description we have to set up a many-body basis for the system. Some

texts on this topic can be found e.g. in [48], [49] and [50].

Usually one sets up the many-body basis from products of single-particle states. To construct a many-body basis in this way one can use the following scheme. We predetermine some arbitrary order of the single-particle basis states. Then, we construct many-body states as products of single-particle states. For a system with N particles, each product consists of N single-particle basis states. When we choose to use in our single-particle basis m states, we get m^N product states. Then we only take those, which follow in the product the order we have set up. Since we have to treat the holes as fermions, we cannot allow two single-particle states in the product to match in every quantum number. So, we have to throw away these states from our set of product states. This will give us an appropriate many-body basis for numerical calculations.

The second-quantisation scheme is a compact and elegant way to describe many-particle physics. In this scheme the Hamiltonian of our system consists of two parts

$$H = H(1) + H(2) \quad (2.66)$$

$$H(1) = \sum_{ij} \langle i | H_{KL} + \mathbb{1}V | j \rangle a_j^\dagger a_i. \quad (2.67)$$

This is the single-particle part. It consists of the Kohn-Luttinger Hamiltonian and the potentials forming the dot.

$$H(2) = \frac{1}{2} \sum_{ijkl} \langle ij | \hat{V}_C | kl \rangle a_i^\dagger a_j^\dagger a_l a_k \quad (2.68)$$

is the part, describing the interaction between two particles. In our case this interaction will be the Coulomb repulsion between the holes. The matrix elements describing this repulsion have the following form [50]

$$\begin{aligned} \langle ij | \hat{V}_C | kl \rangle &= \langle n_i m_i M_i p_i n_j m_j M_j p_j | \hat{V}_C | n_k m_k M_k p_k n_l m_l M_l p_l \rangle \\ &= \delta_{M_i - m_i, M_k - m_k} \delta_{M_j - m_j, M_l - m_l} \delta_{M_i + M_j, M_k + M_l} \frac{1}{4\pi\epsilon\epsilon_0} \\ &\quad \times A_{n_i m_i n_j m_j} A_{n_k m_k n_l m_l} \sum_{\mu = \max(\mu_{min}^{ij}, \mu_{min}^{kl})}^{\min(\mu_{max}^{ij}, \mu_{max}^{kl})} \sum_{\nu = 0}^{\min(\nu_{max}^{ij}, \nu_{max}^{kl})} K_{\nu\mu}^{n_i m_i n_j m_j} K_{\nu\mu}^{n_k m_k n_l m_l} \\ &\quad \times \int dz_1 dz_2 d\xi_{rel} \xi_{rel} \frac{\zeta_{p_i}(z_1) \zeta_{p_j}(z_2) \zeta_{p_k}(z_1) \zeta_{p_l}(z_2) \tilde{\rho}_{\nu_{max} - \nu, m_i + m_j - \mu}^{ij}(\xi_{rel}) \tilde{\rho}_{\nu_{max} - \nu, m_k + m_l - \mu}^{kl}(\xi_{rel})}{\sqrt{l_{rel}^2 \xi_{rel}^2 + (z_1 - z_2)^2}}. \end{aligned} \quad (2.69)$$

The first pair of δ 's represents the fact, that the Coulomb interaction does not affect the Bloch function u_{j_z} . Therefore, these matrix elements have to be diagonal in the band index which is $j_z = M - m$. The third δ represents the conservation of the total angular momentum by this interaction. The total angular momentum z component of the initial states $M_i + M_j$ has to be the same in the final states $M_k + M_l$. For the motion in the xy plane it is possible to change to relative coordinates of the two interacting particles. The Coulomb interaction does not affect the xy motion of their centre of mass. In this manor, we can save the integration over the centre-of-mass variable. The summation over μ and ν represents this basis change. The constants A , K , μ_{min} , μ_{max} and ν_{max} are given in the appendix. The relative characteristic length is $l_{rel} = \sqrt{2}l$. The lack of symmetry in z direction forbids this procedure for this part. Here, we have to carry out all the integrations. We have chosen to describe the z part of the envelope function by two sets of functions, one with heavy-hole mass and one with light-hole mass. Therefore we now have to calculate the matrix elements for all possible combinations of heavy- and light-hole functions. Even when we use the symmetries of the integral, $z_1 \leftrightarrow z_3, z_2 \leftrightarrow z_4$ and $z_1 \leftrightarrow z_2, z_3 \leftrightarrow z_4$, we end up with 76 possible combinations for only the first two functions for each mass.

2.9 Manganese Impurity

The manganese atom has an atomic configuration of $[Ar]3d^54s^2$. When we introduce it into a III-V semiconductor like $GaAs$ or $InAs$ it will most likely substitute the Ga atoms in the lattice[51]. The Mn atom can also substitute the As or take an interstitial position. These situations, however, are less common than the substitution of the tri-valent atom. We will not consider them here. At the place of e.g. Ga in $GaAs$ the two $4s$ orbitals change to sp^3 orbitals to participate in the diamond like bounds. The Mn has only two electrons in the $4s$ orbital so one electron is missing, since the As atom contributes five electrons to these bounds. The electronic configuration of the Mn atom then becomes $3d^5 + \text{hole}$ [52]. Electrons from neighbouring bounds can fill this hole, which causes a detaching of the hole from the impurity. Then, the missing of one positive charge in the Mn core results in a negative charge in the vicinity of the Mn atom relative to the background. The interaction potential between the manganese and the hole can be modeled in the envelope function approximation as a Coulomb-like acceptor potential. This potential of the Mn is, however, screened by other atoms in the lattice. To describe this effect we have to modify the Coulomb potential of the impurity by an additional screening potential. This additional potential deviates remarkably from a constant only in the vicinity of the manganese impurity. We split the screening up in a constant part and a changing part. This second part is different from zero only close to the manganese impurity. The form of the screened Coulomb potential is then $1/r$ with an effective dielectric constant. Its value is $\epsilon_r = 13.1$ for $GaAs$ [32]. To take the rapid change of the screening in the vicinity of the manganese into account we have to add another part to the screened potential. This one is typically of

such a short range, that it has only influence on the ground state of the bound hole, where the hole is typically closest to the manganese. The addition of this second potential is called the Central Cell Correction. Experimentally, one can find that Mn in $GaAs$ is a moderately shallow acceptor with a binding energy for the lowest level of 112.4 meV [53] in the bulk crystal. This potential significantly changes the shape of the quantum dot potential and cannot be omitted, if a quantitative description of the dot eigenstates is intended. In our calculations we will nevertheless omit this correction. In the quantum dot eigenstates the hole is less concentrated around the manganese than for pure acceptor states. So we can expect, that the influence of the correction will be less prominent. The symmetry of the system is determined by the dot potentials. So the additional potential would have less influence on the character, i.e. the spin, of the holes and merely change the energy of the lowest states. In our model quantum dot we assume also, that we have control over the amount of charge carriers in the dot. We will treat cases, where the number of Mn atoms and holes differ. In our basis we have to calculate the matrix elements describing the Coulomb $1/r$ operator numerically.

The reason for introducing a Mn atom into the quantum dot is its large magnetic moment of $5/2\mu_B$. It is formed by the five $3d$ electrons. The $3d$ orbital is half filled, so according to Hund's rule all electrons align their spins parallel. Unlike the $4s$ orbital, which becomes delocalised and forms a band in the crystal lattice, the d electrons stay in the d orbital and remain localised at the place of the Mn . Nevertheless there is an interaction between the d orbital and the s and p band of the crystal. This interaction has its origins in a spin-dependent Coulomb interaction between the orbital and these bands [54]. Notice that this effect differs from the Coulomb force described above stemming from the missing electron in the top shell of the manganese. The exact form of the pd interaction can be found in [51], [55], [56]. We can cast the whole interaction in a spin-like term. The matrix elements of the interaction are then

$$\langle \Psi_{j_z} | \mathbf{J}(\mathbf{R}_I - \mathbf{r}) \mathbf{S} \cdot \mathbf{j} | \Psi_{j'_z} \rangle = \overline{|f(\mathbf{R}_I)|^2} \frac{J_{pd}}{3} \langle S_z, j_z | \mathbf{S} \cdot \mathbf{j} | S'_z, j'_z \rangle. \quad (2.70)$$

Ψ_{n, S_z, j_z} , Ψ_{n', S'_z, j'_z} are some basis states with manganese and hole spin S_z and j_z respectively and the multi-index n describes the orbital movement. \mathbf{j} is the total (atomic scale) angular momentum of the hole. \mathbf{S} is the total spin of the Mn impurity. The interaction between the hole spin and manganese $3d$ spin depends on the alignment of the spin of the hole rather than its total angular momentum \mathbf{j} . Now, within the basis states with $|\mathbf{j}| = 3/2$ of the four topmost valence bands the operator describing this interaction is diagonal. It is proportional to the operator $\mathbf{S} \cdot \mathbf{j}/3$. So the total angular momentum \mathbf{j} of the Bloch function $u_{j_z}(\mathbf{r})$ can also for this interaction be treated as a pseudo spin with four alignments. The strength of the interaction is proportional to the probability for the hole to be in the cell containing the manganese impurity. This probability is determined by the envelope function and is represented here by $\overline{|f(\mathbf{R}_I)|^2} = \langle F_{n, j_z}^*(\mathbf{r}) F_{n', j'_z}(\mathbf{r}) \rangle_{u.c.}$. The integration goes over the manganese unit cell. \mathbf{R}_I is the position of the Mn atom and F_{n, j_z} are the envelope function basis states. Since the envelope functions do not change very much over the

cell volume, we can also take the value of the envelope functions at the position of the impurity and multiply it by the volume of the cell. We also assume, that the presence of the manganese atom can change the orbital movement of the hole i.e. can change the envelope function. This behaviour is modeled by a δ like function, which acts only on the envelope functions

$$\langle F_{n,j_z}^*(\mathbf{r})F_{n,j_z}(\mathbf{r}) \rangle_{u.c.} = V_{u.c.} \int d\mathbf{r} F_{n,j_z}^*(\mathbf{r}) \delta(\mathbf{R}_I - \mathbf{r}) F_{n',j_z} = V_{u.c.} F_{n,j_z}^*(\mathbf{R}_I) F_{n',j_z}(\mathbf{R}_I). \quad (2.71)$$

Where $V_{u.c.}$ is the volume of the unit cell of the crystal. The details of the interaction on the atomic scale are inaccessible to our model. We use a parameter to account for the correct strength of the interaction. This interaction constant is J_{pd} . It gives a value for the interaction energy between a hole spin in the p band and the d electrons of the Mn . This value is hard to determine. I used $J_{pd} \approx 40 \text{ meV nm}^3$ [53]. Treating the total (atomic scale) angular momentum of the hole \mathbf{j} as a pseudo spin, the spin part of the basis for the hole and the Mn is just the tensor product $|S_z\rangle \otimes |j_z\rangle$. The states $|S_z\rangle$ are eigenstates of $\hat{\mathbf{S}}^2, \hat{S}_z$ and $|j_z\rangle$ are eigenstates of $\hat{\mathbf{j}}^2, \hat{j}_z$. In this basis we can describe the spin operator part of the interaction term as

$$\mathbf{S} \cdot \mathbf{j} = S_z j_z + \frac{1}{2}(S_+ j_- + S_- j_+). \quad (2.72)$$

S_+, S_-, j_+, j_- are rising and lowering operators for some angular momentum [42].

When we introduce several Mn impurities in our semiconductor, there is also an interaction between the d orbitals of these impurities. The interaction aligns the magnetic moments anti parallel to each other. However this interaction is very short ranged. Its strength is proportional to the overlap of the d orbitals of the participating Mn atoms. The energy splitting caused by this interaction is about 6 meV for atoms in a distance equal to the distance between the Ga - and As -atoms in the lattice [57]. The lattice constant in $GaAs$, which should be larger than this distance, is $a(GaAs) = 5.65 \cdot 10^{-10}$. Therefore, we can assume, that this interaction can be neglected, if we separate any two Mn atoms by some nm .

2.10 Time Inversion Symmetry

Without an applied magnetic field our system will be invariant under the inversion of the time degree of freedom. Performing this transformation on our system will change the sign on every z component of a spin or angular momentum present in the system. The theorem of Kramer [58] states, that a state with a non-integer total spin can not be mapped onto itself by the inversion of time. Thus such states must be doubly degenerate in energy in a time invariant system. This degeneration occurs in nearly all configurations considered by Me in the present work. At $B = 0 \text{ T}$ all states will be degenerate with a state with exact the opposite angular momentum. So, without defining the angular momentum of the system, we will not see any magnetisation of the manganese. They will be degenerate with their opposite alignments. Actually the spin of

optically created holes and electrons can be controlled by the polarisation of the light used for their creation. We do not encounter any spontaneous breaking of this symmetry as discovered in ferromagnetic materials. Ferromagnetism is the collective effect of a large number of symmetrically arranged atoms. As quantum dots were often considered as artificial atoms, maybe a investigation of quantum dot arrays could find a link. Such an investigation, however, has to be postponed to future work.

Chapter 3

Quantum Dot With Holes

In this chapter I want to present the results of my work. I will start with quantum dots with only a single hole. This shall help to understand basic mechanisms peculiar to a quantum dot containing holes. Then I will gradually introduce additional features into the calculations. First it will be the Coulomb interaction with other holes inside the dot. Second I will discuss the interaction of a single hole with one and two manganese impurities also located inside the dot. Finally I will examine the interplay between the two kinds of interaction.

3.1 Single-Particle States

First I want to present my calculations for eigenstates and eigenenergies of a single hole confined inside a quantum dot. Such calculations have been performed before [59], [60], [38], [61], [62]. Apart from [61] all other authors deal with holes confined in z direction by a quantum well. In my calculations the holes in growth direction are confined at a heterojunction between $GaAs$ and $GaAlAs$. The two systems differ in the form of the confinement potential in this direction. This changes the spectrum of the dot slightly in comparison to the spectrum of a dot formed in a quantum well. In a quantum well there is often a mirror plane perpendicular to the growth direction z . It lies in the middle between the potential walls. This symmetry is represented by the conserved parity quantum number. A heterojunction lacks such a symmetry. Also in a quantum well with high potential barriers modeling of the penetration of the hole wave function into the potential wall is crucial. It has a strong influence on the mixing of the light and heavy hole states and thus on the spin-character of the eigenstates. In a heterojunction the holes are strongly constricted only in one direction of the z axis. This results in rather large band mixing in comparison to the quantum well. Despite this differences it is possible to compare my work with the earlier results. The single-particle spectrum is the simplest model system to explain all the influences of different potentials on the energy of the hole. I present the calculations for several potential configurations of $GaAs$ dots as well as for a dot made of $InAs$. Thereby I will emphasise the

differences between the two systems.

3.1.1 GaAs Quantum Dots

The influence of the host material enters the model via the Luttinger parameters. For *GaAs* they are: $\gamma_1 = 6.85$, $\gamma_2 = 2.1$, $\gamma_3 = 2.9$ and $\kappa = 1.2$. The harmonic confining potential in xy direction should represent a quantum dot with the size of several tens of nanometres. Such dots can be formed by lithographic processes. For the electrons the energy spectrum inside a harmonic dot is equidistant. The strength of the confining potential is given in terms of the energy spacing between these equidistant states. A value for experimentally realised dots lies between 3 and 5 meV [63], [64]. For the starting point of my calculations I will take a value of 4 meV. In such dots the strength of the interaction of the holes with the different potentials we are interested in is of approximately similar magnitude: The dot potential, the magnetic field, the mutual Coulomb repulsion between several holes and the acceptor potential of a manganese impurity. By varying the dot-potential strength we can also change the impact of the other potentials. The fabrication of such dots appears possible, since they differ from dots with electrons by the exchange of doping ions. The experimental study of the hole eigenstates in such dots is difficult. Nevertheless, there are investigations on the eigenstates of holes in a two-dimensional quantum well [65]. These lie in the same energetic regime.

In the description of electrons in quantum dots the influence of the dot potentials, the magnetic field and the Coulomb interaction can be summarised in just one constant [50]. In this elegant description, however, the electrons have to be confined in a δ layer in z direction. Also the effective mass has to be constant. Both of these conditions are not complied for holes. Therefore, we have to resort to the more cumbersome description using the explicit values of all the potentials. The dot confinement energy of $\hbar\omega = 4$ meV is only valid for electrons in the conduction band of *GaAs* with an effective mass of $0.067m_e$. The strength of the xy potential itself is characterised by the “force constant” K_0 . We can calculate this value from the energy spacing of the electrons

$$4[\text{meV}] = \hbar\omega_0 = \hbar\sqrt{\frac{K_0}{0.067m_e}} \quad \rightarrow \quad K_0 = 0.067m_e \left(\frac{4[\text{meV}]}{\hbar}\right)^2. \quad (3.1)$$

With K_0 we can then calculate the confinement energies in the same dot ¹ for the holes with their particular effective masses:

$$E_{HH/LH} = \hbar\sqrt{0.067m_e \left(\frac{4[\text{meV}]}{\hbar}\right)^2 (\gamma_1 \pm \gamma_2) \frac{1}{m_e}} \quad (3.2)$$

¹Since the holes have the opposite charge than electrons the sign of the charge carriers creating the dot potentials has to change. Their number and position shall stay the same

With “+” (“−”) for the heavy(light) holes we get $\omega_0^{HH} = 3.097$ meV ($\omega_0^{LH} = 2.257$ meV). These values, however, are only valid for holes occupying only the $j_z = \pm 3/2$ respective only the $j_z = \pm 1/2$ Bloch bands. In quantum dots, where the energies due to confinement in z and xy direction are of similar magnitude, the hole eigenstates are mixtures of all four bands. These mixtures change strongly depending on the total energy of the state. Thus the effective mass of the particle changes and so the influence of the confining potential. The energy dependence of the effective mass makes the spectrum of the dot not equidistant.

The strength of the linearly rising confinement potential in z direction we will denote by its slope. I assume a field strength of $F = 7$ mV/nm. For the heavy holes this gives z confinement energies² in the lowest two states of 39.84 meV and 69.65 meV. For the light holes we have 64.12 meV and 112.12 meV. This z potential is achievable for experimentally realised $GaAs - (AlGa)As$ two-dimensional heterostructures [66]. In the following I will refer to these values for the xy and z potentials as the standard values. Variations of the confining potentials will be given in relation to these values.

$$\hbar\omega_0 = 4 \text{ meV (for electrons)} \quad F_0 = 7 \text{ mV/nm} \quad (3.3)$$

Notice that according to the Kohn-Luttinger Hamiltonian (2.12) the masses of the heavy holes are larger in z direction than the ones of the light holes, resulting in a smaller energy spacing. In contrast, the masses of the heavy holes in the xy plane are smaller than the ones of the light holes. So, the energy quantisation due to confinement in this plane is bigger than for the light holes.

The quantum dots we treat here are quite large. The exact spatial extend of the hole wave function in an eigenstate has to be calculated numerically. An approximation give the chosen basis functions. With the standard potential values (ω_0, F_0) the characteristic length in the xy direction for a heavy hole is 14 nm . The wave function has a slightly larger extend. In z direction the hole wave function falls to 10% of its peak value around 10 nm .

Figure [3.1] shows the energy spectrum of a hole confined in the quantum dot with confining potentials described above. The spherical approximation is used, i.e. $\gamma_2 = \gamma_3$ is set. Due to the coupling in the Kohn-Luttinger matrix all states consist of different mixtures of the four Bloch bands. The double degeneracy for zero magnetic field arises due to time inversion invariance of the Hamiltonian. In the two ground states the hole has the same density distribution and only the expectation value of the spin and orbital angular momentum differs in sign. This degeneracy is lifted by the magnetic field.

A good quantum number in this system is $M = m_{FD} + j_z$. It is the sum of the z component of the band total angular momentum j_z and the orbital angular momentum of the envelope function m_{FD} . The spectrum exhibits large anticrossings between states with the same M . This leads to a flatter spectrum in comparison with the spectrum of electrons.

²These are the $0D$ counterpart of the subband energies for a $2D$ system.

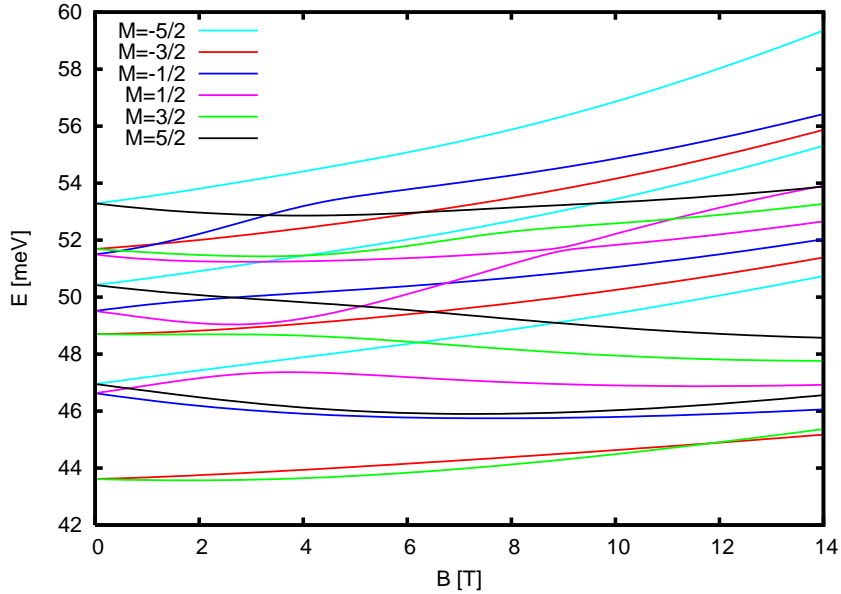


Figure 3.1: One hole confined in a heterojunction quantum dot. Depicted are the three lowest eigenstates for each of the total angular momenta $M = -5/2, \dots, 5/2$.

The confinement in z direction is much stronger than in the xy plane for this configuration of the confining potentials. Thus, the energy due to the confinement in z direction is much larger than the energy due to xy confinement. The basis states with the lower z energy compose the ground state of the dot. The main component of the two ground states $M = \pm 3/2$ is the basis state $|00, j_z = \pm 3/2\rangle$. The $j_z = \pm 3/2$ bands have a lower z confinement energy in comparison with the $j_z = \pm 1/2$ bands due to their larger mass in this direction. The ground state is thus mainly composed of heavy holes. Superimposed on the z energies the ordering is determined by the smaller xy confinement. The Fock-Darwin envelope with $|n = 0, m = 0\rangle$ is the lowest basis state for the xy potential. The R and S operators from the Kohn-Luttinger matrix are responsible for an admixture to the ground state of the $j_z = +1/2, j_z = -1/2$ bands with envelopes $|0 \pm 1\rangle$ and $|0 \pm 2\rangle$ respectively. The next higher states, with $M = \pm 1/2$ and $M = \pm 5/2$, consist also mainly of the $j_z = \pm 3/2$ bands with envelope functions $|01\rangle, |0 - 1\rangle$. This resembles to some extent the spectrum for electrons, where the Fock-Darwin states are eigenstates. There, the lowest envelope is $|00\rangle$ followed by $|0 \pm 1\rangle$. The reason for this similarity is the relatively large z confinement. Therefore, the $j_z = \pm 1/2$ Bloch band dominated states are energetically far away (≈ 25 meV, outside figure 3.1) and the admixture of light holes is relatively small. In conclusion the effective mass of the hole is almost constant in the lowest states. The spectrum resembles the one of a particle described by only one (spin degenerate) band and with an effective heavy hole mass. Actually, with this potential values we are on the edge of the similarity to electrons.

It becomes more pronounced when the splitting to the light-hole bands becomes larger. For higher magnetic fields we see that the slopes of the lowest states are nearly the same. They approach asymptotically Landau levels [67]. For very high magnetic fields the xy potentials forming the dot will play a minor role. The spectrum has to resemble that of a particle confined in the xy plane only by the magnetic field applied in z direction. Then, the quantum dot states resemble more and more those of a two dimensional hole gas in a strong magnetic field. The small spacings between different states approaching the same Landau level scale with the strength of the dot xy potential and vanish for a perfectly two dimensional system.

3.1.2 Band Coupling Effects

The crossing between the lowest eigenstates with total angular momentum z component $M = \pm 3/2$ arises due to competition of different potentials. The xy potential, the influence of the magnetic field on the orbital movement of the holes and the Zeeman energy the holes experience change the hole energy differently. It is instructive to take a closer look at this effect. We have defined the Zeeman energy as $E_Z = -\hbar e/m_e \kappa B j_z$. This term describes the influence of the magnetic field on the Bloch-band part of the holes wave function. The spin of the hole j_z in an eigenstate M is not a good quantum number. Nevertheless, the expectation value of the hole spin at $B = 0$ T is close to $3/2$ and has the same sign as M . So the Zeeman energy rises the $M = -3/2$ state energetically and lowers the $M = +3/2$ state. The influence of the xy potential and the magnetic field on the orbital movement of the hole is opposite to the Zeeman term. The mechanism is the following: They both enhance the coupling between the light and heavy holes. The light holes ($j_z = \pm 1/2$), have a bigger mass in the xy direction than the heavy holes ($j_z = \pm 3/2$). So their quantisation energy in the xy potential is smaller. The magnetic field in z direction acts only on the xy motion of the holes. Again the eigenstates dominated by the light holes rise slower with stronger magnetic fields than the heavy-hole states. The slope of an eigenstate in the magnetic field is dependent on the effective mass of the hole and thus on the admixture of the $j_z = \pm 1/2$ light-hole states to this eigenstate. Now, the magnetic field changes the mixture of Bloch bands in the two lowest $M = +3/2$ and $M = -3/2$ eigenstates differently. This can be seen when we look at the Landau levels which the two ground states approach in high magnetic fields. In this regime the hole is confined in a two dimensional plane by some potential in z direction. Using the envelope function approximation we can describe an eigenstate of this system by

$$\Psi_L = \begin{bmatrix} c_{3/2} f_{HH}(z) \Phi_N(y) \\ c_{1/2} f_{LH}(z) \Phi_{N-1}(y) \\ c_{-1/2} f_{LH}(z) \Phi_{N-2}(y) \\ c_{-3/2} f_{HH}(z) \Phi_{N-3}(y) \end{bmatrix}, \quad c_i = 0 \text{ for } N_i < 0, \quad N = \begin{cases} n & m \geq 0 \\ n - m & m < 0 \end{cases} \quad (3.4)$$

The $f(z)$ are the envelope functions in z direction. In the Landau gauge, $\mathbf{A} = B(-y, 0, 0)$, we get Hermite polynomials as envelope functions $\Phi_N(y)$ in the y direction, and plane waves in x direction [60]. The last part in (3.4) shows us how the quantum numbers of a Landau level are related to the ones of a Fock-Darwin state, which approaches this level asymptotically in high magnetic fields. When the $M = +3/2$ eigenstate approaches the Landau regime, then the $|n = 0, m = 0\rangle$ Fock-Darwin envelope of the $j_z = +3/2$ Bloch band approaches the Φ_N Landau level envelope of the same Bloch band. We have then $N = 0$ according to the last part in 3.4. For the $M = -3/2$ dot eigenstate the $|00\rangle$ Fock-Darwin envelope of the $j_z = -3/2$ Bloch band approaches the Φ_{N-3} Landau level envelope of the same Bloch band and the quantum number N is now $N_{-3/2} = 0 = N - 3$. The $M = +3/2$ dot eigenstate approaches a Landau level, where, because of the condition $N_i < 0 \Rightarrow c_i = 0$ in (3.4), the $N = 0$ Landau level consists only of the $j_z = +3/2$ Bloch band. The envelopes for all other Bloch bands are zero due to the c_i coefficients. In high magnetic fields, the $M = +3/2$ dot state develops towards a state consisting only of holes from the $j_z = +3/2$ Bloch band. The admixture of light holes vanishes. The $M = -3/2$ dot eigenstate approaches a Landau level, where the holes has access to all four Bloch bands. It remains a mixture of all four Bloch bands. This larger admixture increases the effective mass in the xy plane and, therefore, lowers the energy of this state relatively to the $M = +3/2$ state.

In the spectrum of Fig.(3.1) this effect compensates the Zeeman energy at around 12 T where the lowest states cross. By varying the confining potentials we can enhance and lower the coupling between the Bloch bands and can tune the position of this crossing. Figures 3.2(a) to 3.2(d) show the change of the lowest two states of the quantum dot with increasing confinement in xy direction.

The label “for electrons” in the figure caption has the following meaning: When we confine conduction band electrons with an effective mass of $0.067m_e$ in a dot with this xy potential, they will show an equidistant level spacing with the given energy. In the case of conduction band electrons this quantisation energy is experimentally accessible while the constant describing the potential strength is not. Therefore, the notation convention developed, to describe the dot potentials in terms of the level spacing $\hbar\omega$. When we describe valence band holes in a quantum dot we lack such a prominent quantity. The advantage of using in our case this somewhat cumbersome notation is the possibility, to compare the size of the treated dots with the real electron dots mentioned at the beginning of the section. Finally the force constant K_0 determining the strength of the xy potential is inaccessible to experiments. There is also no simple way to describe the strength of the potential by means of the non-equidistant level spacing. Also the frequency $\omega_{Basis} = \sqrt{K_0\gamma_1/m_e}$ we used to determine the spatial extend of our basis states is an arbitrary value since the mass of the holes changes and is never m_e/γ_1 . To represent the potential strength we choose here a value which has in our opinion the most relevance. In the following we will use ω_0 for the standard potential values and give other xy potentials only in relation to this potential.

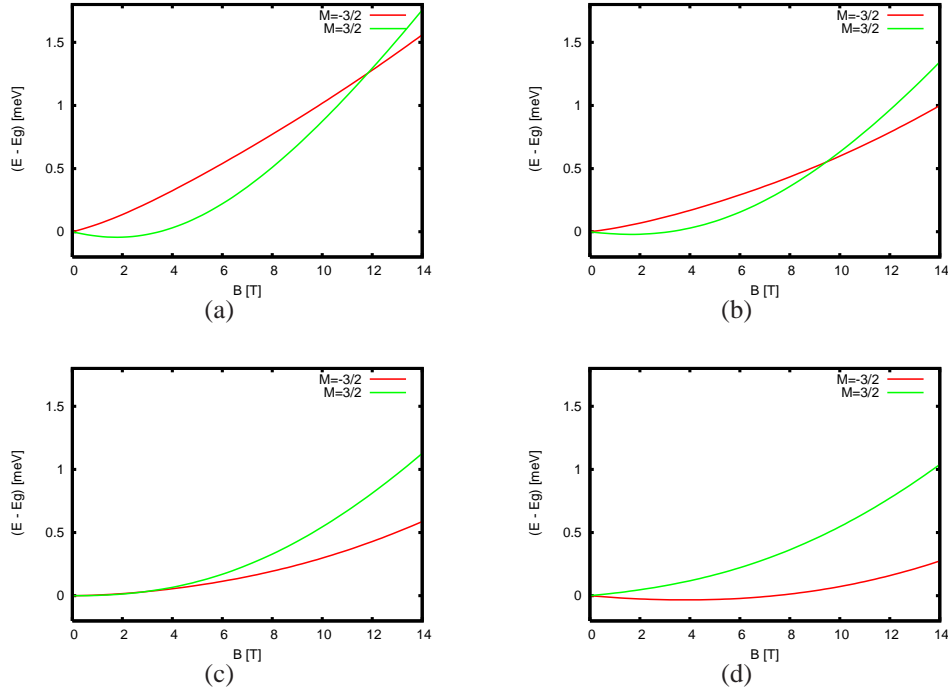


Figure 3.2: Energy (for electrons) due to xy confinement : (a) $\hbar\omega_0 = 4$ meV; (b) $\hbar\omega_0 = 5.5$ meV; (c) $\hbar\omega_0 = 7$ meV; and, (d) $\hbar\omega_0 = 8.5$ meV

With increasing xy potential the crossing between the two lowest states appears at lower magnetic fields. For approximately $\omega_0 = 8$ meV there is no crossing at all. To better compare the different plots, in each of them the energy of the states at $B = 0$ T was subtracted. The energy scale in each picture is the same. Note that with increasing xy confinement the slopes of both states are lowered, but the reaction of the $M = -3/2$ state on this change is much stronger. One can even obtain a negative slope for this state (Fig. 3.2(d)). This happens because the energy lowering admixture of $j_z = 1/2$ holes rises faster with magnetic field than the increase of the confining energy due to the stronger field. For small xy confinements such a negative slope of the states arises due to the Zeeman term (Fig. 3.2(a)).

As already mentioned, the magnetic field changes the mixture of the Bloch bands and thus changes the effective mass of the hole. It is, therefore, not possible to find a new constant effective mass for the hole and describe the system in a single-band picture for different values of the magnetic field.

In general one can find several regimes. When the confining potentials in xy and z direction are weak, the system is determined by the magnetic field and its eigenstates resemble Landau states for even weak fields. When the z confinement is the strongest, i.e. gives a much larger energy separation than the xy potential and the magnetic field, the hole behaves very much like

an electron. It can be described as a particle with a constant effective mass and a two-level spin of $3/2$. Then its effective mass is close to the mass of a heavy hole. For z confinement potentials much smaller than the xy potential the xy potential determines the order of the states. The heavy holes from the $j_z = \pm 3/2$ band have a light xy mass that rises their eigenstates up in energy and the lowest states are mainly composed of the $j_z = \pm 1/2$ bands. When neither of the potentials is dominant the holes states are mixtures of all four bands.

3.1.3 InAs Quantum Dots

We can describe an *InAs* quantum dot in our model by merely changing the Luttinger parameters. They are for *InAs*: $\gamma_1 = 19.67$, $\gamma_2 = 8.37$, $\gamma_3 = 9.29$ and $\kappa = 7.68$ [32]. The difference between γ_2 and γ_3 is again not very large so we are allowed to use the axial approximation. The largest difference compared to *GaAs* is the large value of κ . This parameter corresponds to the Landé factor of atomic states. We thus expect that the dependence of the states on the Zeeman energy will be much stronger, than in the *GaAs* dot. This fact will become important when we introduce a manganese impurity into the dot.

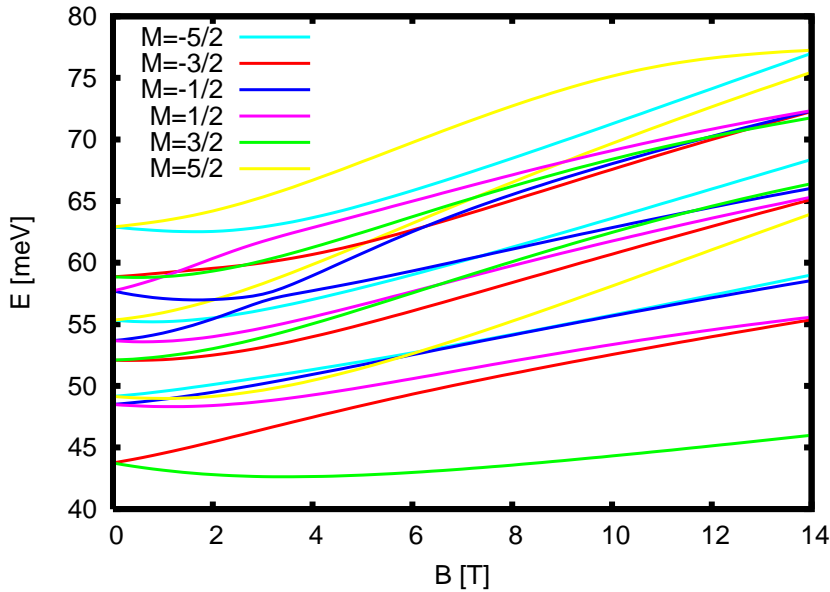


Figure 3.3: *InAs* quantum dot with standard potential values.

Figure (3.3) shows the energy eigenstates of a single hole in an *InAs* quantum dot with standard values (Eq. 3.3) for the confining potentials. The material independent constants K_0 and F are the same. The mixture of Bloch bands constituting the lowest states is comparable

to the one in a *GaAs* quantum dot. The same ratio of the confining potentials in *InAs* leads to a very similar character of the eigenstates in the *InAs* dot. The density of the hole has the same oblate form. The ground state is now $M = +3/2$ throughout the whole range of the magnetic field considered here because of the large negative Zeeman energy. It seems impossible to change the order between $M = +3/2$ and $M = -3/2$ by varying the confinement potentials. To enhance the band mixing and to lower the energy of the $M = -3/2$ state, we have to choose a strong xy confinement and comparatively weak z confinement. For a confining xy potential nine times stronger than the standard value the lowest states run parallel with each other until a field strength of $B = 1$ T but $M = -3/2$ never becomes the ground state. For even higher values of the potential the splitting between the states becomes stronger again. $M = +3/2$ is still the ground state but the mixture of bands in this state differs strongly from the standard potential regime. When the energy due to the xy confinement becomes even bigger than the energy due to z confinement the main components of the ground state again become light holes from $j_z = \pm 1/2$ bands.

3.1.4 Elliptical Quantum Dots

The common situation when dealing with real quantum dots will be that the dots will not possess cylindrical symmetry. This can be due to failures or inherent constraints of the growth and lithographic processes. We want to simulate this lack of circular symmetry and the violation of the conservation of angular momentum in the eigenstates. We, therefore, also investigate quantum dots with an elliptic potential in the xy plane. An additional harmonic potential in y direction creates this elliptic potential profile. In our calculations we considered this anisotropy potential to vary between one and two times the potential strength in x direction, i.e. $\omega_x = \omega_0$ and $\omega_y = 2\omega_0$. For electrons a small additional potential of the form (2.60) can split the $|n, \pm m\rangle$ Fock-Darwin states, which are degenerate at zero magnetic field. Each such state is, however, also degenerate in spin. For a particle with non-integer spin like an electron or a hole it follows from the theorem of Kramer [67] that an additional potential that is invariant under time inversion can not lift the degeneracy of the eigenstates due to time inversion invariance. Electric fields like the additional elliptic potential are invariant under the time inversion. The z component of the total angular momentum of the hole M is a half-integer number. Consequently all hole eigenstates are degenerate in $\pm M$ at $B = 0$. They still remain degenerate in an elliptic quantum dot. Different as for electrons the degeneracy at $B = 0$ T is not lifted by the elliptic potential. Figure 3.4 shows the lowest states of a dot with standard potential values (black curves) and in a dot with an additional harmonic potential of ω_0 in y direction (red curves). All states remain degenerate at $B = 0$ T. All are shifted up due to the stronger total confinement. The doublets, however, experience a different shift in energy due to their different density distribution. Two states $|M\rangle$ and $|M'\rangle$ can become coupled through the additional potential. This coupling is especially prominent when $M \pm 2 = \pm M'$ is fulfilled and their main spin component stems

from the same Bloch band. This is fulfilled for the second and third pair with $M = \pm 1/2$ and $M = \pm 5/2$ respectively. In comparison, the crossing of these states in the circular potential around 0.6 T transforms to a strong anticrossing in the elliptic dot. The reason is the mixing of the $m = \pm 1$ Fock-Darwin orbitals, which partially constitute these eigenstates. The ground states $M = \pm 3/2$ become coupled with the $M = \pm 7/2$ states (not shown in Fig. 3.4). These are energetically far away from the two ground states so their influence on them is small.

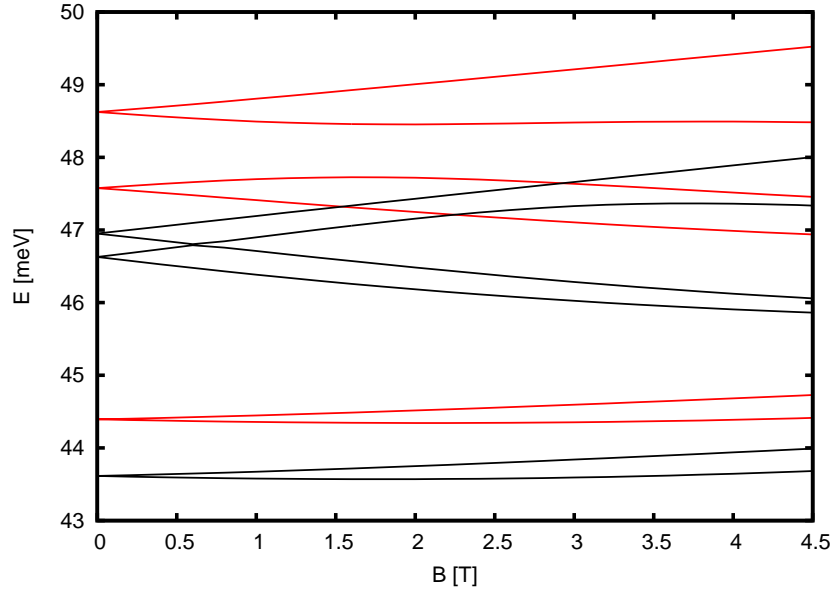


Figure 3.4: Six lowest hole states in a dot with standard potential values (ω_0, F_0) (black) and in an elliptic dot with an additional potential ω_0 in y direction (red).

3.2 Many-Particle States

The eigenenergies of two holes in a quantum dot have been calculated in [59],[62]. With increasing computational power it now becomes possible to treat more than two holes by exact diagonalisation. I will focus on the influence of the different configurations of the confining potentials on the eigenstates of several holes inside the quantum dot.

For conduction-band electrons inside a quantum dot one can show [50] that Coulomb-interaction energy is proportional to $\propto \sqrt{\omega_0}$ while the energy of the electrons due to confinement is proportional to $\propto \omega_0$. So the impact of the interaction energy on the whole system should increase for larger dots with smaller ω_0 . Self-assembled quantum dots have usually a radius of some nanometres. In this system the quantisation energy is very high due to the strong localisation of

the hole. Here the influence of the Coulomb interaction can even be neglected. For larger dots, however, it can have a strong influence. In the case of holes in degenerate bands there is no such simple relation between dot potential and Coulomb interaction. Thus it is important to investigate the effects leading to the different behaviour of the Coulomb interaction. Nevertheless, we can expect that the influence of the Coulomb potential will rise in larger dots, i.e. with weaker confining potentials.

3.2.1 Two Holes

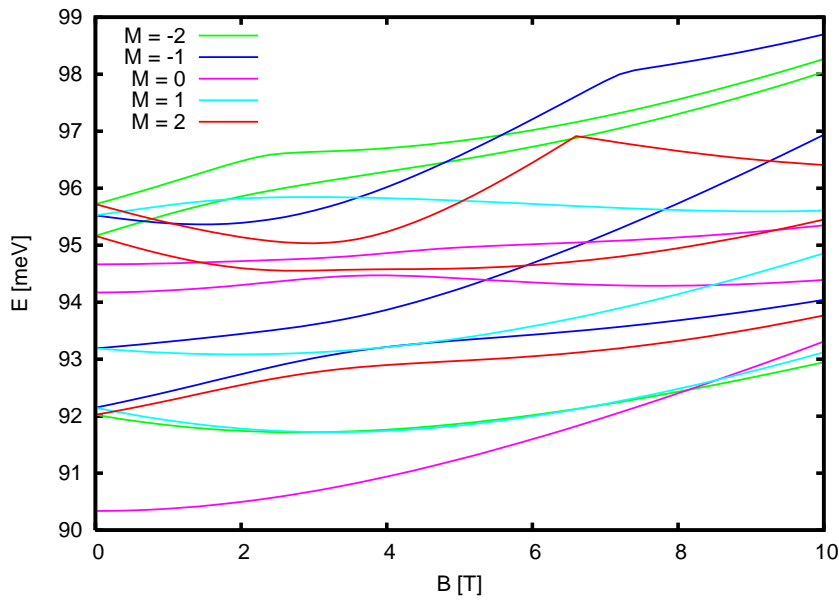


Figure 3.5: Energy spectrum of two holes in a dot with standard potential values ω_0 and F_0 .

Figure 3.5 shows the eigenstates of two holes in a *GaAs* quantum dot with standard potential values. Now, only the sum $M = M_1 + M_2$ of the z components of the total angular momenta of the single holes is a good quantum number. For every value of M there are infinitely many combinations of M_1 and M_2 . We take for each M only sums, which consist of the energetically lowest single-hole states with $M_{1,2} \in (-5/2, -3/2, -1/2, 1/2, 3/2, 5/2)$.

The z component of the total angular momentum is an integer number. So, according to Kramers theorem the states at $B = 0$ T do not need to be degenerate due to time inversion invariance of the system. The symmetry operation of time inversion creates a mapping between the eigenstates of the system. States with an integer number for the total spin can be mapped onto itself. Thus there is no need for a different associate state at the same energy. The lowest state with $M = 0$ is such a not degenerate eigenstate. It is invariant under time inversion. The next higher states are

still twofold degenerate. This is because the time inversion changes the sign of angular momenta. It maps $M = +1$ to $M = -1$, $M = +2$ to $M = -2$ and vice versa.

In the ground state at $B = 0$ T the envelope functions of the two holes both differ little from the lowest Fock-Darwin basis state. This lowest eigenstate has the highest hole density in the centre of the dot and thus the biggest Coulomb energy. This implicates that for our standard potential values we are in a regime, where the dot potential dominates over the Coulomb repulsion. Since the dot potential is dominant, we can use the picture, where the two holes occupy different one-hole orbitales. We approximate the two-hole eigenstate by a product of two single-hole states. In the first excited states one hole occupies an excited orbital while the other hole stays in the ground state. Therefore, the excited states in the present spectrum resemble to some extent the lowest four excited states from the single-particle spectrum (fig. 3.1). This can be especially seen in the development of the states in the magnetic field. For higher magnetic fields the ground state develops very much like the sum of the two single-hole states. The spins of the holes in the ground state point opposite to each other at $B = 0$ T. The different admixture of light holes in the two single-hole states constituting this eigenstate is again visible. While the spin of one hole gains continuously a stronger $j_z = +3/2$ part the other hole with initial $j_z = -3/2$ spin is coupled to the light hole bands by the magnetic field (see discussion in Sec.3.1.1). Thus the expectation value of the hole spin in the two-hole state changes. From 0 at $B = 0$ T it rises continuously with the field. Without magnetic field the spins of the two holes exactly compensate each other. Due to the different band mixture in the two single-hole states with magnetic field this is no longer possible at larger fields. This resembles the behaviour described in [55]. The states with $M = 1$ or $M = -2$ fall below the $M = 0$ eigenstate at a field above $B = 8$ T. The spin expectation value in these states stays nearly unchanged in the magnetic field. For $M = -2$ this spin of the holes points opposite to the alignment favoured by the Zeeman term. What makes it still energetic favourable is its envelope functions, i.e. the orbital movement of the hole inside the dot. These envelope functions consist of basis states with positive magnetic quantum number m , which lower the energy in the magnetic field.

In comparison to the single-particle spectrum the energy difference between the lowest state and the first excited state in the two-hole spectrum is smaller by ≈ 1.5 meV. This energy difference accords the difference in the Coulomb energy between the excited and the ground state in the present spectrum. It occurs, because the hole wave function is more spread out in the excited state. The absolute amount of the Coulomb energy, e.g. in the ground state, can be obtained by comparing energy of the system with Coulomb interaction to the system with the Coulomb interaction turned off. This latter energies are just the sums of the single-particle energies from figure 3.1. The additional energy due to the Coulomb interaction in the ground state then results to ≈ 3 meV (see Fig. 3.9(b)). This is the same magnitude as the excitation energy of one hole and twice the Coulomb energy of the first excited state. We have investigated the interplay of the mutual Coulomb repulsion and confining potentials below. Figure 3.6 illustrates the values for the dot with two holes. The red dots show the additional energy of these two holes due to

Coulomb interaction in the $M = 0$ ground state. The orange dots depict this Coulomb energy in one of the next excited states with $M = 1$. Finally the blue dots show the additional energy between the $M = 0$ and $M = 1$ states only due to the confinement³. Clearly for the $M = 1$ excited state the sum of the dot-(blue) and Coulomb-(orange) energy stays above the ground-state Coulomb energy (red). The $M = 0$ state remains the ground state. The reason for this is the large Coulomb energy in both states. Its dominance is clearly visible in figure 3.6.

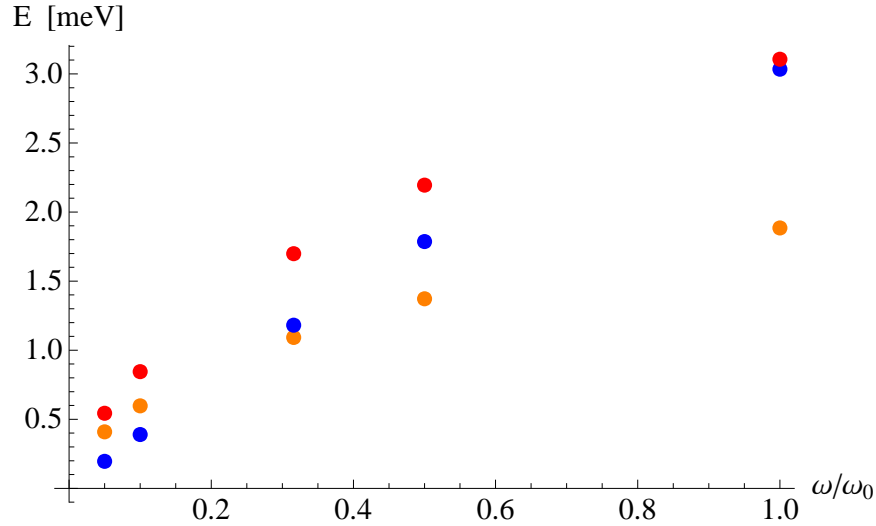


Figure 3.6: Coulomb energy of the $M = 0$ state (red), Coulomb energy of the $M = 1$ state (orange) and energy splitting between these states only due to confinement (blue) for two holes in different xy potentials.

For stronger dot potentials the shape of the ground-state hole density has a Gaussian shape. For the weakest calculated values of the xy potential this shape changes. Figure 3.7 shows the form of the ground-state wave function in the xy plane for the lowest four values of ω from figure 3.6. The xy plane is positioned at the maximum of the density in z direction. The tip of the density becomes gradually blunt with lower lateral confinement. Finally a dip forms in the centre. With weaker lateral confinement the two-hole state can no longer be described in terms of one product state of single-particle states. The eigenstates become a mixture of many such product states.

To sum up we saw that for the standard potential values (ω_0, F_0) the dot potentials dominate over the Coulomb energy of the system. A description of the two-hole state in terms of one single-particle product state is possible. The ground state is not degenerate due to time inversion invariance and is a singlet. Nevertheless, in stronger magnetic field the spin expectation value

³This is the excitation energy in the single-hole spectrum.

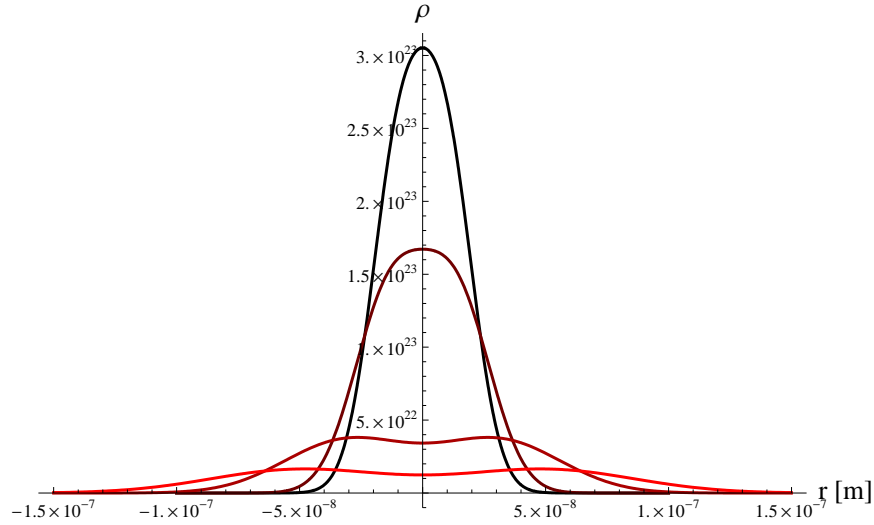


Figure 3.7: Form of the ground state hole density for the lowest four lateral confinements (0.05, 0.1, 0.32, 0.5) from figure 3.6. The z potential is F_0 .

in the ground state rises from zero and points opposite to the direction preferred by the Zeeman term. With smaller lateral potentials the single-particle product states become less accurate. The form of the density of the ground state changes gradually.

3.2.2 Three Holes

Figure 3.8 depicts the eigenstates of three holes for my standard dot. The good quantum number is the sum of the z components of all three total angular momenta. Since the z component of the total angular momentum of the system is again not an integer number, all states have to be twofold degenerate without magnetic field due to the time-inversion invariance [58], [68]. The states with $M = \pm 1/2$ are the ground states closely followed by the $M = \pm 5/2$ states. In all these eigenstates two of the holes stay approximately in the lowest Fock-Darwin state $|00\rangle$. Their spins point opposite to each other. The third hole occupies a mixture of excited single-particle states. The mutual Coulomb repulsion of the holes is considerable. The ground state of the interacting holes lies about 11 meV higher than it would without the mutual repulsion. We can no longer use the picture of independent particles described by a single-particle product state. For the standard potential value the total density of the holes in the two lowest pairs of eigenstates is approximately of Gaussian shape. The density in the somewhat energetically lifted third eigenstate pair with $M = \pm 3/2$ shows a small dip in the centre of the dot. In these both higher states only one hole stays in the $|00\rangle$ Fock-Darwin state. This change in the density resembles the evolution shown in figure 3.7. The dip in the centre arises from the admixture of

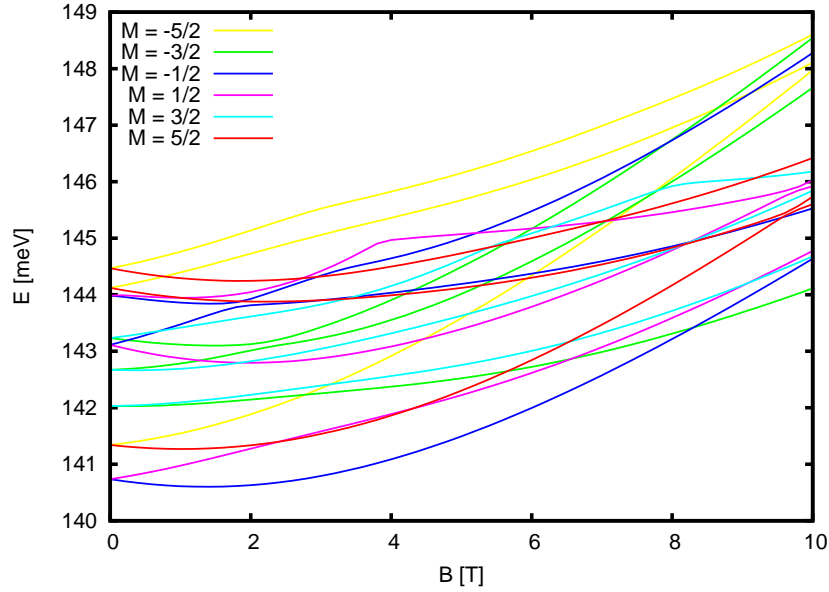


Figure 3.8: Energy spectrum of three holes in a dot with xy potential ω_0 and a z potential of F_0 .

higher Fock-Darwin basis states to the eigenstate. While in figure 3.7 this happens due to the enhanced relative strength of the Coulomb energy, the change in the $M = \pm 3/2$ eigenstate for the present three-hole spectrum arises due to excitation of one hole to higher single-particle states. For the standard potential values the state with the highest density in the dot centre and smallest extend in the xy plane is the ground state. The next state with a considerably lower density in the centre of the dot ($M = \pm 3/2$) is still ≈ 1.4 meV above the ground state. So the system is in a regime that is still determined by the confining dot potentials and not by the Coulomb repulsion. Nevertheless, this repulsion changes strongly the eigenstates of the system. Many different basis states constitute now the eigenstates of the dot. So also no hole spin component is dominant for the particular holes. In the ground state still the spins and angular momenta of two holes cancel. The expectation value of the spin also changes spatially inside the dot. This is due to the coupling of the spin to the orbital movement and to the different spatial extend of the basis functions.

To sum up the three hole dot with standard potential values is still dominated by the confinement potentials. Though the addition of the third hole further enhances the influence of the Coulomb energy. This now considerably blurs the shell-structure of the dot. The spin expectation value in the ground state is not zero. The states are all doubly degenerate at $B = 0$ T.

3.2.3 Variation of Confining Potentials

We investigated the dependence of the Coulomb interaction inside the dot on the dot potentials. We calculated the eigenstates and eigenenergies of several dots at $B = 0$ T with different confining potentials for two and three holes. Figures 3.9(a) - 3.9(c) show the additional energy of the ground state when the Coulomb interaction is turned on.

$$\Delta E = E_g(\text{w Coulomb}) - E_g(\text{w/o Coulomb}) \quad (3.5)$$

The three investigated z potentials amount to $F_a = 0.38 \cdot F_0$, $F_b = F_0$, $F_c = 2 \cdot F_0$. The x axis shows the ratio between the actual xy potential and the one of my standard dot ω_0 . The red(green) dots show the additional energy for two(three) holes. For small xy potential the system follows the square-root like dependence but for higher potential values one clearly sees a divergence from this behaviour. We have fitted corresponding square-root functions to illustrate the effect, using the first five points to fix the coefficients. Beyond the regime of the lateral confinement, where the additional Coulomb energy shows the square-root behaviour, this energy first rises slightly above the square-root law. With stronger lateral potentials it falls then significantly below the square-root curve. For stronger z potentials the effect is weaker. This change in ΔE can be connected with the band mixing due to the dot potentials. Stronger xy potentials in comparison to a fixed z potential increase the mixing of bands. This changes the effective mass of the holes. The strength of the Coulomb interaction between the holes depends only on their charge and not on their mass. The change in mass, however, strongly influences the confinement due to the dot potentials, which is the opposing force to the mutual Coulomb repulsion. The extend of the wave function determines the strength of the Coulomb energy. In a first approximation we can look at the lowest Fock-Darwin basis state for the lateral confinement to estimate the influence of the changed mass. The spatial extent of this state is governed by the characteristic length l . Equation 3.6 shows the dependence of l on the lateral confinement constant K_0 and the effective mass m of the hole inside the crystal. The length l_{ab} is the characteristic length for a particle with mass $a \cdot m$ in a dot potential $b \cdot K_0$:

$$l = \sqrt{\frac{\hbar}{\sqrt{m}\sqrt{K_0}}} \quad l_{ab} = \sqrt{\frac{\hbar}{\sqrt{am}\sqrt{bK_0}}} \quad (3.6)$$

When we increase the lateral potential $K_0 \rightarrow b \cdot K_0$ with $b > 1$ the extend of the function will fall differently for the different masses

$$\Delta l = l - l_b = l \left(1 - \frac{1}{\sqrt[4]{b}}\right) \quad \Delta l_a = l_a - l_{ab} = l_a \left(1 - \frac{1}{\sqrt[4]{b}}\right) = \frac{1}{\sqrt[4]{a}} l \left(1 - \frac{1}{\sqrt[4]{b}}\right) \quad (3.7)$$

So, for a particle with a larger mass $a \cdot m$, $a > 1$ the extend of the function will change less for the same change in K_0 . So when the hole mass rises, the same increase in the lateral confinement

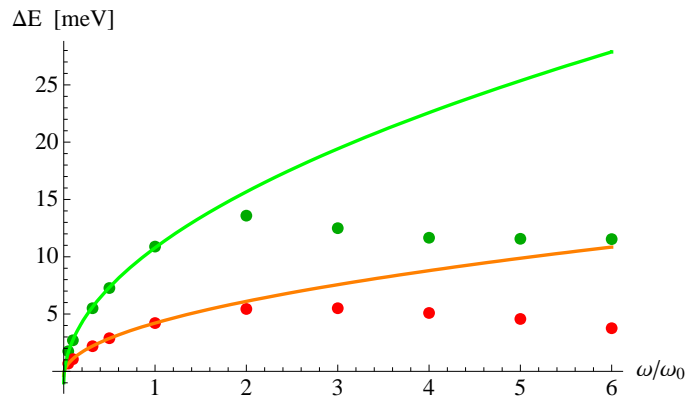
results in a smaller contraction of the wave function. This on the other hand results in a smaller increase of the Coulomb energy. The same process also acts in z direction. Here the decrease of the relative strength of the z potential enlarges the extend of the wave function in z direction. Therefore, the Coulomb energy can even fall with increased lateral confinement as in figure 3.9(a) for $\omega > 2 \cdot \omega_0$. With higher z potentials (fig.3.9(b), 3.9(c)) this decrease of the Coulomb energy shifts to higher values of lateral confinement ω . The square root dependence of the Coulomb energy on the confinement ω is known from quantum dots with electrons. They have a constant effective mass and their extend in the z direction of the dot is mostly considered constant. We observe such a behaviour also for holes for small ω/ω_0 . In this potential configuration the band coupling is small and does not change much with ω . So does the effective mass of the hole. Also the extent of the wave function in z direction is constant due to the relative large z potential. The hole behaves also very much like an electron. Notice that even in this case a magnetic field still leads to a strong change in the band coupling and thus in the effective mass.

The lowest xy potential we investigated in this way was $\omega_0 * 0.05$. The characteristic length l of the system becomes 62.1 nm for this potential values. So this quantum dots are huge in comparison to their usual sizes of some nm to some tens nm . Even for this very low potential the ground state of two holes was among all eigenstates the one with the highest hole density and thus the biggest Coulomb energy.

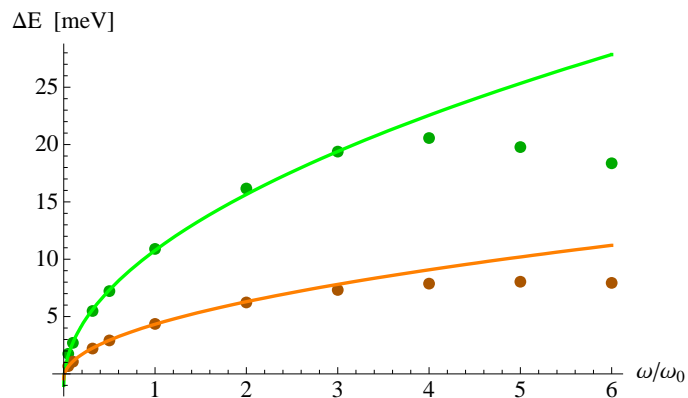
As a conclusion we can draw that for strong z confinements in relation to the lateral potential the holes behave very much as electrons with an effective two-level spin of nearly $3/2$. For comparable xy and z potentials the band coupling changes the effective mass of the holes. With the different masses the holes change their behaviour in further rising potentials. An increase of one confining potential rises the quantisation energy but does not change the extend of the wave function. Thus there is no simple coupling scheme between the evolution of the Coulomb energy and the dot potentials.

3.3 Quantum Dot with One Mn Impurity

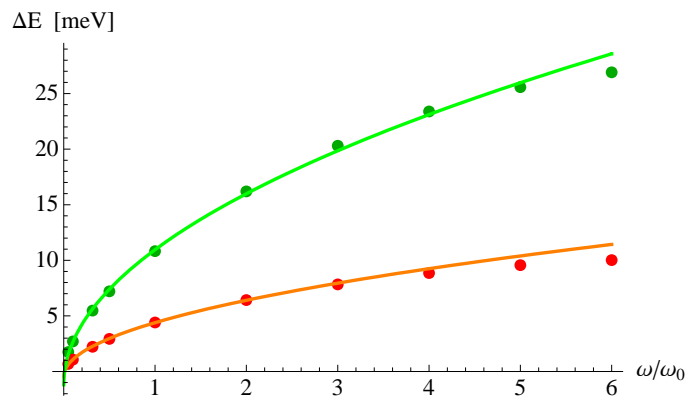
There have been different approaches to treat a manganese impurity inside a quantum dot. Govorov [69] assumed a hole bound to the Mn atom. The interaction between the hole and manganese spins he described in terms of the pd interaction and treated the dot potentials as a perturbation to the impurity states. He then calculated the excitonic states and their selective excitation by a laser pulse. In [55] Climente et al. calculated the Zeeman energy of a Mn atom in $GaAs$ under the influence of an effective magnetic field stemming from a hole confined in a disk-shaped quantum dot. Temperature dependence as well as an addition of a second hole were considered. Fernández-Rossier [70] calculated the spectrum of excitons in a II-VI semiconductor dot with up to three Mn atoms. He used a box potential with large single-particle energy spacing. Only the



(a)



(b)



(c)

Figure 3.9: Coulomb energy for two (red) and three (green) holes. The dots are calculated values. The curves are squareroot-like functions fitted to the first five values. The z potentials are: (a) $F = 0.38 \cdot F_0$; (b) $F = F_0$; and, (c) $F = 2 \cdot F_0$;

lowest eigenstate was considered and the Coulomb interaction between electron and hole was neglected. Bhattacharjee [71] calculated the response of the manganese spin in a quantum dot on the creation of an exciton by a laser pulse. He used a model similar to [59]. Together with Chutia [56] he calculated the dependence of the hole eigenstates on the variation of the confining potentials in a quantum dot with a central manganese impurity. The effects of single electrons and holes in *CdTe* dots were investigated in [72]. Experimental investigations on excitonic spectra in *InAs* can be found in [73].

Our investigations will differ from the aforementioned work in that we will try to include all significant interactions in our calculations. We will calculate the common eigenstates of a hole and a manganese atom inside a circular quantum dot. Since we are dealing with relatively large quantum dots the orbital magnetism as well as the Coulomb interaction between the holes will have an impact on the states. We will also consider a quantum dot formed at a heterojunction. Here the triangular potential couples the light- and heavy-hole bands stronger than a square well potential. Finally we will show the changes in the eigenstates depending on the magnetic field, on a variation of the confining potentials and a change in the position of the *Mn* atom.

We represent the envelope part of the *pd* coupling term (2.70) in our basis of Fock-Darwin basis functions and add it to the one particle matrix. We have to increase the size of our basis to take account for the spin state of the manganese. The matrix elements for the acceptor potential of the manganese are first calculated numerically and stored. The Hamiltonian matrix including all interactions is then diagonalised to obtain the eigenvalues and eigenvectors.

3.3.1 Strength of the Used Potentials

In the investigations on the influence of a manganese acceptor inside the dot, different dot-potential configurations will be used. The results can partially be explained by the dominance of one or several of the used potentials over the remaining ones. In this section we will refine the meaning of a “dominant” potential.

The strength of a potential can be seen e.g. by considering the energy necessary to free the confined particle. The constant potential in our investigations will be the acceptor potential of the manganese. In bulk *GaAs* the manganese acceptor can confine a hole 112 meV above the valence band. In the negative-energy picture used here this accords to -112 meV. In our model, however, we can never reach this energy. In the model for the acceptor states in the frame of the envelope function approximation [74] the ground-state energy results only to $V_{acc} = -26$ meV [71]. The energy of the excited states is predicted in congruity with the measurements. To cure this inaccuracy a correction to the potential of the acceptor atom has to be introduced. It is called the Central Cell Correction. We omitted this correction. This may seem a prohibitively rough approximation. Now, our investigation depends on the relative strengths of the used potential and not on their absolute value. So when the acceptor potential used in this calculations is underestimated the values for its competitors, the dot potentials, are also chosen smaller. The

reported effects depend on the geometric form of the potentials confining the holes. Since the central cell correction changes the Coulomb potential of the acceptor in a radius of $\approx 0.3 \text{ nm}$ from the impurity, it will also have a strong influence on the geometric form of the confinement potential in this radius. Hole states in dots have an extend of at least ten times this value. The dot potentials are positive repulsive potentials. Among them the confinement in growth direction is the strongest. In *GaAs* our standard potential strength in z direction, F_0 , leads to a ground-state confinement energy of a heavy hole (mass $m_e/(\gamma_1 - 2\gamma_2)$) of 39.84 meV and for a light hole (mass $m_e/(\gamma_1 + 2\gamma_2)$) of 64.12 meV. In comparison to the energy of $V_{acc} = -26 \text{ meV}$ this potential is larger but we will not call it dominant. The stronger z potential of $4.3 \cdot F_0$ leads to confinement energies of 105.12 meV and 169.19 meV for heavy and light holes respectively. This potential will clearly dominate the acceptor potential. The form of the hole wave function in z direction will rather resemble an Airy function, i.e. an eigenfunction to the triangular dot z potential, than a spherical symmetric function belonging to the acceptor potential. The lateral dot potentials in the xy plane are typically smaller than the acceptor potential. For a lateral potential of ω_0 the ground-state energy of a heavy hole is 3.10 meV and for a light hole 2.26 meV. In comparison to this potential the acceptor potential is dominant. This changes for the configuration $5 \cdot \omega_0$. The heavy-hole ground-state energy is 15.49 meV and for a light hole 11.28 meV. So the acceptor potential loses its dominance here. Note that the ground state of the system is a potential dependent mixture of the light and heavy holes.

3.3.2 *GaAs* Quantum Dots

When we include a manganese atom in the dot, we get an additional degree of freedom, which is the manganese spin. It can take six possible directions $S_z = +5/2, +3/2, +1/2, -1/2, -3/2, -5/2$. While the Coulomb potential of the manganese atom affects the orbital movement of the holes inside the dot, the Mn spin will couple to the spin of the holes via the pd interaction. We want to treat the system fully quantum mechanical. So our new Hilbert space for the solutions of the systems Schrödinger equation will be the tensor product $\mathcal{H}_{J_z} \otimes \mathcal{H}_{S_z}$ of the old four dimensional space \mathcal{H}_{J_z} spanned by $|\mathbf{J} = 3/2, j_z\rangle$ and the six dimensional space \mathcal{H}_{S_z} spanned by $|\mathbf{S} = 5/2, S_z\rangle$. Additional to the Hamiltonian describing the motion of the hole in the dot H_h (see Eq.2.20) we have to consider the terms describing the new interactions

$$H = H_h + \mathbb{1}U_{acc}(\mathbf{r}) + \overline{|f(\mathbf{R}_I)|^2} \frac{J_{pd}}{3} \langle S_z, j_z | \mathbf{S} \cdot \mathbf{j} | S'_z, j'_z \rangle. \quad (3.8)$$

Here $\mathbb{1}$ is an identity matrix. The acceptor potential U_{acc} acts only on the orbital part of the hole wave function. The last term acts on the spins of the hole and manganese. The coupling strength is determined by the density of the hole at the site of the impurity $\overline{|f(\mathbf{R}_I)|^2}$. The acceptor potential changes strongly the potential landscape of the dot. The dot potential is repulsive and (approximately) infinitely high, i.e. it can confine infinitely many holes. Contrary the acceptor

potential is attractive and can attract only one hole. Then the charges of acceptor and hole will cancel out any influence on further holes. This picture is, however, strongly dependent on the relative strength of dot and acceptor potentials. For large dot potentials the acceptor will merely disturb the dot eigenstates.

First we put the manganese atom in the centre of the dot's xy plane. In z direction we will always choose the position where the lowest z basis function of a heavy hole has its maximum. In most cases the confinement of the hole in z direction is much stronger than the confinement in the xy plane. It also exceeds the strength of the acceptor potential. So the z dependence of the ground-state hole wave function will be very similar to the lowest z potential eigenfunction. This is the heavy-hole z basis function. Such a choice assures that the manganese will be almost in the maximum of the hole density in z direction. For a quantum dot with standard potential values the probability for a hole to be in the central unit cell, the one that contains the Mn atom, is $P_{CC}^{00} = 0.00039$ for the Fock-Darwin basis state $|00\rangle$. This is the most centred basis state and the main part of the ground state of the dot. The probability for the hole to occupy the central cell will rise strongly in the eigenstate of the system in comparison to this basis state due to the strong acceptor potential of the manganese. Nevertheless, we can expect that with this very small value of P_{CC}^{00} the interaction of the manganese with the hole spin will be very weak compared to the other energy scales. Using (2.70) we can calculate the energy splitting between different mutual alignments of the hole spin j_z and the Mn spin S_z . With this probability the splitting amounts to ≈ 0.031 meV. The next higher hole state is ≈ 2.5 meV above and because its envelope function mainly consists of the $|0 \pm 1\rangle$ Fock-Darwin state, the density of the hole in the centre of the dot is almost zero. So we can expect that the manganese will only interact with the ground state of the hole and, as the spin of the hole is concerned, it will be close to $j_z = \pm 3/2$. To increase this small interaction energy between the hole and the Mn atom one has to increase the hole density in the dot by increasing the confining potentials. We calculated the eigenstates of a dot with a Mn atom for standard potential values and also for a dot with a xy confinement $5 \cdot \omega_0$ and a z potential of $4.3 \cdot F_0$. Since $\omega = \sqrt{K_0/m}$ this translates in $K/K_0 = 25$, i.e. the lateral confinement is 25 times as large. Notice that due to the confinement dependent mass of the hole this does not translate in 5 times larger energy spacing. The figures (3.10) and (3.11) show the energy eigenstates of these two different dots.

Let us first consider the dot with standard potential values (Fig. 3.10). The twelve lines represent the twelve different possible alignments between the two lowest hole states and the six possible alignments of the manganese spin $\mathbf{S} = 5/2$, $S_z = +5/2, \dots, -5/2$. The state of the hole is not an eigenstate of j_z but for the lowest two states of the hole one spin component, $j_z = +3/2$ or $j_z = -3/2$ is dominant in one of the two states. The expectation value of the hole spin $\langle j_z \rangle$ is ± 1.42 respectively. As in the dot without the manganese, the coupling between different j_z is an effect of the band coupling in the Kohn-Luttinger matrix. The expectation values of the manganese spin are very close to the eigenvalues of the \hat{S}_z operator. The coupling between different

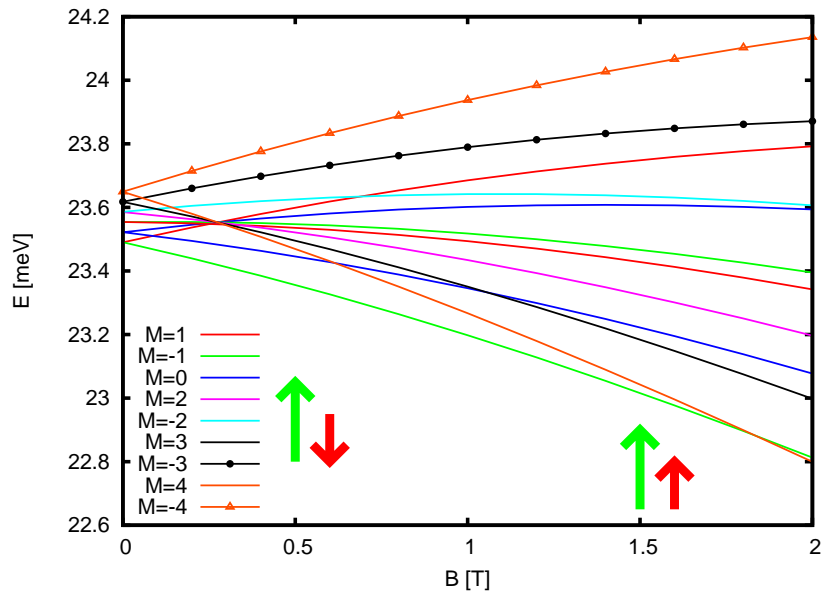


Figure 3.10: Energy spectrum of one hole with standard potential and a Mn atom in the centre.

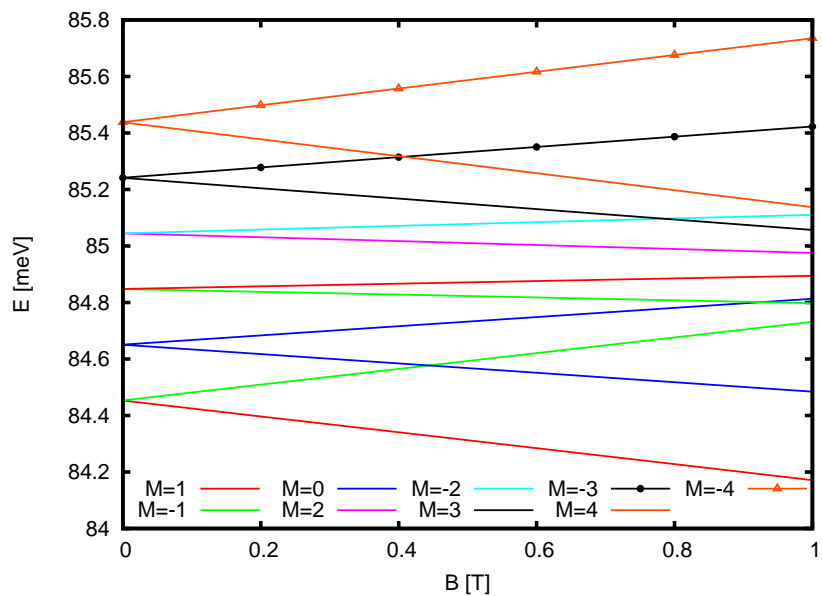


Figure 3.11: Energy spectrum of one hole and a Mn atom in the centre. The dot xy potential amounts to $5 \cdot \omega_0$ and z potential to $F = 4.3 \cdot F_0$.

spin alignments of the manganese almost vanishes when the impurity atom is in the centre of the dot. At $B = 0$ the states with similar mutual alignment of the hole and manganese spins are energetically degenerate. The magnetic field splits these states due to different Zeeman energies. $M = S_z + M_h = S_z + j_z + m$ is here a good quantum number. It is the sum of the z component of the manganese spin S_z , the z component of the hole total angular momentum j_z and the z component of the envelope function angular momentum with the quantum number m . The conserved quantum number M can take the values $M \in (0, \pm 1, \pm 2, \pm 3, \pm 4)$. In the dot with the weaker confining potential (Fig. 3.10) the arrows show the spin alignments in the ground state: Hole spin (red) and manganese spin (green). The state $M = 1$ is the ground state for the most part of the calculated range of the magnetic field. The spins in this state are aligned maximally antiparallel due to the anti-ferromagnetic pd interaction. The dominant spin components are $|S_z\rangle = 5/2$ and $|j_z\rangle = -3/2$. The state $M = 4$ has a stronger negative Zeeman energy and crosses $M = 1$ at $B = 1.7$ T. The spin alignment in $M = 4$ is $|S_z\rangle = 5/2$ and $|j_z\rangle = +3/2$. Notice that the magnetic field points in the $-z$ direction. Due to stronger confinement in the dot in Fig. (3.11) the slopes of $M = 1$ and $M = 4$ differ not much. The now bigger anti-ferromagnetic pd interaction between the spins prevents the hole from aligning following the Zeeman energy even in strong magnetic fields. When the quantum dot is determined by a top metal gate we have control over the lateral confinement. So, by changing the confinement potential one can control the alignment of the hole spin at some fixed magnetic field.

The Landé factor for the manganese spin is $g_{Mn} = 2$ [55] and for the hole $g_h = 2 \cdot \kappa = 2.4$. With the larger manganese spin the Zeeman energy of the manganese is bigger. In the following I will show why it is impossible to control the alignment of the manganese by changing the hole state in the magnetic field: While the magnetic field becomes stronger the pd interaction between hole and manganese is almost constant⁴ while the Zeeman energy of hole and manganese rises linear with it. It can become considerably stronger than the pd interaction energy. Also the band coupling effect which can change the spin of the hole becomes stronger with magnetic field and can even overwhelm the Zeeman energy of the hole. We can expect that for stronger magnetic fields the spin alignments of hole and manganese will be determined by these effects. Only for weak fields the pd interaction can play a significant role. Without magnetic field the two lowest states $|S_z\rangle = \pm 5/2$ $|j_z\rangle = \mp 3/2$ are degenerate. These states have the largest negative pd interaction energy. In a very weak magnetic field this degeneracy is lifted. The pd energy stays the dominant term and is almost the same in both states. The spins stay aligned antiparallel.

In weak magnetic fields we can distinguish two regimes for the hole state. As shown in section 3.1.2 the hole spin here depends on the strength of the xy potential. In weak potentials the hole spin aligns according to the Zeeman term. According to figures 3.2(a)-3.2(d) the band coupling in strong dot xy potentials lowers the energy of the $|j_z\rangle = -3/2$ state, which then becomes the lowest hole state. The manganese atom is influenced besides the pd interaction only by its

⁴For a hole in a quantum dot the magnetic field increases its density in the centre slightly. When the manganese impurity is put here, the interaction energy will rise also only accordingly to the increase of the hole density.

Zeeman energy. In a dot with strong confining potentials (Fig. 3.11) and in weak magnetic fields the state $|S_z\rangle = 5/2 |j_z\rangle = -3/2$ will be at lower energy. The manganese spin in this state has the minimal Zeeman energy and the hole is also in its preferable state due to the influence of the band coupling. For stronger magnetic fields the pd interaction loses influence but with the strong xy potential the same spin alignment of the hole is preferred. The ground state stays the same as for weak magnetic fields. In the second regime with the weaker xy potential (Fig. 3.10) the hole spin will be determined by its Zeeman energy in most realistic magnetic field regimes⁵. In weak magnetic field the spins have to align antiparallel. The Zeeman energy of the manganese atom is stronger than the Zeeman energy of the hole. Here also the state $|S_z\rangle = 5/2 |j_z\rangle = -3/2$ will be the ground state. When the magnetic field grows stronger the interaction energy again loses influence and both spins align according to the Zeeman term. A flip of the hole spin occurs in the ground state. It can be easily shown that no other spin configuration can have a lower energy than the ones mentioned. So in all possible cases the manganese spin points according to the Zeeman term and does not change. The competition between the hole Zeeman energy and the band coupling effect can only change the spin of the hole. Since the Zeeman energy of the hole is lower than the one of the manganese, this change releases not enough energy, to alter the manganese spin. So, to control the manganese spin we have to limit ourselves to the $B = 0$ T case.

The crossing of half of the states at one point in figures (3.10) and (3.11) is caused by the dependence between the energy of the states at $B = 0$ T and their dispersion with magnetic field. Both values depend on the relative alignment of the hole and manganese spin. This alignment determines the pd interaction energy and thus the energy at $B = 0$ T. It also sets the Zeeman energy. The straight slopes point out that this energy term dominates the magnetic field dispersion of the states. In all the crossing states the spin alignment of the hole is $j_z = 3/2$ and only the manganese spin state differs among them. Now, at the crossing point the difference in the pd interaction energy between any two of the crossing states is exactly compensated by the difference in the Zeeman energy between these states. In experiments sensitive to the hole spin a prominent difference for the two spin alignments can be expected at this value of the magnetic field.

In the dot with the large confining potentials (Fig. 3.11) the energy difference between the lowest two alignments of hole and manganese spin amounts to 0.197 meV at $B = 0$ T. This is 6.2 times the value of the small-confinement dot. The density of the hole at the manganese site in the strong confinement regime is 6.3 times as large as for the low confinement. The increase of the pd interaction energy follows the increase of the hole density. In this spectrum the states follow the Zeeman term. In figure (3.11), however, also a deviation from this scheme can be observed. $|M = \pm 1(2)\rangle$ are the first excited states with total angular momentum z component $M = \pm 1$. They arise from the third doublet at 84.85 meV and have a slope opposing their Zeeman energy. The spins in these states are $|M = 1(2)\rangle = |S_z = -1/2, j_z = 3/2\rangle$

⁵For our standard configuration this ordering is present between 0 T and 9 T (see figure 3.2(a)).

and $|M = -1(2)\rangle = |S_z = 1/2, j_z = -3/2\rangle$. According to the Zeeman term, the slope of the $|M = -1(2)\rangle$ state should be positive while the one of the $|M : 1(2)\rangle$ state should be negative. The reason for the inversion of the slopes in the spectrum is the influence of the band coupling on the hole states. In this two states the Zeeman energies of the hole and the manganese atom nearly cancel out and the strong in-plane confinement of the hole pushes the $|j_z\rangle = -3/2$ state below the $|j_z\rangle = 3/2$ state. This influence on the hole spin is present in all states. In the remaining states, however, the Zeeman energies of the hole and especially of the manganese are stronger and determine the alignment of the spins. In the case of the weak confinement the states are not inverted. In figure 3.10 beyond $B = 0.5$ T these are the 6th and 7th lowest state. So here their ordering resembles their Zeeman energies. Also in a dot without the manganese atom for this xy potential $|j_z\rangle = 3/2$ should be lower in energy. However, these both states have a very parallel dispersion in the magnetic field and the splitting between them is small. The reason for this change is the acceptor potential of the manganese atom. It changes significantly the dot potentials and changes thus the band coupling.

The third potential configuration we calculated with a manganese atom in the centre was $\omega_0 \cdot 5, F = 7$ mV/nm (not shown). For this potential configuration the band coupling is strong and the lowest hole states have already a large light-hole admixture, i.e. of states with $j_z = 1/2$. This changes considerably the hole spin expectation value, which is $\langle j_z \rangle = \pm 1.21$ in the lowest two states. The hole density at the manganese site is 0.57 of the value in the configuration in figure 3.11 with a 4.3 times larger z potential. The lowering of the hole density in this configuration is due to the larger spread of the lowest envelope function in z direction in the lower confining potential. The splitting between two of the doublets amounts to 0.11 meV. This is 0.56 times the value of the configuration with the strong z confinement. This splitting is a measure for the strength of the pd interaction. Again it follows the change in the density of the hole at the manganese site. The change of the expectation value of the hole spin $\langle j_z \rangle$ due to the changed band coupling has no influence on the interaction energy. We give these values for comparison with configurations discussed later in the text.

Here we have shown the dependence of the interaction between the hole and the manganese on the dot potentials. The change in the hole density due to a stronger confinement is the most important factor for the strength of the pd interaction between the spins. This interaction is, however, much weaker than the dot and acceptor potentials. Only the lowest hole state participates in the common interacting hole and manganese state. In this ground state the hole spin is an effective two-level system with expectation value close to $\langle j_z \rangle = \pm 3/2$. It is changed by different admixtures of light holes due to changed dot potentials. In magnetic field the alignment of the manganese spin is determined only by its Zeeman energy. In weak fields the spin of the hole aligns antiferromagnetically to the manganese spin due to the pd interaction. In stronger fields the hole spin aligns ferromagnetically due to its rising Zeeman energy. The magnetic field where the change between these two alignments occurs is for weak band mixing dependent on the pd

interaction. When the band mixing is large the spin of the hole is aligned opposite to its Zeeman term even without the interaction to the manganese. Here the ground state may never change from the weak field alignment. An investigation on the effects of different potential aspect ratios on the hole spin in diluted magnetic semiconductors can be found in [75].

3.3.3 Influence of the Lateral Confinement

We have also varied the strength of the confining potential in the xy plane at zero magnetic field. The range went from $0.1 \cdot \omega_0$ to $6 \cdot \omega_0$. The z confinement was constant at $F = F_0$. Figure 3.12 shows the energy of the ground state. The energy drops slightly with increasing potential until $3 \cdot \omega_0$ and then rises slowly. The lowering of the ground-state energy with increasing potential is in striking difference to the undoped dot, where the energy rises linearly. This effect arises due to the competition of the confining- and the acceptor-potential. The energy of the hole changes differently in these two potentials with the distance from the centre of the dot. The stronger localisation due to the larger dot potentials creates a stronger proximity to the acceptor atom. In the potential range used here this effect lowers the total energy. Also the effective mass of the hole is changed with the dot potential. The light-hole character of the states increases with stronger xy potential. Nevertheless, the dominant hole-spin state stays $j_z = \pm 3/2$ even for $6 \cdot \omega_0$. The change of the hole effective mass influences the impact of the dot potential on the movement of the hole. It changes the ratio at which the hole wave function shrinks with increasing dot potential. All these effects sum up to the shown behaviour. Figure (3.13) illustrates the absolute value of the energy splitting between the two lowest doublets in the spectrum of a hole and a manganese atom $E_{pd}(\omega/\omega_0)$. This value represents the strength of the pd interaction between the spins. The change of the pd interaction energy can result from different sources. The most likely reason is the change of the hole density at the site of the impurity. Another reason could be a change in the spin expectation values of the hole and of the manganese. To compare the evolution of the density $\rho(\omega/\omega_0)$ and pd splitting energy $E_{pd}(\omega/\omega_0)$ we normalise both. We divide the evolution of the density by the density value at $\omega/\omega_0 = 1$ and the evolution of the pd splitting by the splitting at $\omega/\omega_0 = 1$:

$$\frac{E_{pd}(\omega/\omega_0)}{E_{pd}(1)} = \frac{\rho(\omega/\omega_0)}{\rho(1)}. \quad (3.9)$$

These normalised diagrams match exactly in all calculated points. The diagrams of both evolutions look exactly like the one depicted in figure (3.13). Therefore, the gain in E_{pd} can be attributed solely to the change of the hole density.

We notice a slower gain in E_{pd} with the confining xy potential beyond $\omega/\omega_0 = 2$. Around this point we also see a change in the behaviour of the ground-state energy gain with the xy potential in figure (3.12). The growth of the hole density is the only relevant factor in the change of the pd splitting. The relevant effect on the hole density here is similar to the one described in section

3.2.3. The change in the effective masses lowers the contraction of the hole wave function with the increasing dot potentials. The change of the hole-spin expectation value due to the changed admixture of the light holes, in contrast, has no effect on the interaction energy between the spins of the hole and the manganese. This higher admixture makes the hole spin expectation value deviate stronger from $\pm 3/2$ which would be the value for pure heavy-hole bands. With the changed spin for the holes also the expectation value of the manganese spin deviates stronger from the eigenvalues of \hat{S}_z . This behaviour is what one can expect: Without a magnetic field the manganese spin has no preferable direction. It aligns according to the hole spin. When the direction the hole spin changes the manganese spin is aligned accordingly to it. For this reason, only a change in the hole density at the manganese site has an influence on the energy splitting due to pd interaction.

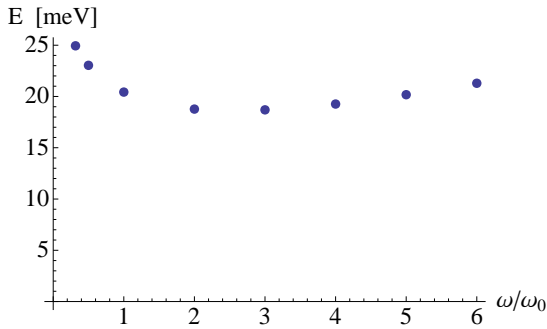


Figure 3.12: Ground state energy in a dot with one Mn atom in the centre for different values of the xy potential and a z potential of $F = F_0$.

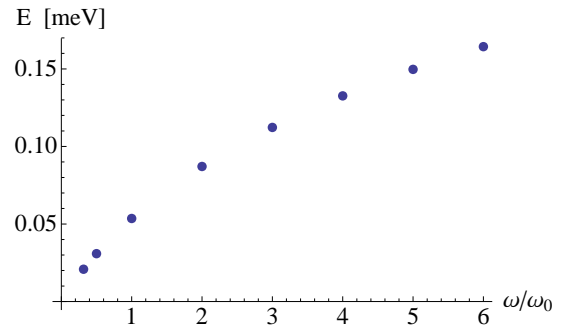


Figure 3.13: Splitting of lowest states due to pd interaction in a dot with one Mn atom in the centre E_{pg} for different values of the xy potential and a z potential of $F = F_0$.

The total spin in the present configuration is an integer number. So, the eigenstates do not have to be degenerate at vanishing magnetic field. Still a degeneracy occurs between the states with $\pm M$. Without a magnetic field no net magnetisation of the dot is possible.

In our calculations we have not taken into account the central cell correction. This correction to the Kohn-Luttinger theory is necessary to reproduce the experimentally measured value of the ground-state energy of the hole [53]. The energies of excited states of the hole are predicted accurately by the $\mathbf{k} \cdot \mathbf{p}$ theory and the envelope function approximation even without this correction. Its addition would lead to a stronger localisation of the hole at the manganese position. The influence of the acceptor potential would, therefore, rise relative to the dot potentials. If the dot potentials are weak the acceptor potential dominates and the system resembles more a single acceptor impurity in bulk $GaAs$ [69]. In the spherical symmetric potential of an acceptor

different alignments of the hole spin j_z are not degenerate. Hence the total angular momentum $\mathbf{F} = \mathbf{S}_{Mn} + \mathbf{J}_h$ (particularly F^2) is a good quantum number. The eigenstates of the system hole + manganese belong to the subspaces with $F = 1, 2, 3, 4$. The states with $F = 1$ are lowest in energy. The ground state is then threefold degenerate and formed by the $|\mathbf{F}, F_z\rangle$ states $|1, 1\rangle$, $|1, 0\rangle$ and $|1, -1\rangle$.

The ground state we found has a different spin alignment. In our calculations the hole takes predominantly only the two $j_z = \pm 3/2$ states, i.e. has only two alignments. The interaction of the manganese impurity with a similar system was studied in [76], [77]. Here the interaction with excitons in a *CdTe* quantum dot was investigated. In this II-VI semiconductor manganese is isoelectric. So, it only introduces its $|\mathbf{S}| = 5/2$ spin into the quantum dot. The exciton spin takes only the values ± 1 . In its spectrum the recombination energy splits in six peaks. They resemble the six possible alignments of the $5/2$ manganese spin to one spin state of the exciton, each with a different *pd* interaction energy. For the standard values of quantum dot potentials chosen by us we are far away from the $|\mathbf{F}, F_z\rangle$ regime. Especially the strong confinement in z direction splits the j_z states of the hole energetically and the total angular momentum \mathbf{F} ceases to be a good quantum number. An addition of the central cell correction would at most change the values of the dot potential, where a clear transition between the two regimes is visible. The addition of the correction would not change our qualitative explanation. The results of the variation of the confining potentials in a quantum dot with a manganese impurity also including a central cell correction were published in [56]. Their results agree qualitatively with our calculations. The quantum dots used in their investigations were much smaller and their potential in z direction was a symmetric quantum well.

To sum up we have shown that within our model and dot potentials range the spin states $j_z = \pm 3/2$ and $j_z = \pm 1/2$ of the hole in a dot with manganese are not degenerate. So the system does not resemble a bulk acceptor state. The density of the hole at the position of the manganese impurity is the only factor determining the strength of the *pd* interaction. During the variation of the dot potentials we see the influence of the change in the hole effective mass on the wave function evolution, as in section 3.2.3. Due to the acceptor potential, the extend of the hole wave function also strongly affects the energy of the ground state.

3.3.4 *InAs* Quantum Dots

Compared with *GaAs*, the response of the hole spin to the application of a magnetic field in an *InAs* quantum dot is different. Due to the strong Landé factor $g(\text{InAs}) = 2 \cdot \kappa$ with $\kappa = 7.68$ for the hole, the Zeeman energy of the hole is bigger than the one of the manganese atom. The *InAs* effective masses of light- and heavy-holes in z direction differ much more than in *GaAs*. While the heavy hole z masses are comparable, the light hole mass is only 0.25 times the mass in the former material. This splits the heavy and light hole subbands far apart. The lowest levels

in the quantum dot have, therefore, a strong heavy hole character. The *InAs* heavy hole mass in *xy* direction is 0.32 times the one in *GaAs*. The characteristic length for eigenstates of the two-dimensional harmonic oscillator in the *xy* plane is

$$l_i = \sqrt{\frac{\hbar}{m_i \omega_0}} = \sqrt{\frac{\hbar}{\sqrt{m_i} \sqrt{K_0}}} \quad \text{and with} \quad m_1 = a \cdot m_2 \quad \Rightarrow \quad \frac{l_2}{l_1} = \frac{1}{\sqrt[4]{a}}. \quad (3.10)$$

With the *InAs* lateral mass $m_{InAs} = 0.32 \cdot m_{GaAs}$ the characteristic length in *InAs* is 1.33 times the value of *GaAs* in the same *xy* potential. The hole density is more spread out in *InAs* within the same potentials. We, therefore, have to use stronger confinement potentials to achieve a comparable hole density at the manganese site and thus a comparable interaction with the manganese spin. To describe the Coulomb attraction between the manganese impurity and the hole in *InAs* we used for the dielectric constant $\epsilon_r(InAs) = 15.15$ [78]. J_{pd} , which describes the strength of the *pd* interaction between the hole and *Mn* spins, is not known for *InAs* to our knowledge. The value for *GaAs* is also not known exactly [71]. These two materials have the same crystal structure with a similar lattice constant. On the atomic length scale the *pd* interaction depends on the overlap of the hole valence band *p* orbitales with the localised manganese *d* orbitals. The *p* orbitals originate from the arsenide atoms, while the manganese typically substitutes a gallium atom in the lattice. So this overlap will certainly depend on the lattice constant. It is reasonable that the values should be of the same magnitude for both materials. We will take, therefore, the same value for *InAs* as for *GaAs*: $J_{pd}(InAs) = J_{pd}(GaAs) = 40 \text{ meV nm}^{-3}$. As in *GaAs*, in *InAs* the energetic splitting between the hole ground states and the first excited ones is much larger than the splitting due to the *pd* interaction. Even with a $J_{pd}(InAs)$ value twice as large the influence of the excited states would be negligible. Apart from a larger splitting we would get qualitatively the same spectrum. Note that in our calculations we did not account for any strain inside the dot. This approximation is justified, because the dots we are investigating are larger than self-assembled dots and the influence of strain for our dots is smaller. Moreover strain in self-assembled quantum dots typically further splits the states dominated by the $j_z = \pm 3/2$ and $j_z = \pm 1/2$ Bloch bands. The influence of the $j_z = \pm 1/2$ bands on the ground state is remarkable in our calculation. We can vary their admixture by changing the aspect ratio of vertical and lateral dot potentials. So a further splitting of the bands would alter the ratio needed to achieve a certain admixture.

In figure 3.14 we see the spectrum of an *InAs* dot. To avoid only a small splitting of the eigenstates at $B = 0 \text{ T}$ and fit the strength of the *pd* interaction better into the magnetic field range being under investigation we increase the strength of the lateral confinement. The confining potential in *xy* direction accords to a potential of $6.3 \cdot \omega_0$ in a *GaAs* dot. The potential in *z* direction is $F = 4.3 \cdot F_0$. The spectrum is dominated by the hole Zeeman energy which splits the states into two bunches with dominant hole-spin component $j_z = +3/2$ and $j_z = -3/2$. The alignments of the manganese spin relative to the hole spin splits both bunches in six states.

As described in section (3.1.3) no inversion of the ordering of the hole ground states is possible for *InAs* quantum dots by variation of the dot potentials. This is in contrast to *GaAs* quantum dots. For these we have shown such an inversion in section 3.1.2. In *InAs* quantum dots the ordering of the two lowest states is always determined by their Zeeman energy. The state with the lower energy in magnetic field has a total hole angular momentum $M_h = +3/2$. For a dot with the manganese atom and in magnetic fields below 0.8 T, the ground state of the system is $|M = -1(1)\rangle = |S_z = -5/2\rangle |M_h = 3/2\rangle$. Different from *GaAs*, the hole is aligned according to its Zeeman term while the manganese points opposite to it. For stronger magnetic fields the lowest state becomes $|M = 4(1)\rangle = |S_z = 5/2\rangle |M_h = 3/2\rangle$. Here, the Zeeman terms become dominant and align the spins parallel. Opposite to the *GaAs* quantum dot now the *manganese* spin flips when we increase the magnetic field. The splitting between two doublets at $B = 0$ T is a measure for the strength of the interaction between the hole and the manganese. It amounts to 0.092 meV here. This is slightly above the value from the *GaAs* configuration (0.084 meV) in Fig. 3.11 where the *xy* potential was 0.79 times as high. This depicts the lesser confinement of the hole by the potentials in *InAs*. Moreover, the state with parallel alignment of the spins becomes the ground state at lower magnetic fields as in *GaAs* even in comparison to a *GaAs* dot with weaker confinement (see Fig. 3.10). We see such a behaviour although the *pd* interaction in the present *InAs* dot is stronger than in that case. This happens because now the spin of the manganese flips and not the spin of the hole. The *pd* interaction energy and the Zeeman energy of the flipping particle compete. The flip occurs when the Zeeman energy overtakes the *pd* interaction. Since in *GaAs* the Zeeman energy of a hole is smaller than the Zeeman energy of the manganese and smaller than the Zeeman energy of an *InAs* hole, the flip will occur in *GaAs* at a stronger magnetic field than in *InAs*.

As in *GaAs* the crossing eigenstates contain all the same hole state. This state has the dominant $j_z = 3/2$ spin component. As mentioned in section 3.3.2 at the crossing point the sum of the Zeeman energy of the manganese atom and its *pd* interaction energy with the hole is constant. Now the crossing lies not in the centre of the spectrum any more. This is again due to the hole Zeeman energy being stronger than the manganese Zeeman energy. Independent of the alignment of the manganese spin all states with $j_z = 3/2$ hole spin alignment have a negative slope in the magnetic field. So, the crossing point has to be located energetically below the lowest state at $B = 0$ T. In *GaAs* the slope of a state was determined by the Zeeman energy of the manganese. In this material, states with the same alignment of the hole spin could rise and fall depending on the manganese spin S_z . The crossing was located in the centre in the spectra.

3.3.5 Off-Axis Mn Atoms

Currently (2009) it is technologically not possible to gain precise control over the manganese atom in a quantum dot. The position of the impurity is determined randomly during the growth

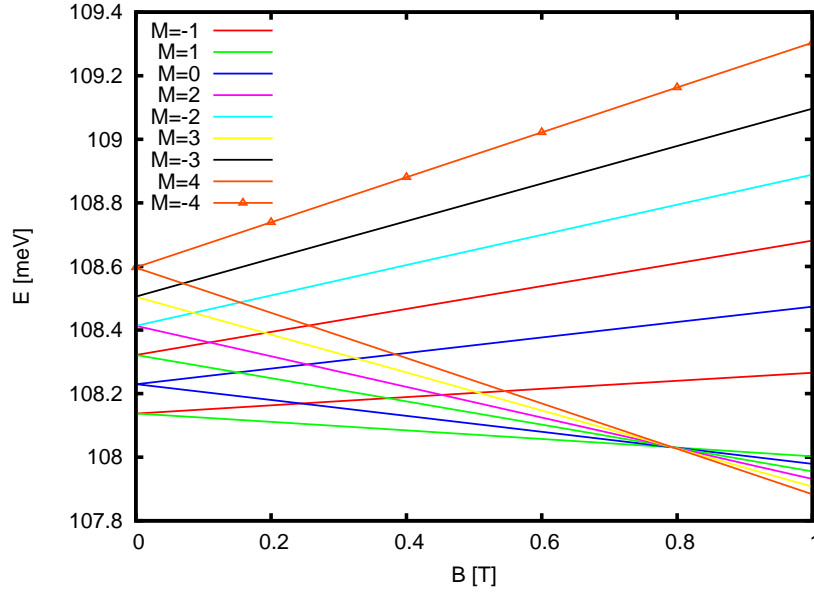


Figure 3.14: Energy spectrum of an *InAs* QD with one hole and a *Mn* in the centre. A xy potential of $6.3 \cdot \omega_0$ and a z potential of $F = F_0$ is used.

process and it will be rare to find it in the centre of the dot. It is, therefore, of major importance to examine an off-axis manganese position. Nevertheless, we will not choose it arbitrarily. The strong spread of the hole wave function and thus a lower density in large dots we are interested in yields only a very weak pd interaction between the hole and the *Mn* atom. We have to assure that the probability to find the hole at the *Mn* position remains relatively high. Figure 3.15 shows the chosen position. In the expansion of the lowest-states envelope functions, the Fock-Darwin function $|0, 0\rangle$ has a large weight. It has its maximum in the centre of the dot. The second biggest part is the basis state with $|0, \pm 1\rangle$. So, we choose the position of the off-axis impurity at the maximum of the $|0, \pm 1\rangle$ basis function. At this point the value of $|0, 0\rangle$ equals that of $|0, \pm 1\rangle$. This assures a large hole density at the manganese site and yields a noticeable interaction of the manganese atom with the hole ground state. The maximum of the $|0, \pm 1\rangle$ Fock-Darwin state lies just at the distance of one characteristic length l (2.31) from the centre of the dot. This characteristic length changes with the dot potential. So, in this arrangement, for different values of the xy potential the distance of the manganese from the centre of the dot will also change. Its position is adapted to the varying extend of the hole wave function. Otherwise, when the xy potential is increased, an off-axis manganese atom will typically lose overlap with the hole wave function. We are not interested in this effect but want comparable set-ups for all potential values. The z position will remain at the maximum of the lowest heavy hole z basis function. This function deviates only slightly from the exact envelope function in z direction.

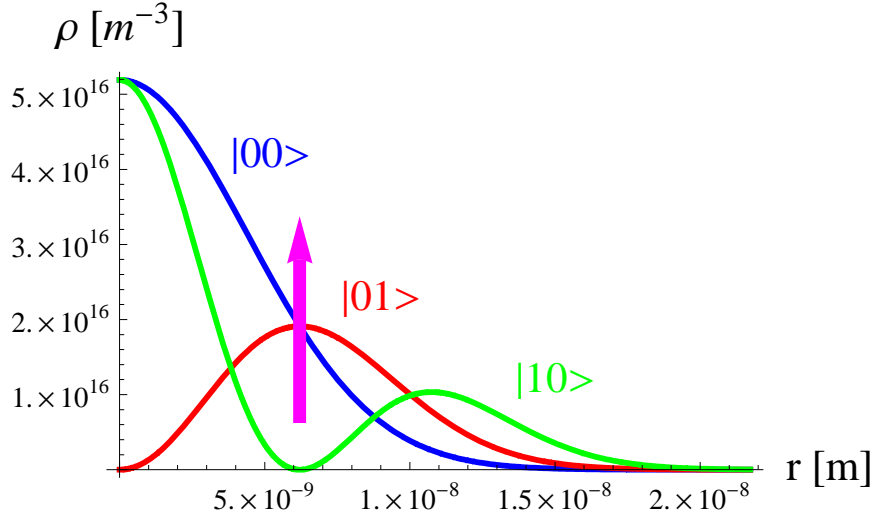


Figure 3.15: Off-axis position of the Mn impurity (arrow) in relation to the Fock-Darwin basis states.

An off-axis position of the Mn breaks the cylindrical symmetry of the system. The Hamiltonian no longer decomposes into blocks of total angular momentum z component $M = S_z + M_h$. We now have to include all possible values of the total angular momentum of the hole and the manganese spin in our calculations. To maintain computability we will always include all possible states of the manganese spin S_z and only the energetically lowest states of the hole $M_h = j_z + m$ with $M_h \in \{-7/2, \dots, 7/2\}$. This resulted in a basis size of 60 states for each hole spin j_z . The precision of the calculations is treated in section 3.6.

3.3.6 GaAs Dots, Mn Off-Axis

Fig. 3.16 shows a quantum dot with a manganese atom at a distance of 14 nm from the centre of the dot. The dot potentials are at standard values. Because the centre of the xy confining potential and the centre of the manganese acceptor potential are not located in the same point anymore, the density of the hole at the manganese site is smaller. The splitting of the six doublets is smaller than for the manganese in the centre. It amounts to 0.026 meV between each doublet at zero magnetic field. This is 83% of the in-centre energy splitting. Without conserved angular momentum different mutual alignments of hole and manganese spin are possible within one eigenstate. The degeneracy at zero magnetic field can now be broken. This is an effect of the spin flipping terms $j_{z+} S_{Mn-}$ and $j_{z-} S_{Mn+}$ in the $\mathbf{j} \cdot \mathbf{S}$ operator and of the broken circular symmetry. A splitting at $B = 0 \text{ T}$ is, however, not prominent here. Only in the 5th and 6th state the hole and manganese spin expectation values are lower than in the other states. This lowering results from a coupling between these two states. When the coupling becomes stronger the states

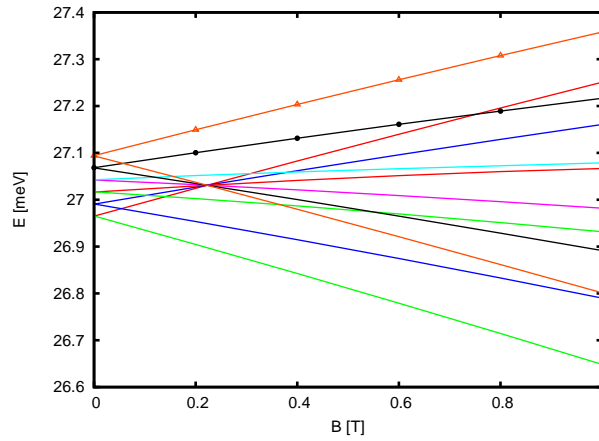


Figure 3.16: Energy of one hole and a Mn atom 14 nm from dot center, xy potential of ω_0 and z potential of $F = 7 \text{ meV/nm}$.

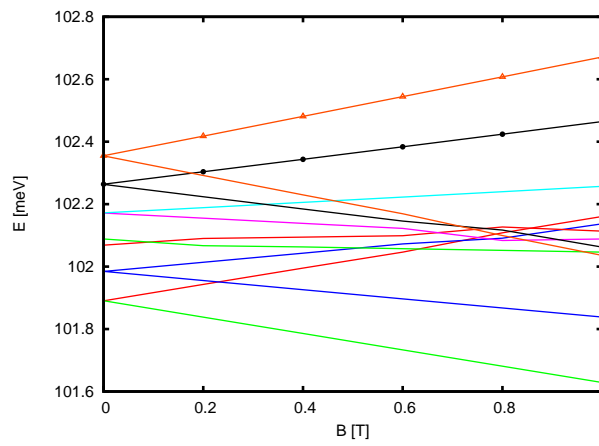


Figure 3.17: Energy of one hole and a Mn atom 6.2 nm from dot centre, xy potential of $5 \cdot \omega_0$ and z potential of $F = 30 \text{ meV/nm}$.

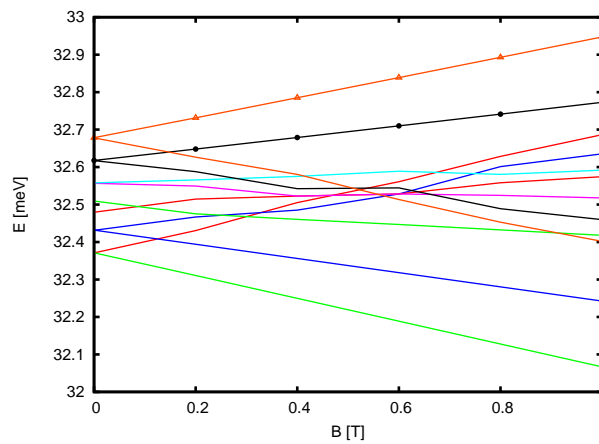


Figure 3.18: Energy of one hole and a Mn atom 6.2 nm from dot centre, xy potential of $5 \cdot \omega_0$ and z potential of $F = 7 \text{ meV/nm}$.

can even split. To explain the coupling mechanism and the special situation in the states 5/6 let us make the following considerations: When the interaction between the hole and the manganese is turned off, the lowest eigenstates of the system can be described by the tensor product of the six possible alignments of the manganese spin with the lowest two empty-dot hole states. Let us denote this hole states by $\pm h_1$

$$|S_z, \pm h_1\rangle \approx a F_{\pm 3/2} |S_z\rangle |\pm 3/2\rangle + b F_{\pm 1/2} |S_z\rangle |\pm 1/2\rangle + c F_{\mp 1/2} |S_z\rangle |\mp 3/2\rangle. \quad (3.11)$$

Here F_j is the appropriate envelope function for the Bloch band j . The coefficients a, b, c are weighting factors describing the admixture of the light hole Bloch bands with $j_z = \pm 1/2$. They show the strength of the band mixing and their values are finally determined by the aspect ratio of the confining potentials, i.e. the ratio of the z potential to the xy potential. S_z is the spin of the manganese. For lens-shaped dots the z potential is much stronger than the xy potential and a becomes much bigger than b and c . This is the case of moderate band coupling. With increased band coupling the admixture of the light holes with spin $j_z = \pm 1/2$ to the ground state is increased and the values of the a, b, c come closer together. The interaction that determines the relative alignment of hole and manganese spins is the pd interaction. When we turn it on, the undisturbed states (3.11) become coupled. This is, however, not possible to the same extent for each pair of states. The flipping terms $j_{z+}S_{z-}$ and $j_{z-}S_{z+}$ change the spin of the manganese by one. The only pairs with this difference in S_z are the fourth doublet $|\pm 1/2 \pm h_1\rangle$ and the third doublet $|\pm 1/2 \mp h_1\rangle$. The application of the flip operator on one state from each of the two pairs gives e.g.

$$\begin{aligned} j_{z+}S_{z-} | +1/2 - h_1 \rangle &= \tilde{a} F_{-3/2} | -1/2 - 1/2 \rangle + \tilde{b} F_{-1/2} | -1/2 + 1/2 \rangle \\ &+ \tilde{c} F_{+1/2} | -1/2 + 3/2 \rangle \end{aligned} \quad (3.12)$$

$$j_{z+}S_{z-} | +1/2 + h_1 \rangle = \hat{b} F_{+1/2} | -1/2 + 3/2 \rangle + \hat{c} F_{-1/2} | -1/2 + 1/2 \rangle \quad (3.13)$$

The matrix element of the pd operator (Eq. 2.70) between the states in these pairs is (apart from constants) given by

$$\begin{aligned} \langle -1/2 + h_1 | J(\mathbf{R}_I) \mathbf{S} \cdot \mathbf{j} | +1/2 - h_1 \rangle &\approx a\tilde{c} \langle F_{+3/2} | \delta(\mathbf{R}) | F_{+1/2} \rangle + b\tilde{b} \langle F_{+1/2} | \delta(\mathbf{R}) | F_{-1/2} \rangle \\ &+ c\tilde{a} \langle F_{-1/2} | \delta(\mathbf{R}) | F_{-3/2} \rangle \end{aligned} \quad (3.14)$$

$$\langle -1/2 - h_1 | j_{z+}S_{z-} | +1/2 + h_1 \rangle \approx c\hat{c} \langle F_{+1/2} | \delta(\mathbf{R}) | F_{-1/2} \rangle, \quad (3.15)$$

where we have substituted the averaging over the impurity unit-cell by a delta function. Upon diagonalisation of the system matrix the states coupled by non-vanishing matrix elements repel each other and their possible degeneracy is removed. When the impurity is placed in the centre of the dot the same matrix elements arise. In this case, however, the integration over the

envelope functions F_j vanishes and prevents a splitting. Since the angular momentum must be conserved in this case, the envelope functions of a Bloch-band j_z have a defined angular momentum $m = M_{tot} - S_z - j_z$. Now, for an impurity in the centre of the dot the matrix element $\langle F_j | \delta(\mathbf{R}) | F_{j'} \rangle$ can only differ from zero when both envelope functions have $m_1 = m_2 = 0$. This condition can never be fulfilled for two different j_z in this configuration⁶. Therefore, all states were degenerate at $B = 0$ T for dots with manganese in the centre. This is no longer true for the present off-centre dot configurations.

For the potential values used here and the pair with parallel spins $|\pm 1/2 \pm h_1\rangle$ the coupling (3.15) is very weak. So, no enhanced spin mixing is noticeable. The other strong influence on the hole in the dot comes from the acceptor potential of the off-axis manganese atom. The peak density of the hole appears at 12.3 nm from the centre and the impurity is located at 14 nm. The acceptor can localise the hole wave function nearly at its position. This gives a clue about the relative strength of the dot and the acceptor potential. In comparison of the present dot containing the off-centre manganese to a dot with the same dot potential values and a central impurity the density at the position of the impurity in the present configuration amounts to 82% of the in-centre value. This ratio also appears in the splitting between the two lowest doublets in these two configurations. It again shows that the splitting due to the pd interaction is mainly determined by the density of the hole at the manganese site. The slight change in the expectation values of the hole and the manganese spin do not contribute to the change of the pd interaction energy.

In the dot with the standard potentials and manganese in centre the ground state changes at about $B = 1.8$ T (see Fig. 3.10). Below the crossing point $|S_z = 5/2\rangle |j_z = -3/2\rangle$ is the ground state and beyond it is $|S_z = 5/2\rangle |j_z = +3/2\rangle$. This crossing must occur for the off-centre configuration at much higher magnetic fields. In figure (3.16) the mentioned states are beyond $B = 0.4$ T the lowest and third lowest one. Their slopes are almost parallel in the calculated range of the magnetic field. This is remarkable because the hole density at the Mn off-axis site is lower than in the dot with the central impurity. Thus the transition of the ground state to the Zeeman-energy dominated spin alignment should occur at lower magnetic field. In both configurations the hole spin expectation value in the lowest states is comparable due to the same strength of band coupling. The manganese spin is in both states and both configurations in the $S_z = 5/2$ state. So, the Zeeman energies in the dot with the central and in the one with the off-centre impurity are not very different. What makes the difference between both states is the expectation value of the hole orbital-movement angular-momentum quantum number $\langle m \rangle$ in the two aforementioned states. While for the in-centre case $\langle m \rangle$ is small in both states and has the same sign as the hole spin, in the off-centre case $\langle m \rangle$ is two to three times larger and its sign in both considered states points opposite to the hole spin expectation value. This behaviour lowers the slopes of both these states in the magnetic field for the off-axis configuration. It shifts their crossing point towards

⁶ Note that the coupling between the particular spin states crucially depends on the form of the operator describing the exchange interaction. This form depends on many factors like the crystal symmetry, on the number of bands taken into account, approximations like the spherical approximation and the interacting particles [79].

higher field values. This change of the orbital movement of the hole depends crucially on the strength of the acceptor potential. When the lateral dot potentials are strong in comparison with an off-axis acceptor potential, the wave function of the hole will be localised near the centre of the dot. When the acceptor potential is much stronger, the hole will be localised in the vicinity of the acceptor. In both cases the potential in the xy plane will have a symmetry close to circular symmetry because the dominant potentials have it. Only when the lateral dot potential and the off-axis acceptor potential are of comparable strength the hole will be localised between them. Then the circular symmetry in the xy plane will be strongly violated. The present configuration can be classed as the regime with dominating acceptor potential and with a strong disturbance of the *dot* lateral potentials. This disturbance is responsible for the change in the orbital movement of the hole in the two aforementioned states. It changes their expectation value $\langle m \rangle$. So an off-axis impurity disturbs the circular symmetry in the dot only if the dot potentials are of comparable strength.

Figure 3.17 shows a dot with $\omega_{xy} = 5 \cdot \omega_0$ and $F = 4.3 \cdot F_0$. The splitting at zero magnetic field amounts to ≈ 0.094 meV between the lowest doublets. This is 46.4% of the manganese in-centre configuration value. Again the densities of the hole at the manganese site in these both configuration have a very similar ratio. The value of the hole density at the position of the impurity is in this case 47% of the in-centre value. The maximum of the hole density lies 3.94 nm from the centre of the dot potential. The impurity is again located at the maximum of the $|01\rangle$ Fock-Darwin basis function, which is at $R_I = 6.2$ nm for this xy potential. So, for this configuration the hole is localised stronger towards the centre of the dot than in the case of figure (3.16). In dots with weak confining potentials in comparison to the acceptor potential the impurity can localise the hole in its vicinity. Thus the hole density and the strength of the pd interaction depends little on the position of the manganese atom. This is no longer true when the dot potentials become stronger. The position of the hole density peak in this potential configuration is localised at approximately half the way between dot centre and acceptor atom. From this we can deduce that the dot potential strength is comparable with the acceptor potential, but not dominant. In a very strong dot xy potential the acceptor potential will play a minor role. In such a strong potential, moving the manganese atom from the centre of the dot will not change the hole wave function much. It will merely result in a decrease of the hole localisation at the manganese site and thus a lowering of the splitting between the doublets. The other features of the spectrum should remain qualitatively the same. This strong lateral confinement regime is not reached by far in the present potential configuration. Now the spectrum experiences significant changes from the in-centre configuration with the same dot potentials. One eye-catching feature of the spectrum is the broken degeneracy at $B = 0$ T in the 3rd doublet. This was predicted by Eq. (3.14). The hole and manganese spin expectation values are nearly zero in these states due to the mixing between them introduced by the pd interaction term (2.70). The spin expectation values are also lowered in the 4th doublet as predicted by Eq. (3.15). In these states no splitting is noticeable within the numerical precision of our calculations. Other features, not seen in dots

with a manganese atom in the centre and in dots with an off-axis manganese and weak xy potential, are the anticrossings between states which cross in one point in the former configurations. In these states the dominant hole spin component is $j_z = 3/2$. The anticrossings occur not between particular states, but all states mutually repel each other. Again the spin-flip terms are responsible for the mixing of different spin states. As shown before, this mixing is strongly dependent on the admixture of light holes with $j_z = \pm 1/2$ to the eigenstates. In the present potential configuration ($5 \cdot \omega_0, 4.3 \cdot F_0$) this admixture is bigger than in the weak dot potential configuration. Also the localisation of the hole, in the middle between the dot centre and the manganese atom, strongly disturbs the circular symmetry in the xy plane. This makes coupling between different orbital hole states possible. The ground state consists mainly of the $|S_z = 5/2\rangle |j_z = -3/2\rangle$ state. This configuration is very preferable for these potentials. The large band mixing lowers the energy of the $j_z = -3/2$ hole state. Due to the strong dot potentials the hole density at the manganese site is high and thus the pd interaction is large.

We also calculated the spectrum of a dot with the xy confinement potential of $\omega_{xy} = \omega_0 \cdot 5$ and a z confinement of $F = F_0$. The energy quantisation due to the confinement in z direction is still larger than for the confinement in the xy plane. Nevertheless, this configuration comes closer to a cylindrical dot shape rather than the oblate form of the former dots. Figure (3.18) shows the corresponding spectrum. The kinks in the spectrum result from a small number of calculated points (one each 0.2 T). The lines represent states with the same dominant basis state and, therefore, the same dominant spin alignment. Anticrossings in this spectrum appear as a symmetric displacement in energy of two states with their crossing in the middle. Again the manganese atom is located at $6.2nm$ from the centre of the dot. The density of the hole at the manganese site is 0.55 of the in-centre configuration value with the same dot potential strength. The splitting between the lowest two doublets at $B = 0$ T has the same ratio for these two configurations. The peak of the density is at $4.24nm$ from the centre. In comparison with the configuration from figure (3.17), i.e. the one with manganese at the same position, the same xy potential, but stronger z potential of $F = 4.3 \cdot F_0$, the hole is now localised closer to the acceptor atom. This displacement is also the result of the competition between the dot potentials and the acceptor potential. With the lower z potential the wave function spreads further in this direction. The proximity of the hole to the acceptor becomes smaller. In the xy plane the wave function is shifted in x direction towards the acceptor atom. This results again in a stronger proximity to the acceptor. In the present case, however, there is no gain in hole density at the manganese spin site. Due to the further spread of the wave function in z direction, the hole density at the position of the manganese is lowered more than the increase in density due to the shift towards the acceptor can make up for. The ratio of xy to z potentials yields a large admixture of the $j_z = \pm 1/2$ Bloch bands to the ground states of the hole. The large band mixing enhances the spin flip mixing mechanism described in (3.14) and (3.15). We see the splitting of doublets at $B = 0$ T and anticrossings in the $j_z = +3/2$ states seen in the preceding configuration. The effects are now more pronounced. Even the 4th doublet shows a small splitting described by (3.15). The states exhibit not only one

anti crossing in the region where they come together. During the anticrossing the eigenstates are mixtures of many different hole- and manganese-spin states. The states with dominant hole spin contribution $j_z = -3/2$ do not cross. For the states not participating in the anticrossings and for the other states away from the anticrossing region the expectation value of the hole spin is constant around ± 1.15 . This value is typical for the large band coupling regime treated here. The expectation value of the manganese spin is close to the eigenvalues of \hat{S}_z for all states away from the crossing region. In the ground state the manganese is aligned following the Zeeman term. As mentioned before the hole spin states are now strongly mixed, but the dominant component is still $j_z = -3/2$. The only competitor for the lowest eigenstate is the one with $S_z = +5/2$ and dominant $j_z = +3/2$. It has a very similar slope in the magnetic field. A crossing with the ground state can occur only in magnetic fields far beyond the calculated range.

We can divide the spectrum of a dot with an off-axis manganese impurity into several regimes. The first one can be set when the dot potentials are much stronger than the acceptor potential of the manganese and the band coupling is small due to a relatively large splitting of the light- and heavy-hole bands. Here an off-centre position of the atom does not change the spectrum of the system very much. It is comparable with the on-centre spectrum except for a smaller splitting between the six doublets due to the smaller hole density at the manganese site. A second regime can be defined, where the band coupling is still small but the dot potentials are considerably weaker than the acceptor potential of the manganese atom. Here the hole becomes localised almost completely at the site of the manganese impurity. When the dot potentials are very weak the circular symmetry is not violated very much. Then the centre of symmetry is the impurity site. The spectrum does not change much from the on-centre case. In such a system the dependence on the actual manganese position is very weak, since the acceptor atom takes the hole with it. To achieve a stronger change in the spectrum we require a strong band coupling and a broken circular symmetry. So we can set up a third regime where these requirements are fulfilled. The strong band mixing occurs when the dot z potential is low in comparison with the xy potential of the dot. To break the circular symmetry we must localise the hole between the centre of the dot and the acceptor atom. So, the xy potential must be of comparable strength as the acceptor potential. This enables spin-flip processes. Then splitting of several doublets at $B = 0$ T occurs as well as strong anti crossings.

In all regimes the pd interaction strength is mainly determined by the density of the hole at the site of the manganese atom. A change in the band mixture of the hole state has only a minor direct influence on this value. Outside the crossing points of the states with strong spin-flip probability the alignment of the manganese spin is close to the eigenvalues of \hat{S}_z and the alignment of the hole spin is determined by the strength of the band coupling.

In all the potential configurations considered here the ground state was dominated by the heavy-hole bands with $j_z = \pm 3/2$. By a change of the ratio of the confining potentials we can also enforce the light-hole bands with spin $j_z = \pm 1/2$ to provide the main spin component in the

ground states of the dot. In [80] such a transition is investigated, however, in a very different system. The spectra of the dots will, however, not deviate qualitatively from the heavy-hole ones. With the actual form of the pd interaction term the coupling between $j_z = \pm 1/2$ hole states will be stronger than for the $j_z = \pm 3/2$ ones. In the highest and lowest of the six degenerate doublets the alignment of the manganese spins deviates maximally. It is $+5/2$ and $-5/2$. The coupling between the states and thus the splitting of these doublets will be still small even with dominating $j_z = \pm 1/2$ bands.

In this work I consider only one off-axis manganese position. We have found that for different off-axis manganese positions the observed effects change only slightly. An according investigation for valence band electrons (holes) in II-VI semiconductors can be found in [81]. In that work the effects are more pronounced, since without an acceptor potential the manganese disturbs less the eigenstates of the dot.

3.3.7 *InAs* Dots, Mn Off-Axis

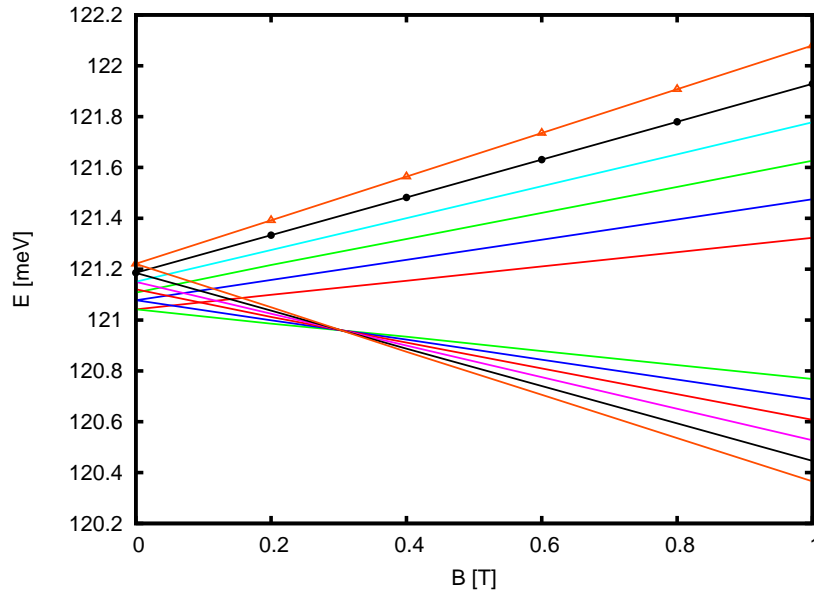


Figure 3.19: Energy of one hole and Mn atom $7.2nm$ from centre in an *InAs* QD, xy potential of $6.3 \cdot \omega_0$ and z potential of F_0 .

Finally we investigated off-axis manganese atoms in quantum dots made from *InAs*. Figure 3.19 shows the spectrum. We used the same potential values as for the *Mn* in-centre case of *InAs*. The manganese atom is positioned in the same way as for the *GaAs* case, i.e. in the maximum of the $|01\rangle$ basis state. With the effective masses in *InAs* the absolute position is $R_I = 7.18 nm$ from the centre of the dot and $z_I = 2.04 nm$ from the heterojunction plane. The

peak density of the hole lies 3.26 nm from the centre. The hole density at the manganese site in the off-axis configuration is 50% of the in-centre configuration value. This high ratio and the localisation of the hole almost in the middle between the dot centre and the acceptor site show that the two present potentials are of comparable strength for the *InAs* effective masses. The circular symmetry is broken for the hole. Also the second requirement for strong spin-mixing is present. The admixture of the light holes to the two-hole ground-states results for the *InAs* dot in a expectation value of the hole spin of $\langle j_z \rangle = 1.35$. This value is comparable to the dot from figure 3.17 with comparable dot potential values. We also see the splitting of the third doublet at $B = 0 \text{ T}$. At the crossing point of the $j_z = +3/2$ states, at $B = 0.3 \text{ T}$, anticrossings occur. These are, however, very small. The expectation value of the manganese spin at the calculated points, at 0.2 T and 0.4 T , is only slightly lowered in the crossing states in comparison with the non-crossing $j_z = -3/2$ states. The *pd* interaction is so small that the Zeeman energy is dominant already beyond $B = 0.3 \text{ T}$. Again the hole spin is constant in the magnetic field and at the crossing point it is the manganese spin which changes its alignment.

3.3.8 Elliptic Dots with Mn

We calculated the eigenstates of elliptic *GaAs* quantum dots with manganese impurities at $B = 0 \text{ T}$. The elliptic potential was created by considering an additional harmonic potential in the y direction. We varied the strength of the additional potential K_e (2.60) from 0 to $1 \cdot K_0$, i.e. the harmonic potential in y direction was at most twice as high as the one in x direction. For the strong potential configuration $5 \cdot \omega_0$ the additional potential was increased appropriately to keep the 2 : 1 ration of the y to the x harmonic dot potential.

In a dot with standard potential values and a manganese atom in the centre the hole density does not change much upon application of the additional potential. The circular symmetric acceptor potential is strong in comparison with the elliptic dot potential and conserves the circular shape of the hole density even at the maximal value of the elliptic potential $K_e = K_0$. Still we notice a small lowering of the manganese spin expectation value in the 3rd doublet. The violation of the circular symmetry starts the spin-mixing mechanism as described in Eq. (3.14). In the strong-potential configuration $5 \cdot \omega_0$ and $F = 4.3 \cdot F_0$ the elliptic dot potential is comparable with the acceptor potential. The hole density shows a slightly elliptic contour. The density at the centre of the dot drops to 97% of the circular value. The influence of the spin-mixing terms rises with the now stronger broken circular symmetry. The third doublet shows now a small splitting of 0.01 meV . The third configuration $5 \cdot \omega_0$ and $F = F_0$, with strong band coupling, shows again a different behaviour. The density of the hole in the centre rises to 104% of the circular value. The strong band coupling enhances the spin-mixing mechanism, so that the third doublet is now split by 0.03 meV .

In the configuration, where the additional potential is applied in y direction, and the man-

ganes atom is located on the x axis, the additional potential has the smallest influence on the hole. Again we are interested in the change in the character of the hole eigenstates due to the additional potential. At the same time we do not want the hole density at the manganese site to be considerably lowered. For the standard values of the dot potentials, the acceptor potential dominates. The hole density and the spin alignments of hole and manganese barely change. In the strong dot potential configuration the now stronger additional potential squeezes the hole density in y direction. This leads to an increase of the hole density at the site of the manganese to 105%. The splitting between the lowest doublets follows this increase. The expectation values of both spins and the splitting of the third doublet changes only little. The third potential configuration, where the band coupling is strong, shows again a different behaviour. The density at the manganese site rises to 103% of the circular value upon application of the maximal additional potential. In contrast to all preceding cases, the splitting between the lowest two doublets does not follow this change and drops slightly to 97%. This is not true for the distance between the two topmost doublets, where no change in the splitting is visible at all. In all cases the changes due to the additional potential are small. The impact of the elliptic potential can be considered strongest in the case of a central impurity, where the violation of the circular symmetry can lift the degeneracy of some of the doublets.

Nevertheless, we could proof our spin-mixing mechanism. As predicted in Eq. 3.14 spin-mixing via the pd interaction is only possible in a broken circular symmetry for the orbital movement.

3.4 2 Mn 1 Hole

In this chapter we will investigate the interaction of two manganese impurities and one hole inside the quantum dot. The costly calculation of the matrix elements describing the acceptor Coulomb potential of the manganese in our basis, suggests to choose the same positions of the manganese impurities as in the former chapters. So in our configurations one of the atoms will be located in the centre of the dot while the other will be in the maximum of the $|0 \pm 1\rangle$ basis function. This is for the standard potential ω_0 at $14nm$ from the centre and for $5 \cdot \omega_0$ at $6.2nm$. In both cases this is far enough apart to neglect the anti ferromagnetic interaction between the manganese spins. The antiferromagnetic $Mn-Mn$ interaction acts on the length scale of the crystal lattice constant [82]. The potential values in $InAs$ were $(6.3 \cdot \omega_0, F = F_0)$. This yields the position for the off-axis manganese to $7.18nm$ from the centre of the dot.

3.4.1 $GaAs$ Dots

We have seen that in the case of one manganese impurity atom and one hole in the quantum dot the spin alignment of the manganese atom in magnetic field is determined only by its Zeeman energy. The spin alignment of the hole, in turn, can be changed by all potentials: the magnetic

field, the dot potentials and the alignment of the manganese spin. The Zeeman energy of the hole competes with the anti ferromagnetic pd interaction. In case of one hole in a dot with two manganese impurities we can surely expect that the hole will have even less influence on the spins of the two manganese atoms. In contrast the influence of the two manganese atoms on the hole spin stays large. We can only control on the manganese spins by means of the hole state at $B = 0$ T.

Even for the strongest dot potentials and thus the largest density of the hole at the position of the manganese atoms the splitting in energy between the different alignments of the hole and manganese spins never rises above 0.2 meV. This is at least an order of magnitude smaller than the splitting between the ground state and the next excited states. So, the lowest states of this system will consist of the two hole ground states and the six states of the spin for each manganese atom. This results in $2 \cdot 6 \cdot 6 = 72$ states. Depending on the relative strength of the dot- and the acceptor-potential the hole envelope function can be changed considerably by the acceptor potentials. We will, therefore, use the same number of hole orbital basis states in our calculation, as in the preceding cases. Figures (3.4.1), (3.4.1) and (3.4.1) show the spectrum of the 72 lowest states of the system.

First we want to consider the dot with the strongest confining potential values $5 \cdot \omega_0$ and $F = F_0$ (fig. 3.4.1). The two manganese atoms now compete in attracting the hole and the density at each manganese site drops in comparison to the preceding cases with only one-manganese atom. Nevertheless, with the strong dot potentials localising the hole towards the centre, the peak of the hole density lies at 0.96 nm from the centre of the dot between the two impurity atoms. The density at the site of the second atom, the one off-axis, is about 20% of the density of the one in the centre. The splitting between the highest and lowest doublet at $B = 0$ T amounts to 0.93 meV. The lowering in the pd interaction energy becomes clear, when we compare this value to the sum of the splittings in the two preceding one-impurity cases. It yields 1.455 meV. The quantum numbers of the z components of the two manganese spins, $S_z^{(1)}$ and $S_z^{(2)}$, and the one of the hole spin z component j_z are not conserved. This is due to the broken circular symmetry and the spin-mixing terms. The spin expectation values of the off-centre impurity $\langle S_z^{(2)} \rangle$ and the hole spin $\langle j_z \rangle$ deviate stronger from the eigenvalues of the corresponding operators. The different spin states of the particles are coupled. This effect is smaller for the in-centre impurity in this potential configuration. The reason for the different spin expectation values of the two manganese atoms is the spatially dependent alignment of the hole spin. To describe the spatial change of the hole spin we defined in appendix A the polarisation $\pi(\mathbf{x})$. It is the expectation value for the hole spin at position \mathbf{x} normalised by the total hole density at this point. At the site of the central impurity we have $\pi(0, 0, 1.9 \text{ nm}) = 1.496$. At the site of the second impurity it amounts to $\pi(6.2 \text{ nm}, 0, 1.9 \text{ nm}) = 1.400$. Without an external magnetic field the hole spin is the only influence on the spin of the manganese. The manganese spins align according to it, i.e. antiparallel. The overall variation of the polarisation in the dot is rather small. Figure 3.20 shows

the form of $\pi(\mathbf{x})$ in the plane containing both impurities with $z = 1.9 \cdot 10^{-9} \text{ nm}$ for the strongest dot potentials ($5 \cdot \omega_0 F = F_0$) at $B = 0 \text{ T}$. A stronger deviation from the mean value of the hole spin occurs only at the very edge of the hole density.

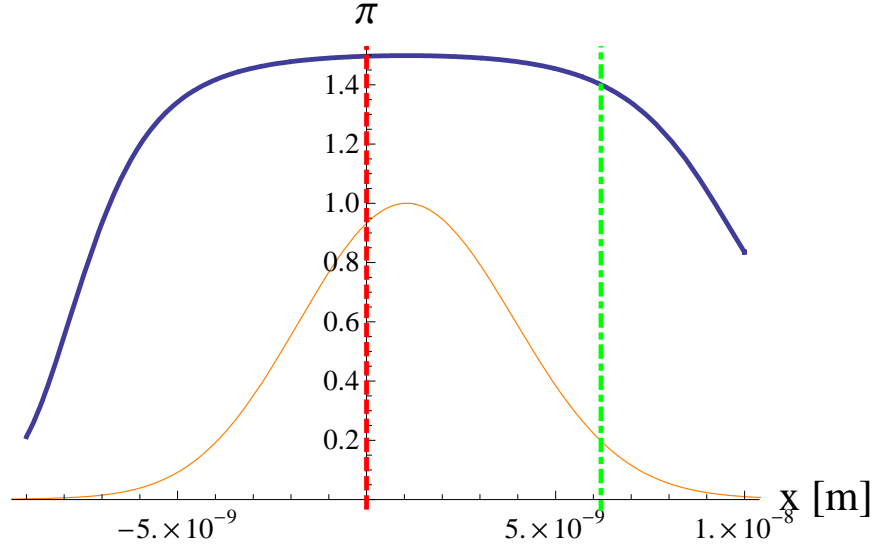


Figure 3.20: Polarisation π of the hole (blue curve) normalised to the hole density. The red(green) line shows the position of the central(off-axis) Mn atom. The orange curve shows the total hole density normalised to its peak value.

The coupling of different spin states is most prominent when states with the appropriate spin alignments (see Eq. 3.14) are close in energy, e.g. when they cross. At $B = 0 \text{ T}$ all states are doubly degenerate. This is in contrast to the case with one off-axis impurity. In that case, for those potentials values one doublet splits. The spin expectation values of the hole and the manganese in these states become nearly zero. This difference is again consistent with Kramers theorem. The total spin of the particles is not an integer number anymore. So, without a magnetic field each state must be at least doubly degenerate due to the time-inversion invariance. Without magnetic field the spins align according to the pd interaction. The states with the largest negative pd energy, $|S1_z = 5/2\rangle |S2_z = 5/2\rangle |j_z = -3/2\rangle$ and $|S1_z = -5/2\rangle |S2_z = -5/2\rangle |j_z = 3/2\rangle$ form a degenerate ground-state doublet. The ground state in the whole calculated range of the magnetic field is the one with dominant spin states $|S1_z = 5/2\rangle |S2_z = 5/2\rangle |j_z = -3/2\rangle$. This is due to the large negative Zeeman energy of the two manganese spins in this state. The pd interaction then aligns the hole antiparallel to them. The only state with larger negative Zeeman energy is the one starting at the top of the spectrum, where the spin of the hole is aligned parallel to the manganese atoms. The slopes of both states in the magnetic field are parallel. The gain in Zeeman energy of the hole is compensated in this dot potential configuration by the band cou-

pling. Even for magnetic fields several times larger than the 1 T in our calculation we can expect that the ground state will not change. The next higher states differ only in the spin alignment of the off-centre manganese atom. In the first excited state it flips to the $|S_{2z} = \pm 3/2\rangle$ state⁷. It is energetically favourable to change this spin because of the lower hole density at its site and thus a lower pd interaction energy in comparison with the centre atom. The splittings between all the doubly degenerate states at $B = 0$ T are not equidistant. This is due to different pd interaction energies of the two manganese impurities. When the density of the hole is equal at both impurity sites and the spin expectation values of both manganese atoms are comparable, the pd interaction of the two atoms with the hole is the same. In this symmetric case the states at $B = 0$ T then will group in eleven tuples according to the eleven possible values of $S_{tot} = S_z^{(1)} + S_z^{(2)}$ with $S_z \in \{-5/2 \dots + 5/2\}$. This result was already found by Fernandez-Rossier in [70]. In each such tuple S_{tot} is then (roughly) constant. Due to the positioning of one manganese in the centre and one far away on the x axis in our investigations we never had such a symmetric case. The hole densities differ strongly and thus the pd interaction. We can achieve equal densities of the hole at the manganese sites when we align the impurity atoms at equal distances from the centre opposite to each other. A general scheme for the ordering of the different spin alignments at $B = 0$ T can be constructed as follows: For each of the six alignments of the spin of one impurity and a particular spin of the hole, there are six equidistant states belonging to the six alignments of the spin of the second impurity. The splitting in this six-tuple is proportional to the pd energy of the second atom. The energetic splitting between similar states in two different six-tuples, i.e. with different alignment of the first impurity, is determined by the pd energy of the first impurity. If no accidental degeneracy occurs we end up with at most 36 doubly degenerate states. In each of the 36 doublets the spin alignments of all particles in one state is just opposite in sign to the respective spins in the other state. In the present case the splitting between two alignments of the off-centre impurity amounts to 0.032 meV while the difference for the on-axis impurity amounts to 0.155 meV. According to this values and following the mentioned scheme we notice that in the lowest four (doubly degenerate) states the spin of the first impurity is maximal antiparallel to the hole. The second impurity takes four different states meanwhile. In the fifth doublet the central impurity flips once while the second is maximal antiparallel to the hole and so on.

In figure (3.4.1) we see the spectrum of a dot with a xy potential of $5 \cdot \omega_0$ and a z potential of F_0 . The splitting between the highest and lowest state drops in comparison with the former case to 0.543 meV. The hole density at the manganese sites differs now less than in the preceding configuration. The peak of the hole density is 1.59 nm from the centre and the hole density at the off-axis manganese site is about 35% of the value of the central manganese. The lowering of the z potential compared to the former potential configuration changes the position of the hole in the xy plane. This is an effect of the competition between the dot and the acceptor potentials. By lowering of the confinement in z direction, the hole density becomes more elongated in this di-

⁷This means that the dominating spin basis state changes in this eigenstate. The manganese spin is not a good quantum number.

rection. The spread of the hole in the xy plane is then lowered. This changes the potential energy of the hole in the strong xy dot potential as well as in the both acceptor potentials. The balance between all three of them changes and the density of the hole is shifted. This effect corresponds to the one described for the one hole and one off-axis manganese with dot potentials ($5 \cdot \omega_0 F_0$). Remarkable is the low total energy of the system. The eigenstates lie almost at the valence band edge of bulk $GaAs$, which we took to be our zero energy point. This is in consistence to the other configurations. The energy difference due to the different z confinements of a $j_z = \pm 3/2$ hole in the configuration ($5 \cdot \omega_0, 4.3 \cdot F_0$) and the present one ($5 \cdot \omega_0, F_0$) is about 65 meV. For even stronger dot xy potentials or manganese atoms placed closer together the energy of the system will rise over the edge of the valence band. The ground state again has the dominant spin states $|S_z^{(1)} = 5/2 \rangle > |S_z^{(2)} = 5/2 \rangle > |j_z = -3/2 \rangle$. With the strong band coupling the spin alignment of the hole is determined by this effect. So even without the interaction with the manganese spins the hole will be aligned opposite to the Zeeman term. The stronger band coupling in this potential configuration lowers the absolute hole spin expectation value and changes its spatial distribution. It amounts to 1.483 at the central impurity site and 1.333 for the off-axis impurity. The manganese spins expectation values change accordingly. While the central impurity does not change much the off-axis value is lowered. The energy change due to a flip of the central impurity at $B = 0$ T amounts to 0.078 meV, for the off-axis impurity to 0.027 meV. For the off-axis impurity the change in the pd interaction energy due to the changed dot potentials does not follow the change of the hole density at this impurity site as seen in the previous configurations. The ratio of the hole density at the site of the off-axis manganese in the present configuration to the ($5 \cdot \omega_0, 4.3 \cdot F_0$) configuration amounts to 0.900. The ratio in the pd interaction energies amounts to 0.855. The interaction energy drops stronger than the hole density. The pd interaction energy of the central impurity follows the change in the hole density. None of the spin components of any particle is a good quantum number. The change in the pd interaction energy of the off-centre impurity with the change of the hole spin is only a small effect in this configuration. To investigate further the mechanism, configurations are needed where the change in the hole spin is larger.

For the dot configuration with ω_0 and F_0 in figure (3.4.1) the splitting between the highest and lowest states drops to 0.13 meV. This is due to the low density of the hole at the manganese sites. The peak density of the hole is at $4.5nm$ while the off-centre impurity is located at $14nm$ for this potential configuration. The density at the off-centre manganese amounts to 40% of the in-centre value. The spins expectation values of both manganese and the hole stay in most part of the spectrum close to the eigenvalues of their corresponding operators \hat{S}_z and \hat{j}_z , i.e. the coupling of different spin states is low in comparison to the preceding configurations. Nevertheless, it is higher in comparison to the dot with only one off-centre manganese. In such a dot the impurity acceptor potential strongly attracts the hole towards its position. The spherical symmetry around the impurity is then destroyed only slightly by the relatively weak dot potential. With two impurities the hole is localised in between the two spherical potentials of the acceptor atoms. The

circular symmetry is violated strongly. This again enhances the coupling between the different spin states. The ratio of the dot potentials, however, leads not to a strong band coupling. So the second requirement for the strong coupling of the spins fails. Until $B = 0.8$ T the lowest state is the one with the dominant spin components $|S_z^{(1)} = 5/2 \rangle > |S_z^{(2)} = 5/2 \rangle > |j_z = -3/2 \rangle$. Here the anti-ferromagnetic pd interaction between the hole- and manganese spins dominates. Already at $B = 1$ T the state with the biggest Zeeman energy becomes the ground state, which is the one with same manganese spins and with the hole spin $|j_z = +3/2 \rangle$. These two states exhibit an anticrossing. Between 0.8 T and 1.0 T the expectation value of the hole spin $\langle j_z \rangle$ in each of these states drops to zero and rises again with the opposite sign. The manganese spins do not change in the meantime. Such anticrossings appear also in several of the next higher states at lower magnetic field values. Different from the former configuration this anticrossing does not result from couplings between the states by the pd operator. This can be seen because the spin expectation values of the manganese are not lowered during this anticrossing. The origin of the coupling is the violation of the circular symmetry by the off-axis acceptor potential. The anticrossing in the lowest states can also only occur, because for these dot potentials the hole spin at higher magnetic fields is determined by the Zeeman energy. For higher xy potentials the crossing will shift to higher values of the magnetic field and finally disappear.

In conclusion we see, without magnetic field the hole in $GaAs$ can align the spin states of two manganese atoms (almost) parallel. Due to the time inversion invariance the states with opposite spins are energetically degenerated. In optical experiments holes with a definite angular momentum can be created inside a quantum dot by applying circularly polarised light. Recent investigations show that the hole spin lifetimes (T_1^h) in a quantum dot can reach even some tens of μs [83]. Calculations suggest even larger (T_1^h) can be reached for single holes with well separated subbands [84]. Theoretical work [85] and experimental investigations on $CdTe$ quantum dots show that exciton spin can align impurity spins ferromagnetically within its Bohr radius [86], [87]. The exciton recombination time is of the order of hundreds of ps . Recently in $CdTe$ dots manganese orientation times of 20 to 100 nm were measured [88]. In this material also the control of manganese spins in quantum dots was shown [89]. Also the longer lifetime of the hole spin inside the $GaAs$ dot suggests that the manganese spins can be aligned parallel. Polarisation of manganese spins in a diluted magnetic semiconductor $GaAs$ quantum well has already been shown [90].

The thermal stability of the ferromagnetic state depends on the energetical separation between the different spin eigenstates of the system. This, in turn, crucially depends on the density of the hole at the sites of the impurities. Also the densities must be equal for both impurities to get the largest minimal splitting between the states. So, the localisation of the hole wave function inside the dot also matters. To maximise the hole density at all manganese impurity sites the impurities must be positioned symmetrically around the centre of the dot. Yet, this distance must be large enough for the short-ranged anti ferromagnetic mutual interaction of the manganese spins to vanish. Also a strong band-coupling can couple different spin states of the manganese and

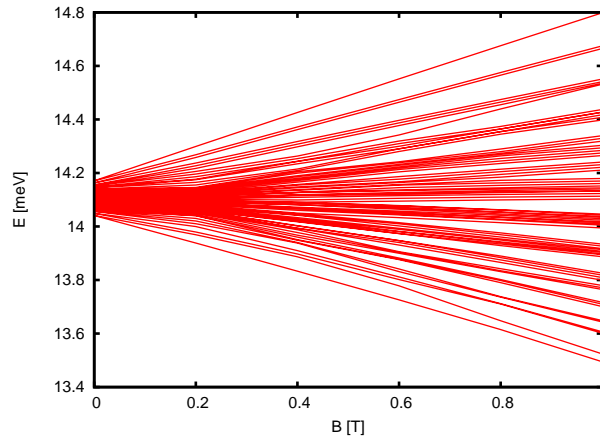


Figure 3.21: Energy of a hole and 2 Mn atoms in centre and $14nm$ from centre, xy potential of ω_0 and z potential of F_0 .

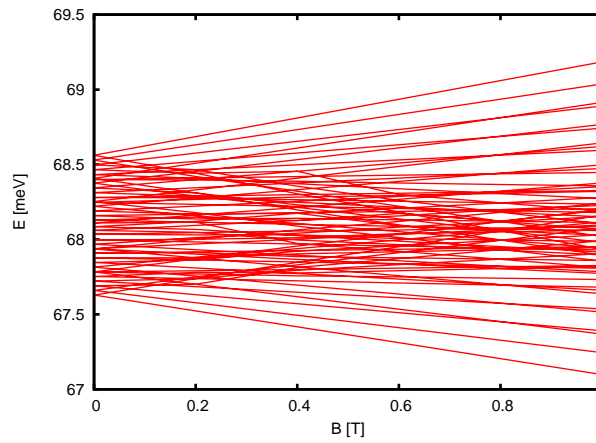


Figure 3.22: Energy of a hole and 2 Mn atoms in centre and $6.2nm$ from centre, xy potential of $5 \cdot \omega_0$ and z potential of $F = 30$ mV/nm.

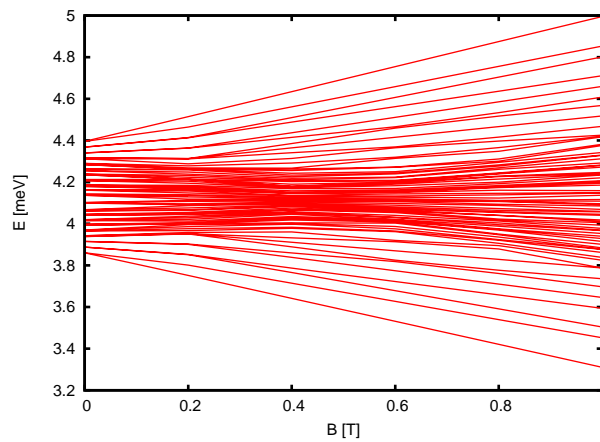


Figure 3.23: Energy of one hole and 2 Mn atoms in centre and $6.2nm$ from centre, xy potential of $5 \cdot \omega_0$ and z potential of $F = 7$ mV/nm.

thus hinder the ferromagnetic ordering.

3.4.2 *InAs* Dots

Finally we calculated the spectrum of two manganese impurities in an *InAs* quantum dot. Again the ordering of degenerate doublets at $B = 0$ T depends on the ratio of the hole densities at the sites of the two manganese atoms. As in the case of one manganese impurity the spectrum again divides into two fans at higher magnetic fields. In all states of the lower fan the alignment of the hole spin is according to the Zeeman term, in the higher one it is opposite to this term. This shows the dominance of the hole spin in the magnetic field for *InAs*. There is only one deviation from this scheme. Both states forming the lowest doublet at $B = 0$ T develop nearly parallel in the magnetic field and their slopes are nearly horizontal. In both of these states the two manganese spins are aligned maximally antiparallel to the hole spin, i.e. $|j_z = \pm 3/2 \rangle$ and $|S_z^{(1)} = \mp 5/2 \rangle, |S_z^{(2)} = \mp 5/2 \rangle$. The lower one has the hole spin aligned according to the Zeeman term with $|j_z = +3/2 \rangle$. The energy of the states is mainly determined by the Zeeman terms. So, we can conclude from the horizontal dispersion of the states that the Zeeman energy of the two manganese is only slightly lower than the Zeeman energy of one hole in *InAs*. These two states are the ground states until about $B = 0.2$ T. Then, between $B = 0.2$ T and $B = 0.7$ T, the ground state is $|j_z = +3/2 \rangle, |S_z^{(1)} = -5/2 \rangle, |S_z^{(2)} = +5/2 \rangle$. In this state the off centre impurity flips at the cost of the pd interaction energy with the hole. Again this energy is lower for the off-centre impurity. Beyond $B = 0.7$ T all three spins are aligned according to their Zeeman terms. The double change in the ground state was not seen in any of the *GaAs* quantum dots. The reason for it is the fact that the Zeeman energy of the hole is larger than this energy for one of the manganese atoms. This can be easily verified using a simple model. We assume the spins of the particles to be conserved and in the vicinity of the eigenvalues of the respective operators. We also assume that the energies of the states are determined only by the pd interaction and the Zeeman energy. The Zeeman energy of a hole will be approximately $\pm 3/2 \kappa B$ while the energy of the manganese will amount to $\pm 5/2 g \mu_B B$. We then calculate the crossing points of straight lines with slope determined by the Zeeman energy of the state and offset determined by the spin dependent pd interaction in the state. Then, one can easily show that there will be always a double change as long as the Zeeman energy of one hole is larger than the maximal Zeeman energy for one manganese. The overall splitting at $B = 0$ T amounts to 0.659 meV. This is 70.9% of the value for the *GaAs* dot with the strongest confinement used there. In the present *InAs* dot the confining potentials are even stronger. The z confinement is the same and the xy confinement 1.6 times as strong. It is, however, not possible to easily calculate this value from e.g. the change in effective length due to the different hole mass and changed confining potential.

In *InAs* the interaction of the confined hole with the manganese impurities is less pronounced compared to *GaAs*. The lighter xy hole mass lowers the hole density at the impurity site sub-

stantially and thus the pd interaction. On the other side the strong Luttinger parameter κ makes the influence of the magnetic field dominant for the hole states. The actual strength of the pd interaction depends, however, on the unknown value of the interaction constant $J_{pd}(InAs)$. In $InAs$ we have the possibility to control the alignment of at least two manganese atoms. Between 0 and 0.2 T the presence of a single hole in the quantum dot inverts the alignment of the two manganese spins. By changing the magnetic field we can manipulate their spin alignment further. The double change in the ground state allows to manipulate the off-axis spin even separately from the central one. This kind of control is not longer possible in a system with three manganese atoms. Their joint Zeeman energies are larger than the Zeeman energy of the hole.

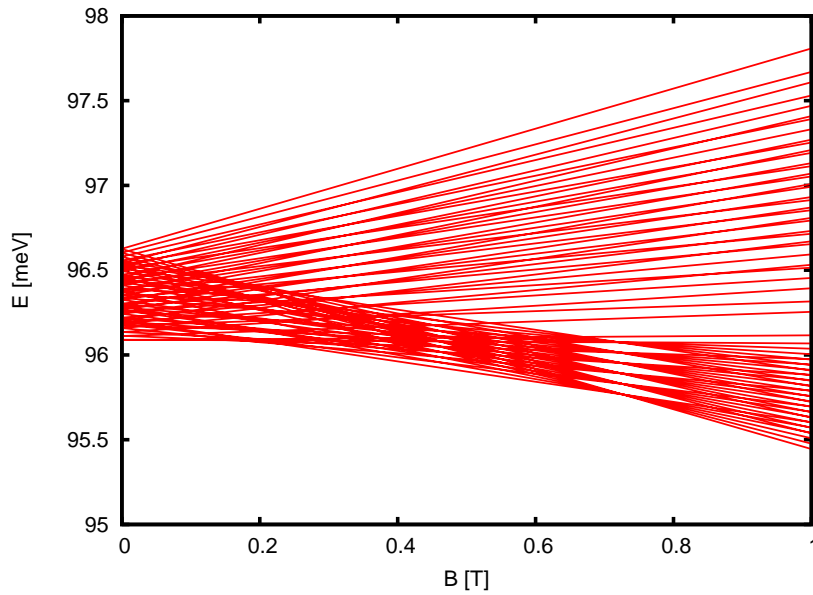


Figure 3.24: Energy of a hole and 2 Mn atoms in centre and 7.18 nm from centre, xy potential of $6.3 \cdot \omega_0$ and z potential of $F = 30$ mV/nm.

3.5 2 Holes with Manganese

In this section we want to report on the impact of a second hole in a quantum dot with manganese impurities. In this configuration all considered interactions contribute to the eigenstates of the dot: confining potentials, magnetic field, acceptor potentials of the manganese, pd interaction of hole and manganese spins and finally the mutual repulsion of the holes. First we want to consider the interaction of two holes with only one manganese impurity. We will present here in detail the dependence of the eigenstates on the manganese position and the confining potentials. Finally we will look at a dot with two holes and two manganese impurities. We will use the

three potential configurations known from the preceding sections and also the same manganese positions. Recent theoretical work on the cyclotron resonance of one and two conduction band electrons in a quantum dot with a manganese impurity can be found in [91], [92].

3.5.1 2 Holes, 1 Manganese

The ground state of a dot with two holes and without a manganese atom is not degenerate and has a total angular momentum of $M = 0$. The holes are in a singlet state with their the spins $j_z^{tot} = j_z^{(1)} + j_z^{(2)} = 0$ and orbital angular momenta z components $m^{1,2}$ pointing exactly opposite to each other at $B = 0$ T. With the addition of the manganese atom the holes stay in the singlet in any of our potential configurations. The hole singlet state interacts with the six manganese states. So, the low part of the dot spectrum constitutes of six states. These are separated by some meV from the next higher ones. In these lowest states, due to the opposite alignment of the hole spins, the interaction of one hole with the manganese atom is compensated by the interaction of the other hole. So, in all the three considered configurations of the dot potentials, (ω_0, F_0) , $(5 \cdot \omega_0, F_0)$ and $(5 \cdot \omega_0, 4.23 \cdot F_0)$, the ground state at $B = 0$ T is sixfold degenerate. The total pd interaction energy is zero. This changes little when we turn the magnetic field on. Due to the different band mixing in the two lowest one-hole states in the magnetic field the spins of the two holes develop slightly different. The interactions of the two holes with the manganese do not compensate each other any longer for higher magnetic fields. This effect, however, is only small in the calculated range of the magnetic field. The degenerated states are still split mainly due to the different alignments of the manganese spin and thus due a different Zeeman energy. The influence of the small hole-spin expectation value due to the incomplete compensation of both spins in the magnetic field is negligible in comparison to the manganese Zeeman energy. The state with manganese spin $S_z = 5/2$ is the lowest one. As depicted in the two-hole spectrum in figure 3.5 a different state becomes the ground state around 8.5 T. At this point two two-hole states are close in energy. In both of them the total pd interaction of the two holes with the manganese does not vanish. So each of the two-hole states splits into six states according to the six possible alignments of the hole spin to the manganese spin. At such high magnetic fields the pd interaction plays an inferior role. The cancellation of the pd interaction for two holes in a $CdTe$ quantum dot was also found in ref. [55]. Also the slow increase of the pd interaction for the ground state in the magnetic field was mentioned there.

We will not show the calculated spectra for lack of new interesting features in the low magnetic field regime. In high fields the states are determined by their Zeeman energy and the pd interaction has no influence. Nevertheless, it is instructive to take a look at the energies of the ground state of the system for different configurations. Table 5.2 shows the energies of the lowest eigenstate for a dot with two holes and one manganese atom in the centre (row C) and on off-centre on the x axis (row X). The columns belong to the three configurations of the dot potentials used before.

	(1) ω_0, F_0	(2) $5 \cdot \omega_0, F_0$	(3) $5 \cdot \omega_0, 4.3 \cdot F_0$
C	57.21 meV	62.06 meV	189.00 meV
X	64.24 meV	77.76 meV	217.27 meV

Table 3.1: Ground state energies for $B = 0$ T, three potential configurations, a manganese in the centre (C) and off-centre (X).

By comparison of these values to the ones for a dot with one hole and one manganese we can see the impact of the mutual repulsion between the holes. Without this mutual repulsion the energy in the present configurations should be just twice the one-hole one-manganese value as long the orbital movement of the holes is considered (see figure 3.10). Now, in the configuration with the weakest dot potentials (column (1)) and the manganese in centre (row C) the energy of the ground state is about 10 meV higher. This is the same order of magnitude as the transition to the next excited many-particle state in the dot. The states next to the six degenerate ground states lie about 8.6 meV higher in energy. We clearly see that the mutual repulsion cannot be considered small in this potential configuration. With increasing confinement potential the influence of the Coulomb energy falls. Nevertheless, for the configuration with the strongest dot potentials (column (3)) the additional Coulomb energy as well as the orbital excitation energy amount both almost to 20 meV. So even in that case the repulsion is remarkable. We want to stress again that we have not taken into account the central cell correction. It would increase the localisation of the hole in the vicinity of the manganese impurity and rise the Coulomb repulsion further.

The cancellation of the hole-manganese interaction occurs, however, only in the ground state. In the excited states the pd interactions of the two holes do not compensate each other any more. The states of the holes are also doubly degenerate. So the spectrum of these states is comparable to the ground state of the one-hole configuration treated in preceding sections. Each of the higher doubly degenerate two-hole states is split into six doubly degenerate states by the interaction with the impurity. The total splittings of these states are small. They lie below 0.1 meV in the first configuration and below 0.7 meV in the third.

The energies of the ground states are lowered strongly in comparison to a dot without the manganese impurity. In the standard potential configuration with the manganese in the centre the relative change is the strongest. The energy is lowered by about 34 meV. This lowering is, however, reduced in comparison with the one-hole configuration. In a dot with standard potentials the total energy-reduction due to the acceptor potential amounts to ≈ 20.2 meV. Without mutual repulsion we would thus expect for two holes a reduction of the double value. The influence of the acceptor atom is also seen in the particle number densities of the holes (see Fig. 3.25). In all the configurations with the manganese atom in the centre of the dot the densities of the lowest and the first excited states are all approximately of Gaussian shape. In comparison to the dots without the manganese the hole becomes now stronger concentrated in the centre of the dot around the acceptor impurity. None of the holes is, however, in a state comparable to the acceptor

state in bulk. While in bulk the extend of the hole wave function is 1 – 2 nm [71], the extend of the wave function of the two holes in the dot amounts to several nm . The dot potentials repel the holes from the very vicinity of the acceptor atom. A discussion about other possible localisations of the two holes in a dot with acceptor is given further down.

For the dot potential values chosen by us the ground states in the configurations with the manganese off-centre (row X) behave very much as in the one hole case. The densities have all a single peak between the dot centre and the acceptor atom (see Fig. 3.26). The positions of the peaks are slightly shifted towards the dot centre. This can be attributed to the larger extend of the two-hole wave function. On large distances in the xy plane from the dot centre the potential of the dot becomes dominant. So, larger wave functions are influenced stronger by the lateral dot potentials. For dots with an off-centre manganese the spins of the two holes do no longer compensate each other even at $B = 0$ T. This is a consequence of the broken circular symmetry of the combined potentials confining the hole. The splitting of the states due to the pd interaction is, however, very small. For the configuration $(X, 3)$ we found a splitting of merely 0.0008 meV. This value lies at the limit of our computational accuracy. For the potential configurations with weaker dot potentials this splitting was even smaller. A further splitting of the ground states of the dot can be achieved by applying an additional elliptic potential in the xy plane. We added to the $(X, 3)$ dot configuration a harmonic potential in y direction making the lateral dot potential elliptic. The additional potential had the same strength as the circular potential $K_e = K_0$ (see Eq. 2.60). In such a dot the splitting of the six lowest states rises to 0.0058 meV. This is still very little in comparison to the splitting for one hole.

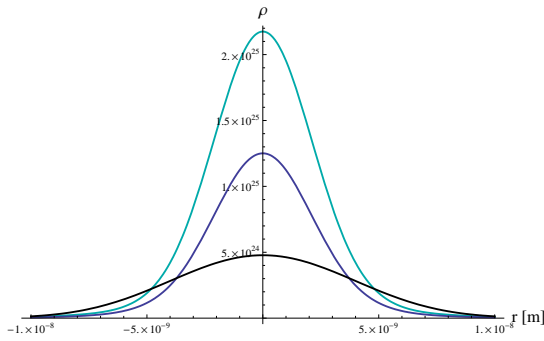


Figure 3.25: Densities of the two-hole ground state in the configurations $(C, 1)$ (black), $(C, 2)$ (blue), $(C, 3)$ (cyan).

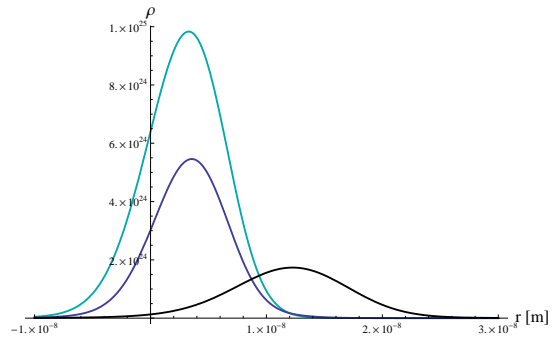


Figure 3.26: Densities of the two-hole ground state in the configurations $(X, 1)$ (black), $(X, 2)$ (blue), $(X, 3)$ (cyan).

We have seen that the two-hole groundstate in our potential configurations is a singlet and the interaction with the manganese vanishes. Nevertheless, the ground state of the dot with a manganese acceptor impurity and two holes is particularly interesting. There are hints (see below)

that the ground state can have also a very different character. The character of the spin alignment of the holes can change significantly depending on the dominance of the participating potentials. In all the potential configurations investigated by us the dot potentials were dominant. The hole was not localised in the very vicinity of the acceptor. Thus the influence of the spherical acceptor potential on the band mixing was small. The splitting of the light- and heavy-hole bands by the strong dot z confinement determined the character of the hole spin as an effective two-level system $j_z = \pm 3/2$. In the case of a manganese acceptor in bulk *GaAs* the z spin components of one hole bound to the acceptor (A^0 configuration [69]) are not separated. In this case the total angular momentum $\mathbf{F} = \mathbf{J} + \mathbf{S}$ (not merely its z components) of the hole and the manganese is a good quantum number. The ground state of this complex is the $F = 1$ state [53]. When the acceptor is placed in a quantum dot and the dot potentials are weak in comparison to the acceptor potential they can merely perturb this configuration. The lowest states $|\mathbb{F} = 1, F_z\rangle$ are then split slightly. For oblate shaped dots the $|\mathbb{F} = 1, F_z = 0\rangle$ state is then shifted upwards and the $|\mathbb{F} = 1, F_z = \pm 1\rangle$ states are shifted down.

For two holes interacting with the manganese acceptor in the dot also the relation of the dot and acceptor potentials to the strength of the pd interaction is crucial. For two conduction band electrons in weak dot potentials and in the presence of a magnetic field or a magnetic moment the ground state can change from a singlet to a triplet state [93], [94], [95]. Then also for two particles there will be a noticeable exchange interaction with the impurity spin. Such transitions have also been postulated for quantum dots with holes [96]. To form a triplet, the holes have to be in different orbital states. Using the magnetic field in our weakest dot potentials (configuration (1)) such a transition occurs in our spectrum beyond 8 T. Accounting for the magnetic moment of the manganese the pd interaction has to be stronger than the dot confinement. We can enforce such a transition in our calculations by artificially enhancing the realistic value of the pd interaction constant $J_{pd} \approx 40 \text{ meV nm}^3$ by a factor of 20. As long as the ground state of the system is concerned and no spontaneous, e.g. thermal, excitations to higher states occur, our system is certainly far away from the transition to a triplet in all considered potential configurations. To find the right potential regime a careful investigation has to be done. The pd interaction is determined by the density of the hole, but to increase the density the confinement and so the quantisation energy have to be raised. For weaker confinements the Coulomb energy can also support a transition. Therefore, the two-hole configuration may show a different behavior in its ground state than for one hole. The results on the ground state of two holes with the acceptor impurity presented here can, however, be attributed to a regime, where the ordering of states is determined by the dot potentials.

There were experimental [73], [97] and theoretical [98] investigations on the photoluminescence of self assembled *InAs* quantum dots containing a single manganese impurity. The photoluminescence of optically injected excitons was measured. The obtained spectra were interpreted in terms of the recombination of a neutral exciton X^0 . The model used to interpret the spectra assumes in the dot without an exciton a hole bound to the manganese impurity (A_0). The exciton

then interacts with this hole-acceptor complex. One hole is localised strongly in the vicinity of the acceptor. With its spin the hole forms the slightly split $|\mathbb{F} = 1, F_z\rangle$ states. So the influence of the dot potentials on this hole is very weak. The spin of the exciton hole is totally determined by the dot potentials, i.e. its $j_z = \pm 3/2$ and $j_z = \pm 1/2$ spin states are strongly split due to the dot z confinement. This strong difference in the splitting of the different spin states j_z of the two holes is unusual. The form of the confinement landscape has a very strong influence on the hole spin in this situation.

In our calculations we have not seen a non-singlet ground state. This is also in accordance with other investigations [56]. The search for the configuration of potentials yielding the unusual two-hole state mentioned above has to be postponed to future work. We have to investigate another potential regime than the one under current treatment. Due to the computationally costly calculation of the matrix elements describing the Coulomb repulsion of the holes and the acceptor potential of the manganese it is not possible within our approach to easily change the potential parameters. Thus we have to stick to our decision on the potential strengths made at the beginning of our investigations. Of particular importance seems the integration of the central cell correction into our model.

3.5.2 2 Holes, 2 Manganese

We use in this section the familiar dot potential configurations. We investigate then the interaction of the two impurities and the two-hole state. For all examined configurations the ground state of the system is a singlet state. The interaction with the manganese atoms vanishes. The hole singlet-state is not degenerate so the ground states of the system consist of this single two-hole state and the 36 possible alignments of the two manganese spins. All states are degenerate without magnetic field. In the magnetic field the degenerate states split up in 11 bunches according to the possible values of the total manganese spin z component $S_{tot} = S_z^{(1)} + S_z^{(2)}$. As described in section 3.4, when the pd interaction of the hole with the manganese is equal for both atoms, the states become degenerate. Here the interaction is zero at both manganese sites. As in the case of one hole the potential of two acceptor atoms compete. This lowers their influence on the hole.

The presence of the second hole effectively destroys any ferromagnetic alignment of the manganese atoms in the dot. The very weak splitting due to the off-centre impurity, seen for one manganese atom in the $(X, 3)$ potential configuration, is not visible any more. This is mainly due to the lower density of the hole at its site. So the hole states follow a shell-structure (at least for two-holes) as shown for electrons [99], [100] with vanishing pd interaction for filled shells. At about $B = 8$ T the lowest two-hole state changes and a non-zero pd interaction occurs. It has, however, no influence on the hole and manganese spin alignment for such large magnetic fields. In [101] a system of several electrons and of two manganese impurities is investigated. There

also the effects of RKKY interaction are included for singlet many-particle states.

To sum up we have shown that for all investigated potential configurations with two holes the ground state is a spin singlet. In this state the particular pd interactions of the two holes cancel each other. The splitting in the ground state can occur, when the confining potentials have no circular symmetry. The energy difference between the split different alignments of the manganese spin stays below 0.005 meV. The vanishing of the pd interaction for two holes makes it possible to effectively control the magnetic properties of the quantum dot by the control of the charge inside the dot. The density distribution and spin alignment of the holes in a dot with a manganese acceptor impurity is strongly dependent on the relative strengths of the dot and acceptor potentials. Also the central cell correction may have a large influence.

3.6 Precision of the calculations

Due to the fact that most of the preceding results were obtained numerically we have to discuss the precision obtained in these calculations. In the procedure of exact diagonalisation used here the approximation in the calculations occurs by the truncation of the basis we use to represent the Hamiltonian. Each term of the Hamiltonian has to be represented in all the basis states. For a dot with only one hole most of the matrix elements describing the xy confinement can be calculated analytically. Confinement in z direction requires to include only a few basis states because it is stronger in comparison to other potentials. The corresponding matrix elements were calculated numerically with high precision. Other terms like the mutual repulsion of the holes and the acceptor potential of the manganese atoms required very costly numerical integrations. These were the strongest constraints in the choice of basis size and thus the achievable accuracy. The model used by us simplifies the actual physical system considerably. Many important terms were dropped. The central cell correction is known to change the eigenenergy of the ground state of a hole bound to a manganese acceptor by at least 50 meV in *GaAs*. The strain in the *InAs* can shift the light-hole bands even more [27], [102]. In these systems we cannot expect to get the correct absolute values for the eigenenergies. However, we always strived to grasp all important features of the investigated systems and let not an insufficient basis blur the effects. The drop of the central cell correction was certainly the biggest cut into the precision of the calculations. While it certainly does not change the quality (e.g. hole spin alignment in the ground state) of the results it will certainly shift the found regimes. Also it would have a strong impact in weak dot potential regimes. We will in the following discuss the quality of the calculations for the different dot configurations.

For most configurations we were only interested in the eigenstate of the system with the smallest energy. For a convenient choice of the basis states one expects the ground state to be the one with the best approximation to the real eigenstate of the physical system. In general many operators have off-diagonal elements in the various terms of the Hamiltonian. Then an addition of basis

states enhances the interaction of basis states and thus repulsion of eigenstates. Their energy then changes. They converge to a limit, which is their true eigenenergy. There is no simple criterion how fast the convergence will be. However, we can expect that the change in ground-state energy by addition of one basis state will be strictly monotonically decreasing. The value of such a change relative to the other important energies of the system can give us a clue on the accuracy of our calculations. Another hint is the character of the eigenstates. In general each eigenstate will contain almost all basis states. When now in a calculated eigenstate, the probability of the system to be in one of the high basis states near the basis cut off is infinitesimally small, the basis size is sufficient. An addition of more basis states will then not change the character of the eigenstate very much. Also the relative strength of the terms in the Hamiltonian is important. The basis states reflect the symmetry of the dot. With increasing dot potentials strength in comparison to other terms, especially the acceptor potential, these weak terms will become merely a perturbation. We can thus expect that for strong dot potentials the approximation to the actual eigenstate will be better with the same number of basis states, than for weak dot potentials. The confinement in z direction is very strong in comparison to all other terms in the Hamiltonian. The system always stays mainly in the lowest basis state. A change of the z basis size has little influence on the eigenstates.

The eigenstates of a dot only with a single hole can be calculated in our model to almost any considerable precision. The spectrum in figure 3.1 was calculated using 20 basis states for the xy motion (Fock-Darwin states) and two states for the each hole mass to describe the z motion. By lowering the xy basis size to 4 states in the xy direction gives a change 0.001 meV while the absolute value of the eigenenergy in this state is 43.614 meV. In the calculations containing the Coulomb repulsion and the acceptor potentials we tried to take the maximal possible number of basis states. We prove the accuracy by reducing the basis sizes and comparing the change to the absolute value of the eigenenergy of the ground state. Typically the addition of a basis state changes the calculated energy less, than the removing of a basis state. So the presented energy change can be considered as an upper bound to the change in energy while the basis changes by one state. The standard potential values with the lowest dot confinement should be most susceptible to the basis size. In the calculations of the two hole spectrum with standard potential values the reduction of the one-particle xy basis size by one state from their maximal number results in a change of the ground-state energy of 0.262 meV. The absolute eigenvalue is 89.951 meV. This is a change of 0.3%. We can expect that our calculated value deviates not more than 1% – 2% from the actual value. For configurations with stronger dot potentials this deviation is again even smaller. When considering the acceptor potential the crucial configuration is the one with the off-axis manganese atom and standard dot potentials. The off-axis position contradicts strongly the symmetry of the basis states. This makes it necessary to use more states to resolve that symmetry. For this configuration the accuracy of our calculations is lower in comparison to the preceding. A reduction of one state in the xy basis changes the eigenenergy of the lowest state by about 0.0029%. We can, therefore, expect that our calculations will deviate at most by

a few per cent from the actual value. With stronger dot potentials the influence of the acceptor potential will fall and the basis states resemble more the exact eigenfunction. With the same number of basis states the approximation should become better. For the calculations including two holes and one manganese we investigated the configuration $(X, 1)$. Here we found a deviation of 0.67% in the ground-state energy with the reduction of one lateral one-hole basis state. This deviation is the largest among all calculated configurations. We can expect that with the addition of one basis state the energy of the ground state will differ by several per cent. We want to stress that we could properly represent the controversial ground state in the configuration with standard dot potentials and one manganese in the centre, albeit without the central cell correction.

All the reached computational precisions can be strongly enhanced by using more basis states. The only restriction is the computational time needed to calculate the matrix elements that representing the acceptor potential and the Coulomb interaction.

Chapter 4

Conclusions and Outlook

In this work I have investigated the interaction of up to two manganese impurities with up to three holes in different quantum dots. The changing dot potentials and the magnetic field influenced this interaction in many ways. The most widely investigated topic is the influence of the hole band mixing induced by varying ratios of the lateral potential to the potential in growth direction of the dot. We found that in the case of a small mixing of the $j_z = \pm 3/2$ and the $j_z = \pm 1/2$ Bloch bands, e.g. because of a large subband splitting, the hole behaves very similar to a conduction band electron with an effective two-level spin of $j_z = \pm 3/2$. This similarity appears in the shell structure of the quantum dot, the Coulomb energy in the dot and in the interaction with a manganese impurity. When the band coupling increases the dot shell-structure becomes blurred. The Coulomb energy stays almost constant with increasing confinement and several mutual alignments of the hole and the manganese spin begin to mix.

The ground state of a manganese acceptor in a quantum dot with holes crucially depends on the ratio between the acceptor potential and the dot potentials. If the acceptor potential dominates, the lowest state differs little from a bulk acceptor state. In contrast, in this work I concentrated on the regime dominated by the dot potentials. Especially the splitting of the light- and heavy-hole bands by a strong confinement in growth direction changes the character of the ground state. It then consists of six doubly-degenerate states. The splitting between the doublets is solely determined by the density of the hole at the position of the impurity. Elliptic lateral dot potentials as well as an off-axis manganese position can break the degeneracy but only in some of the doublets, only for dot and acceptor potentials of comparable strength and only for strong band mixing. In *GaAs* dots in magnetic field the spin alignment of the manganese is solely determined by its Zeeman energy. The hole has no influence on it. The hole aligns for weak fields antiferromagnetically with respect to the manganese spin. If it can align ferromagnetically for stronger fields depends again on the band mixing. In *InAs* on the other hand the hole determines the alignment of the manganese spin. The manganese is then aligned opposite to its Zeeman term in weak fields. I have shown the ferromagnetic coupling of two manganese atoms by a single hole and the determined the position of the two impurities, which maximises this coupling for a given

dot potential. With the addition of a second hole the coupling can be turned off. In the dots, superposition of quantum states can be created and destroyed by means of confining potential and magnetic field. This may be interesting for the realisation of quantum bits. In an *InAs* dot with two manganese atoms their spins can be flipped independently by a change of the magnetic field. This results suggest that once the technical difficulties concerning the controlled implementation of impurities in nanostructures are solved, we obtain a rich tool kit for the investigation of quantum mechanical systems and for the design of material properties.

The theoretical investigations in my work yielded a number of interesting results which still lack an experimental validation. The main drawback is the lack of experimental data to validate the results and give the present problem new impulses. Cyclotron resonance techniques on single dots enlightening their inner structure are difficult. The investigation of the small, self-assembled quantum dots via photoluminescence is now well established and attains much interest. Concerning the used model, now at the end of my work it appears, however, a draw-back that I have neglected the central cell correction in my simulations. In contrast to older publications new hints point out its importance to the interaction of the hole and the manganese.

As a continuation to this work it would be useful to implement the central cell correction. Also a concentration on the characteristics of the self-assembled quantum dots can put the work on a broader experimental footing. In this field the present quantum dot model will perform very well. In my belief, it is capable to give a quantitative description of the experiments. Staying in the field of toy models, investigations on the realisation of quantum bits are possible. The present numerical routine is very appropriate to simulate influences of the geometry of nanostructures on quantum mechanical states like the spin of the confined holes. With the ever rising computational power numerical simulations become more reliable and potent.

Chapter 5

Appendix

5.1 Polarisation

The eigenstates of holes in the quantum dot are not eigenstates to the hole spin j_z . The expectation value of the spin can vary spatially. We define the spin density operator by [49]

$$S_z(\mathbf{x}) = \sum_{s=-3/2}^{3/2} s\psi_s^+(\mathbf{x})\psi_s(\mathbf{x}). \quad (5.1)$$

The field operators $\psi_s^+(\mathbf{x})\psi_s(\mathbf{x})$ represent the particle-number density ρ_s of spin- s particles at point \mathbf{x} . The total density at this point is then

$$\rho_{tot}(\mathbf{x}) = \sum_{s=-3/2}^{3/2} \rho_s. \quad (5.2)$$

We define the polarization by dividing (5.1) by the total density

$$\pi(\mathbf{x}) = \frac{1}{\rho_{tot}(\mathbf{x})} \left(\frac{3}{2}\rho_{3/2}(\mathbf{x}) + \frac{1}{2}\rho_{1/2}(\mathbf{x}) - \frac{1}{2}\rho_{-1/2}(\mathbf{x}) - \frac{3}{2}\rho_{-3/2}(\mathbf{x}) \right). \quad (5.3)$$

For an eigenstate to \hat{j}_z , e.g. the eigenstate $j_z = 3/2$, the quantity above gives what one would expect: a constant value of $3/2$ over the whole dot.

5.2 Coefficients for relative coordinates

To calculate the matrix elements of the mutual Coulomb repulsion of two holes we changed the basis states of the motion in the xy plane. We changed to the relative coordinates of the two interacting particles to save one costly numerical integration. The transformation law is given in (2.69). Here we will give the boundaries in the summation and the used coefficients. Their full derivation can be found in [50].

$$\mu_{min}^{ij} = -\frac{2(n_i + n_j) - m_i - m_j + |m_i| + |m_j|}{2} \quad (5.4)$$

$$\mu_{max}^{ij} = \frac{2(n_i + n_j) + m_i + m_j + |m_i| + |m_j|}{2} \quad (5.5)$$

$$\nu_{max}^{ij} = \frac{1}{2} [2(n_i + n_j) + |m_i| + |m_j| - |\mu| - |m_i + m_j - \mu|] \quad (5.6)$$

$$A_{n_1 m_1 n_2 m_2} := (-1)^{(2n_2 + |m_2|)} \left[\prod_{i=1}^2 2^{(2n_i + |m_i|)} \left(\frac{2n_i + m_i + |m_i|}{2} \right)! \left(\frac{2n_i - m_i + |m_i|}{2} \right)! \right]^{-\frac{1}{2}} \quad (5.7)$$

and

$$K_{NM}^{n_1 m_1 n_2 m_2} := C_{\frac{1}{2}(2N+M+|M|)}^{\frac{2n_1+m_1+|m_1|}{2}, \frac{2n_2+m_2+|m_2|}{2}} C_{\frac{1}{2}(2N-M+|M|)}^{\frac{2n_1-m_1+|m_1|}{2}, \frac{2n_2-m_2+|m_2|}{2}}$$

with

$$C_a^{bc} := \sum_{s=\max(a-c, 0)}^{\min(a, b)} \binom{b}{s} \binom{c}{a-s} \sqrt{a!} \sqrt{(b+c-a)!} (-1)^s. \quad (5.8)$$

Bibliography

- [1] G. Janssen, E. Goovaerts, A. Bouwen, B. Partoens, B. Van Daele, N. Žurauskienė, P. M. Koenraad, and J. H. Wolter, *Phys. Rev. B* **68**, 045329 (2003).
- [2] O. Astafiev, V. Antonov, T. Kutsuwa, and S. Komiyama, *Phys. Rev. B* **65**, 085315 (2002).
- [3] S. Raymond, S. Studenikin, A. Sachrajda, Z. Wasilewski, S. J. Cheng, W. Sheng, P. Hawrylak, A. Babinski, M. Potemski, G. Ortner, et al., *Phys. Rev. Lett.* **92**, 187402 (2004).
- [4] H. Drexler, D. Leonard, W. Hansen, J. P. Kotthaus, and P. M. Petroff, *Phys. Rev. Lett.* **73**, 2252 (1994).
- [5] E. E. Vdovin, A. Levin, A. Patane, L. Eaves, P. C. Main, Y. N. Khanin, Y. V. Dubrovskii, M. Henini, and G. Hill, *Science* **290**, 122 (2000).
- [6] T. Fujisawa, D. G. Austing, Y. Tokura, Y. Hirayama, and S. Tarucha, *Nature* **419**, 278 (2002).
- [7] T. Dietl, H. Ohno, F. Matsukura, J. Cibert, and D. Ferrand, *Science* **287**, 1019 (2000).
- [8] J. König, H.-H. Lin, and A. H. MacDonald, *Phys. Rev. Lett.* **84**, 5628 (2000).
- [9] R. Hanson and D. D. Awschalom, *Nature* **453**, 1043 (2008).
- [10] D. Loss and D. P. DiVincenzo, *Phys. Rev. A* **57**, 120 (1998).
- [11] E. A. Stinaff, M. Scheibner, A. S. Bracker, I. V. Ponomarev, V. L. Korenev, M. E. Ware, M. F. Doty, T. L. Reinecke, and D. Gammon, *Science* **311**, 636 (2006).
- [12] D. Brunner, B. D. Gerardot, P. A. Dalgarno, G. Wust, K. Karrai, N. G. Stoltz, P. M. Petroff, and R. J. Warburton, *Science* **325**, 70 (2009).
- [13] A. O. Govorov and A. V. Kalameitsev, *Phys. Rev. B* **71**, 035338 (2005).
- [14] J. Fernández-Rossier and R. Aguado, *Physical Review Letters* **98**, 106805 (2007).

-
- [15] A. L. Efros, E. I. Rashba, and M. Rosen, *Phys. Rev. Lett.* **87**, 206601 (2001).
- [16] W. Kohn, *Phys. Rev.* **123**, 1242 (1961).
- [17] T. Darnhofer, U. Rössler, and D. A. Broido, *Phys. Rev. B* **52**, R14376 (1995).
- [18] M. Kroutvar, Y. Ducommun, D. Heiss, M. Bichler, D. Schuh, G. Abstreiter, and J. J. Finley, *Nature* **432**, 81 (2004).
- [19] I. A. Merkulov, A. L. Efros, and M. Rosen, *Phys. Rev. B* **65**, 205309 (2002).
- [20] A. V. Khaetskii, D. Loss, and L. Glazman, *Phys. Rev. Lett.* **88**, 186802 (2002).
- [21] J. A. Gupta, D. D. Awschalom, X. Peng, and A. P. Alivisatos, *Phys. Rev. B* **59**, R10421 (1999).
- [22] B. D. Gerardot, D. Brunner, P. A. Dalgarno, P. Ohberg, S. Seidl, M. Kroner, K. Karrai, N. G. Stoltz, P. M. Petroff, and R. J. Warburton, *Nature* **451**, 441 (2008).
- [23] G. S. Solomon, J. A. Trezza, A. F. Marshall, and J. S. Harris, Jr., *Phys. Rev. Lett.* **76**, 952 (1996).
- [24] B. Daudin, F. Widmann, G. Feuillet, Y. Samson, M. Arlery, and J. L. Rouvière, *Phys. Rev. B* **56**, R7069 (1997).
- [25] S. Kalliakos, C. P. García, V. Pellegrini, M. Zamfirescu, L. Cavigli, M. Gurioli, A. Vinatieri, A. Pinczuk, B. S. Dennis, L. N. Pfeiffer, et al., *Applied Physics Letters* **90**, 181902 (2007).
- [26] J. M. Luttinger and W. Kohn, *Phys. Rev.* **97**, 869 (1955).
- [27] G. L. Bir and G. E. Pikus, *Symmetry and strain-induced effects in semiconductors* (Wiley, New York, 1974), ISBN 0-470-07321-7.
- [28] G. Bastard, *Wave mechanics applied to semiconductor heterostructures* (Les Ulis Cedex : Les Éd. de Physique, 1996), ISBN 2-86883-092-7.
- [29] P. Pietiläinen and T. Chakraborty, *Physical Review B (Condensed Matter and Materials Physics)* **73**, 155315 (2006).
- [30] P. Lawaetz, *Phys. Rev. B* **4**, 3460 (1971).
- [31] J. M. Luttinger, *Phys. Rev.* **102**, 1030 (1956).
- [32] O. Madelung, *Landolt-Börnstein, Numerical data and functional relationships in science and technology: new series III Vol. 22a* (Springer, Berlin, 1987), ISBN 3-540-16609-2.

- [33] R. Winkler, *Spin-orbit Coupling Effects in Two-Dimensional Electron and Hole Systems* (Springer, Berlin, 2003), ISBN 978-3-540-01187-3.
- [34] L. I. Schiff, *Quantum mechanics* (McGraw-Hill, New York, 1968), ISBN 0-07-085643-5.
- [35] M. G. Burt, *Journal of Physics: Condensed Matter* **4**, 6651 (1992).
- [36] N. W. Ashcroft and M. N. David, *Solid state physics* (Holt, Rinehart and Winston, New York, 1976), ISBN 0-03-083993-9.
- [37] C. Kittel, *Einführung in die Festkörperphysik* (Oldenborg, München, Wien, 2002), ISBN 3-486-27219-5.
- [38] D. A. Broido, A. Cros, and U. Rössler, *Phys. Rev. B* **45**, 11395 (1992).
- [39] D. Pfannkuche, *Aspects of coulomb interactions in semiconductor nanostructures* (1998).
- [40] V. Fock, *Z. Phys.* **47**, 446 (1928).
- [41] M. Abramowitz and I. A. Stegun, *Handbook of mathematical functions : with formulas, graphs, and mathematical tables* (Dover, New York, 1972), ISBN 0-486-61272-4.
- [42] C. Cohen-Tannoudji, B. Diu, and F. Laloë, *Quantenmechanik* (Walter de Gruyter, Berlin, 1999), ISBN 3-11-016459-0.
- [43] T. Darnhofer-Demar, Ph.D. thesis, *Ferninfrarot-Response von Quanten-Dots mit Elektronen oder Löchern*, Universität Regensburg, Regensburg, Germany (1996).
- [44] A. V. Madhav and T. Chakraborty, *Phys. Rev. B* **49**, 8163 (1994).
- [45] O. Dippel, P. Schmelcher, and L. S. Cederbaum, *Phys. Rev. A* **49**, 4415 (1994).
- [46] R. Haupt and L. Wendler, *Physica B* **184**, 394 (1993).
- [47] T. Ando, A. B. Fowler, and F. Stern, *Rev. Mod. Phys.* **54**, 437 (1982).
- [48] F. Nolting, *Grundkurs: Theoretische Physik, Bd. 7 Vielteilchen-Physik* (Zimmermann-Neufang, Ulmen, 2000), ISBN 3-540-42020-7.
- [49] F. Schwabl, *Quantenmechanik für Fortgeschrittene* (Springer, Berlin, 2004), ISBN 3-540-20308-7.
- [50] D. Jacob, Diploma thesis, *Elektronische Eigenschaften gekoppelter Quantenpunkte*, Universität Hamburg (2002).

-
- [51] T. Jungwirth, J. Sinova, J. Mašek, J. Kučera, and A. H. MacDonald, *Reviews of Modern Physics* **78**, 809 (2006).
- [52] M. Linnarsson, E. Janzén, B. Monemar, M. Kleverman, and A. Thilderkvist, *Phys. Rev. B* **55**, 6938 (1997).
- [53] A. K. Bhaattacharjee and C. Benoit a la Guillaume, *Solid State Communications* **113**, 17 (2000).
- [54] J. K. Furdyna and J. Kossut, *Semiconductors and Semimetals, Volume 25, Diluted Magnetic Semiconductors* (Academic Press, 1988), ISBN 0-12-752125-9.
- [55] J. I. Climente, M. Korkusiski, P. Hawrylak, and J. Planelles, *Phys. Rev. B* **71**, 125321 (2005).
- [56] S. Chutia and A. K. Bhattacharjee, *Physical Review B (Condensed Matter and Materials Physics)* **78**, 195311 (2008).
- [57] J. Mašek and F. Máca, *Phys. Rev. B* **69**, 165212 (2004).
- [58] C. Kittel, *Quantentheorie der Festkörper* (R. Oldenbourg, München, Wien, 1970).
- [59] F. B. Pedersen and Y.-C. Chang, *Phys. Rev. B* **53**, 1507 (1996).
- [60] F. B. Pedersen and Y.-C. Chang, *Phys. Rev. B* **55**, 4580 (1997).
- [61] T. Darnhofer, D. A. Broido, and U. Rössler, *Phys. Rev. B* **50**, 15412 (1994).
- [62] L. G. C. Rego, P. Hawrylak, J. A. Brum, and A. Wojs, *Phys. Rev. B* **55**, 15694 (1997).
- [63] V. Gudmundsson, A. Brataas, P. Grambow, B. Meurer, T. Kurth, and D. Heitmann, *Phys. Rev. B* **51**, 17744 (1995).
- [64] S. M. Reimann and M. Manninen, *Rev. Mod. Phys.* **74**, 1283 (2002).
- [65] K. Rachor, T. E. Raab, D. Heitmann, C. Gerl, and W. Wegscheider, *Physical Review B (Condensed Matter and Materials Physics)* **79**, 125417 (2009).
- [66] H. L. Stormer, Z. Schlesinger, A. Chang, D. C. Tsui, A. C. Gossard, and W. Wiegmann, *Phys. Rev. Lett.* **51**, 126 (1983).
- [67] L. D. Landau and E. Lifschitz, *Quantenmechanik* (Akademie-Verlag, Berlin, 1988), ISBN 3-05-500067-6.
- [68] A. Messiah, *Quantenmechanik, Band 2* (Walter de Gruyter, Berlin, New York, 1990), ISBN 3-11-012669-9.

- [69] A. O. Govorov, Phys. Rev. B **70**, 035321 (2004).
- [70] J. Fernández-Rossier, Physical Review B (Condensed Matter and Materials Physics) **73**, 045301 (2006).
- [71] A. K. Bhattacharjee, Physical Review B (Condensed Matter and Materials Physics) **76**, 075305 (2007).
- [72] Y. Léger, L. Besombes, L. Maingault, and H. Mariette, Physical Review B (Condensed Matter and Materials Physics) **76**, 045331 (2007).
- [73] A. Kudelski, A. Lemaître, A. Miard, P. Voisin, T. C. M. Graham, R. J. Warburton, and O. Krebs, Physical Review Letters **99**, 247209 (2007).
- [74] A. Baldereschi and N. O. Lipari, Phys. Rev. B **8**, 2697 (1973).
- [75] F. V. Kyrychenko and J. Kossut, Phys. Rev. B **70**, 205317 (2004).
- [76] L. Besombes, Y. Léger, L. Maingault, D. Ferrand, H. Mariette, and J. Cibert, Phys. Rev. Lett. **93**, 207403 (2004).
- [77] L. Besombes, Y. Léger, L. Maingault, and H. Mariette, Journal of Applied Physics **101**, 081713 (2007).
- [78] O. Madelung, *Landolt-Börnstein, Numerical data and functional relationships in science and technology: new series III Vol. 17a* (Springer, Berlin, 1987), ISBN 0-387-15072-2.
- [79] E. L. Ivchenko and G. Pikus, *Superlattices and Other Heterostructures* (Springer, Berlin, 1997), ISBN 3-540-62030-3.
- [80] L. O. Massa, F. Qu, L. Villegas-Lelovsky, and R. F. K. Spada, Journal of Superconductivity and Novel Magnetism **23**, 121 (2010).
- [81] F. Qu and P. Hawrylak, Phys. Rev. Lett. **95**, 217206 (2005).
- [82] S.-J. Cheng, Physical Review B (Condensed Matter and Materials Physics) **77**, 115310 (2008).
- [83] D. Heiss, S. Schaeck, H. Huebl, M. Bichler, G. Abstreiter, J. J. Finley, D. V. Bulaev, and D. Loss, Physical Review B (Condensed Matter and Materials Physics) **76**, 241306 (2007).
- [84] D. V. Bulaev and D. Loss, Phys. Rev. Lett. **95**, 076805 (2005).
- [85] S.-J. Cheng and P. Hawrylak, EPL **81**, 37005 (2008).

-
- [86] S. Mackowski, T. Gurung, T. A. Nguyen, H. E. Jackson, L. M. Smith, G. Karczewski, and J. Kossut, *Applied Physics Letters* **84**, 3337 (2004).
- [87] A. A. Maksimov, G. Bacher, A. McDonald, V. D. Kulakovskii, A. Forchel, C. R. Becker, G. Landwehr, and L. W. Molenkamp, *Phys. Rev. B* **62**, R7767 (2000).
- [88] M. Goryca, T. Kazimierczuk, M. Nawrocki, A. Golnik, J. A. Gaj, P. Kossacki, P. Wojnar, and G. Karczewski, *Physical Review Letters* **103**, 087401 (2009).
- [89] C. L. Gall, L. Besombes, H. Boukari, R. Kolodka, J. Cibert, and H. Mariette, *Physical Review Letters* **102**, 127402 (2009).
- [90] R. C. Myers, M. H. Mikkelsen, J.-M. Tang, A. C. Gossard, M. E. Flatte, and D. D. Awschalom, *Nat Mater* **7**, 203 (2008).
- [91] N. T. T. Nguyen and F. M. Peeters, *Physical Review B (Condensed Matter and Materials Physics)* **78**, 245311 (2008).
- [92] N. T. T. Nguyen and F. M. Peeters, *Physical Review B (Condensed Matter and Materials Physics)* **80**, 115335 (2009).
- [93] T. Voigt, Diploma thesis, *Diluted Magnetic Quantum Dots*, Universität Hamburg (2007).
- [94] R. M. Abolfath, *Physical Review B (Condensed Matter and Materials Physics)* **80**, 165332 (2009).
- [95] M. Wagner, U. Merkt, and A. V. Chaplik, *Phys. Rev. B* **45**, 1951 (1992).
- [96] A. O. Govorov, *Phys. Rev. B* **72**, 075359 (2005).
- [97] O. Krebs, E. Benjamin, and A. Lemaître, *Physical Review B (Condensed Matter and Materials Physics)* **80**, 165315 (2009).
- [98] J. van Bree, P. M. Koenraad, and J. Fernández-Rossier, *Physical Review B (Condensed Matter and Materials Physics)* **78**, 165414 (2008).
- [99] R. M. Abolfath, P. Hawrylak, and I. Žutić, *Physical Review Letters* **98**, 207203 (2007).
- [100] J. Fernández-Rossier and L. Brey, *Phys. Rev. Lett.* **93**, 117201 (2004).
- [101] F. Qu and P. Hawrylak, *Physical Review Letters* **96**, 157201 (2006).
- [102] O. Stier, Ph.D. thesis, *Electronic and Optical Properties of Quantum Dots and Wires*, Technische Universität Berlin, Berlin, Germany (2008).

Publication

1. Maxim Trushin, Karel Výborný, Peter Moraczewski, Alexey A. Kovalev, John Schliemann, and T. Jungwirth,
Anisotropic magnetoresistance of spin-orbit coupled carriers scattered from polarized magnetic impurities
Phys. Rev. B 80, 134405 (2009)

Dankeschön

Ich möchte den vielen Menschen herzlich danken, die es mir ermöglicht haben, diese Arbeit zu schreiben. Ein ganz besonderer Dank gebührt natürlich Frau Prof. Dr. Daniela Pfannkuche, die mich in ihre tolle Gruppe aufgenommen hat. Sie hat es immer geschafft mich fachlich auf den richtigen Weg zu bringen und mich immer gedrängt hat die Welt positiver zu sehen. Ich möchte mich auch herzlich bei Prof. Dr. Detlef Heitmann bedanken für die übernahme des Zweitgutachtens der Dissertation. Prof. Dr. Ulrich Merkt danke ich auch ganz herzlich für die übername des Zweitgutachtens in der Disputation und die Betreuung des Graduiertenkollegs 1286. Viel mehr noch zu danken habe ich Ihm aber für den Anstoß englisch zu schreiben und die Hilfe beim verfassen der englischen Texte. Thanks. Vielen Dank an PD. Dr. Alexander Chudnovskiy für den Vorsitz des Prüfungsausschusses und den freien Tag den ich Ihm damit klauere. Ich möchte Dr. Karel Vyborny danken für die super Zusammenarbeit und interessanten persönlichen Gespräche. Ein großes DANKE! an Bodo Krause-Kjora, der mit seiner Arbeit an den Wochenenden die Computer am laufen gehalten hat. Einen riesigen Dank für die tolle und freundschaftliche Atmosphäre geht an alle aktuellen und ehemaligen Mitglieder der Gruppe th1 km und insbesondere für: Stellan Bohlens danke ich für die Geduld beim anhören meiner Lebensweisheiten, Daniel Becker und Philipp Knake vor allem für die interessanten Gespräche, Dirk-Sören Lühmann für die immer-währende Hilfe beim allen, Jacek Świebodzinski für seinen Humor, Tobias Voigt, Johann Gutjahr und Benjamin Baxevanis ganz besonderes für die fachlich sehr hilfreichen Diskussionen, danke auch Benjamin Krüger, Hosnieh Safaei-Katoli, Christoff Hübner, Tim Ludwig, Frank Deutzrnbacher, Kim Plassmeier, Frank Hellmuth, Alexander Lieder, Eva-Maria Richter und Christian, Müller. Vielen Dank an Frau Sen und Frau Schmidtke für den unaufhörlichen Nachschub an Kaffee. Ich danke Dr. Kevin Rachor für die interessante Zusammenarbeit. Ich möchte mich bedanken beim allen Mitgliedern des Graduiertenkolleg 1286, die ich hier nicht auch noch aufzählen kann. Es hat immer Spaß gemacht ich konnte einen Blick über den Tellerrand werfen. Ich möchte Bernd Güde für seine gute Laune danken. Für meine gute Laune und Arbeitskraft haben auch entscheidend meine Freunde aus dem “normalen” Leben gesorgt. Ich ganz herzliches Danke! an euch alle. Ich hoffe Ihr bleibt mir erhalten. Ich will meinem Bruder Michael danken für seine kritischen Kommentare zu meinem Leben und meinen Eltern Krystyna und Jerzy.